INFORMATION TO USERS

The most advanced technology has been used to photograph and reproduce this manuscript from the microfilm master. UMI films the text directly from the original or copy submitted. Thus, some thesis and dissertation copies are in typewriter face, while others may be from any type of computer printer.

The quality of this reproduction is dependent upon the quality of the copy submitted. Broken or indistinct print, colored or poor quality illustrations and photographs, print bleedthrough, substandard margins, and improper alignment can adversely affect reproduction.

In the unlikely event that the author did not send UMI a complete manuscript and there are missing pages, these will be noted. Also, if unauthorized copyright material had to be removed, a note will indicate the deletion.

Oversize materials (e.g., maps, drawings, charts) are reproduced by sectioning the original, beginning at the upper left-hand corner and continuing from left to right in equal sections with small overlaps. Each original is also photographed in one exposure and is included in reduced form at the back of the book. These are also available as one exposure on a standard 35mm slide or as a 17" x 23" black and white photographic print for an additional charge.

Photographs included in the original manuscript have been reproduced xerographically in this copy. Higher quality 6" x 9" black and white photographic prints are available for any photographs or illustrations appearing in this copy for an additional charge. Contact UMI directly to order.

U·M·I

University Microfilms International
A Bell & Howell Information Company
300 North Zeeb Road, Ann Arbor, MI 48106-1346 USA
313/761-4700 800/521-0600

Order Number 9009721

Local-field and electromagnetic properties of disordered systems

Chen, Zhe, Ph.D.

City University of New York, 1989

U·M·I
300 N. Zeeb Rd.
Ann Arbor, MI 48106

LOCAL-FIELD AND ELECTROMAGNETIC PROPERTIES OF DISORDERED SYSTEMS

by

Zhe Chen

A dissertation submitted to the Graduate Faculty in Physics in partial fulfillment of the requirements for the degree of Doctor of Philosophy, The City University of New York.

1989

This manuscript has been read and accepted for the Graduate Faculty in Physics in satisfaction of the dissertation requirement for the degree of Doctor of Philosophy.

September 1989 9/14/89
Date

Chair of Examining Committee

September 1989 9/14/89
Date

Executive Officer

Supervisory Committee

The City University of New York

Abstract

LOCAL-FIELD AND ELECTROMAGNETIC PROPERTIES OF DISORDERED SYSTEMS

by

Zhe Chen

Thesis adviser: Dr. Ping Sheng

This thesis regards the investigation of the static and dynamic electromagnetic properties of random systems. In the static limit, a generalized Onsager's approach is developed for the study of local field distribution and its implications for the dielectric properties in random systems. Correlation with the microstructure of random materials is highlighted. We find the distribution of local fields to display a double-peak character in general. This unexpected behavior is explained in terms of two types of local environments defined relative to the applied field. The quantitative characteristics of the distribution are found to be sensitive to the microstructure of a random system. In particular, the standard deviation of the distribution is directly proportional to the product of the polarizability and a parameter that measures the local anisotropy of the medium. The mean of the distribution, on the other hand, is found to be bounded below by the Lorentz local field value, with the fractional deviation from the lower bound proportional to the variance. The later quantity is also identified as the correction factor to the

Clausius-Mossotti relation, and the extended spatial correlation is demonstrated to have a significant effect on this factor.

In the dynamic limit, we study the optical properties of colloidal gold aggregates where the focus is on the effects of multiple scattering on the structure factor $S(q)$ and the consequences of high-order multipole interaction on the absorption and depolarized scattering by the colloidal aggregates. Effects of multiple scattering on the structure factor are examined by relating them to the spatial correlations of the local fields. It is found that the multiple scattering affects only the magnitude of $S(q)$ but not its q-dependence for $q \leq a^{-1}$, where a is on the order of a single particle size. This makes light scattering a viable technique for structure determination. The high-multipole interaction and its implications on the absorption and depolarized scattering characteristics are examined through a rigorous scattering solution of a simple model that consists of a periodic chain of cylindrical particles. Results obtained are in good accord with experimental observations.

To My Parents

Acknowledgements

I would like first to thank Dr. P. Sheng, my thesis advisor at Corporate Research Science Laboratories of Exxon, for his invaluable guidance and active involvement in all the projects we worked on. His unique intuitive style and deep physical insights have not only helped me renew my interests in theoretical physics but also greatly influenced my thinking of physics. I would also like to thank him and Mrs. Sheng for their countless invitations and hospitalities on holidays. They made my bachelor life in the U.S. a happy and memorable one.

I would also like to thank Prof. J. L. Birman, whose encouragement and care has motivated me over the years. I have benefitted from him over many invaluable discussions and physical insights on both my research projects and reading courses (on the Fluctuation Theory of Phase Transitions, and Group Theory and Phase Transitions). I would like to thank Profs. M. Lax, J. Gersten, and A. Genack for serving on my dissertation guidance committee and for making the second examination a happy and learning experience for me.

At Exxon, I would like to thank Dr. D. A. Weitz, who is also a member of my dissertation committee, for numerous helpful discussions and suggestions during the course of the thesis research. I have benefitted from him for both his physical insights and a good deal of personal advice. I have enjoyed collabrating with him and with Drs. M. H. Lindsay, M. Lin, P. Meakin, and R. Klein. I would also like to thank Dr. K. Liang for many helpful advices. I am grateful to R. Rao of Cray Research Inc., and K. Jordan and B. Fornberg of Exxon for their helpful assistances in computing matters.

I am grateful to Prof. K. K. Mon of Georgia University who made my summer stay at the Center for Simulational Physics a joyous learning experience. I am also grateful to Prof. D. P. Landau and the Center for their generousity on the supercomputer time.

I would like to acknowlege many of my fellow graduate students and postdocs at Exxon of whom I would like to mention in particular Dr. S. Troian, for many enlightening discussions ranging from science to sociology, and Drs. M. Murat, W. Xue, Z. Wang, and Z. Q. Zhang for helpful discussions.

I am grateful to Prof. T. D. Lee, who implemented the CUSPEA program, for enabling me to study in the U.S.

Professor R. Tao, my undergraduate thesis advisor at Fudan University, has given me great encouragement and personal care. I share this thesis with him.

I would especially like to thank my parents for their understanding and for letting me be away from them. Their understanding and support made the thesis possible.

Last but surely not least, I wish to acknowledge my indebtness to my wife, Xiaohua Huang, for her selfless support and constant love, and my son Xixi, for making my last dissertation year a joyous one.

TABLE OF CONTENTS

LIST OF FIGURES

CHAPTER 1

INTRODUCTION

The study of physical properties of random systems is of great importance in many diverse areas of science and technology. Current interests range from metal-insulator transition in composite materials[1,2], localization of light[3] and electron[4] in random media, application of amorphous semiconductors in xeroxgraphy and solar cell[5], physical processes in porous media[6], to the wide use of special purpose polymeric materials[7,8]. Common to all random systems is the lack of periodicity in their structural arrangements. Therefore, the scientific insights for these systems must be achieved without the help of mathematical amenities such as Brillioun zone, Bloch states, etc. which we are accustomed to in conventional crystalline solid state physics[9]. In the last two decades, rapid development of computers capable of studying large models of random systems has generated new understanding of the topology and structure of random networks. Advances towards the analytical description of random structures were achieved through the percolation theory[10] and the recent introduction of the fractal concept[11]. Yet, despite of the progress in understanding random structures, the interplay between the microstructues of a random system and its physical properties still remains today a poorly understood subject. The aim of this thesis is to do a systematic study on the issues related to the physical implications of random structures on their dielectric and optical properties. In doing so we hope to bridge a gap in the structure-property relationship for random materials.

In the static limit, the dielectric property of a material is characterized by the dielectric constant ϵ defined by $P = (\epsilon - 1)E/4\pi$, where P and E are the electric polarization strength and the macroscopic field, respectively. Since $P = \sum p/V$, where the induced dipole moment p is proportional to the local field at each molecule, the important quantity for determining the ϵ is obviously the local field. By definition, local field is the sum of the applied field and the dipolar fields at a molecule produced by all other molecules in the material. Calculation of local field is a generic electromagnetic many-body problem which dates back to as early as Faraday[12] who proposed a model of a dielectric, which consisted of a series of metallic globules separated from each other by insulating materials. Mossotti[13] subsequently analyzed the interaction between these polarizable entities, invoking a spherical cavity in the derivation of the local field. This first cavity consideration for deriving local field was later used, with more clarity, by Clausius[14] who took each molecule as contained in a small sphere, cut out of the continuous surrounding medium characterized by the final dielectric constant of the material. In Clausius' derivation, the sphere fits tightly around the molecule, an assumption that obviously neglects the effect of spatial fluctuations in a real material.

This assumption was formally relaxed later by Lorentz[15], who introduced a large spherical cavity (known as Lorentz cavity nowadays) separating the far away molecules, whose interactions with the center one could be approximated by a dielectric continuum, from the nearby molecules which need more explicit consideration. In his calculation, however, the complexity of the many-body interaction was reduced by assuming the molecules in the cavity to be distributed on a simple cubic lattice so that the combined contribution from all the other molecules to the local field at the center vanishes. In terms of Lorentz's local field,

$E_L = E + \frac{4\pi}{3}P$, the Clausius-Mossotti (CM) relation was easily rederived. Despite of the overwhelming success of the CM relation and the Lorentz local-field* in non-polar materials, the assumed cubic symmetry in molecular arrangement still leaves the effect of spatial fluctuations unexamined.

In the context of calculating the effective dielectric constant of inhomogeneous materials, Maxwell[22] in 1873 considered a large sphere containing spherical inclusions of different resistivity, and calculated their effective dielectric constant. Later, Garnett[23] based on the maxwell's equation for propogating waves, also derived a CM-like relation for glasses containing metal spheres. This formula, known as Maxwell-Garnett (MG) formula nowadays, has been widely used for estimating the effective dielectric constant for random inhomogeneous materials[12]. Although the MG formula was able to predict qualitatively a resonance absorption, as observed in experiments[24], for the composites consisting of metal inclusions in an insulating matrix (at some negative ratio of the dielectric constants between the two phases), it failed to produce a metal-insulator transition also observed in these composites. In 1935, Bruggeman[25] proposed an effective medium theory for the random composites, in which all the independent phases were treated equivalently. The Bruggeman effective medium theory was able to yield a percolation threshold for the metal-insulator composites, but it could not explain the observed absorption resonance. The physical understanding on these discrepancies was achieved only recently with the recognition that each effective-medium theory is associated with an underlying microstructure[26]. In fact, Milton[27] has shown that there always exists a composite geometry for which the predictions

* Apart from the spherical point-like molecules, Lorentz's cavity was shown[12] to yield unreasonable results for molecules with needle-like or flat-disk-like shapes. Wiener[16], Bragg and Pippard[17], Pollark[18,19,20], and later Landauer and Woo[21] proposed an excluded volume approach for the calculation of local field, which allows more flexibility in accommodating different molecular shapes.

of an effective-medium theory are rigorously valid. Hashin and Strikman[28] later derived rigorous bounds for the dielectric constants (of all possible microstructures) based on the consideration of the general symmetries of the composites. However, the realization of the roles of microstructure in the effective-medium type theories immediately raises the importance of developing a theory or calculational methods in which the microstructure of a random material could be treated explicitly.

Explicit consideration of the effects of spatial fluctuations on the local field and the dielectric constant has been pursued by Kirkwood[29] and Yvon[30] (KY) since mid-thirties, followed by de Boer, van der Maesen and ten Seldam[31], and Brown[32], who calculated the deviation S from the CM relation using statistical mechanics, where S is defined as

$$\frac{\epsilon - 1}{\epsilon + 2} = \frac{4\pi}{3}\alpha\rho(1 + S), \tag{1.1}$$

here α is the dipole-polarizability of the molecules, and ρ is the particle number density. The correction factor S, arising from spatial fluctuations, was expressed in terms of the correlation in molecular positions. The above authors expanded S in powers of α and calculated only the lowest non-vanishing order $S^{(2)}$, i.e. the term proportional to α^2. In this level of approximation, $S^{(2)}$ already involves contributions from two- and three-body correlations. Kirkwood applied the superposition approximation[33] in evaluating the three-body correlation and used the density expansion for the evaluation of two-body correlation function. However, the validity of the density expansion is restricted to low concentrations. In 1974, Stell and Rushbrooke[34] showed that even with the Percus-Yevick pair-correlation function[35], application of the Kirkwood superposition approximation still yields results which deviate significantly from that of Monte Carlo simulation by Alder,

Weis and Strauss[36]. Generalization of the KY theory to include higher-order multipole interactions has been investigated by Felderhof[37,38], by using density expansion of the two- and three-body correlation functions in the weak-coupling limit*. More recently, similar consideration was also pursued by Geigenmüller and Mazur[41], who examined the effect of the spatial fluctuations in a random system of dielectric spheres by using a modified density expansion formulation, in which the correction to the CM relation was expanded in the density-fluctuation correlation functions. Although they could show that the high-order correction in S is small, the formal nature of these theories, like the KY theory, precluded their studying the specific issues of the structure-property relationships of random dielectrics.

Another formulation of the local-field calculation was introduced by Onsager[42] in 1936 in an effort to resolve the so-called polarization catastrophy[43] difficulty encountered by the Lorentz theory in polar liquids. Here the dipolar interaction of a molecule with the rest of the material was approximated by placing a molecule in an empty spherical cavity cut out of a dielectric continuum. The size of the cavity was set to be equal to the average molecular volume. This model, in fact, is quite similar to that of Clausius'[14] except the molecule now possesses a permanant dipole moment in addition to the polarizable part. The genius of Onsager's approach is in the division of local field into a cavity field, arising from the polarization of the cavity wall by the applied field, and a reaction-field, due to the additional polarization of the cavity by the molecule's own dipole moment. He found that the reaction-field was always parallel to the direction of the dipole moment, so that it would not affect the spatial orientations of the molecule. By

* Felderhof, Ford, and Cohen[39,40] also examined the non-local effect on the CM relation using the cluster-expansion method for dielectric constant.

using Onsager's local field, a better formula for the dielectric constant of polar liquids was obtained in which the polarization catastrophy was absent. Like all other single particle approaches, Onsager's approach also ignores the effect of the microstructure of a random medium.

In a random medium, the diversity of local environments is expected to generate a distribution of local field values. It is therefore clear that a proper theory of local field should have as its focus the local field distribution functions. To obtain this distribution in terms of the microstructure of a random medium, we first note that there generally exists a correlation length ξ in a random medium characterizing the size of the spatial inhomogeneities of the medium. The medium may be regarded as homogeneous only on scales larger than ξ. However, its physical properties are known to be influenced by both the size and the characteristics of the correlation[44]. Therefore, for a calculation to be truely representive of the real medium, one must take into account explicitly the spatial correlations. Owing to its inherent mathematical generalizability, in Chapter two, the Onsager approach is generalized to a cluster of particles of size larger than ξ, so that the interactions between particles within the correlated region can be treated explicitly. Using this approach, the local field distribution and its relations to microstructure are studied for random media charaterized by either uniform or percolative spatial correlations.

We found that the local field distribution[26] displays a double-peak character in general with the Lorentz local field value situated in between. This unexpected behavior is found to be associated with the existence of two types of local environments, defined relative to the applied field, in a random medium. Indeed, the quantitative characteristics of distribution are shown to be sensitive to the microstructure of a random medium. In particular, the variance (or the second

moment) of the distribution, as measured by the standard deviation, is directly proportional to the product of a parameter that measures the local anisotropy of the medium and the particle polarizability. The mean of the distribution, on the other hand, is found to be bounded below by the Lorentz local-field value consistent with other variational calculations[45]. The fractional deviation S from the lower bound is identified as the correction to the Clausius-Mossotti relation. Our calculation also indicates that the correction factor S is proportional to the variance of distribution.

In terms of the correction factor S, the effect of microstructure is vividly demonstrated by comparing the S for both the uniform and the percolative random media in the low density region. In this region, the requirement that the particles to be connected in a percolative structure makes the microstructure of the percolative structure more anisotropic than that of an uniform one. As a result, the S for a percolative medium increases as the density ρ decreases, contrary to the behavior for an uniform medium where S decreases to zero when $\rho \to 0$. Therefore the Lorentz local-field and the CM relation would be a poor approximation for fractal and growth structures and the CM like relation with the correction of S may now be regarded as a new effective-medium theory for these correlated structures.

In the dynamic limit, the response of a material to an incident wave is generally characterized by the optical index of refraction and the structure factor $S(q)$. Great progress was made on the study of wave propogation and scattering in random media when Foldy[46] showed how the effective index of refraction could be related to the averaged forwarding scattering amplitude in a random medium. Lax[47] then extended the theory by introducing an effective medium in which the scatterers are embedded and the theory is proven to be quite general.

Due to the sensitivity of light scattering behavior to those structures of a medium whose scales are comparable with or larger than the wavelength, light scattering has also been used for structural determination. However, the traditional relationship between the structure factor and the light scattering intensity is based on the single scattering Born approximation. Yet, when a system is dense and the polarizability of the particles is large, multiple scattering can be strong and this naturally raises the question whether light scattering can remain a viable technique for structural determination of such systems.

For random fractal systems, the multiple scattering effect has been considered recently by Berry *et al.* [48] for smoke clusters and by Chen *et al.* [49] for metallic colloidal aggregates. By using a mean-field approximation, Berry *et al.* made a mean-field estimation on the importance of the multiple scattering during the coagulation process. However, the question about the multiple scattering effect on the structure factor can not be studied with this mean-field approximation.

In Chapter three, we provide a general multiple scattering formulation for the scattering fields in particulate aggregates. The effects of multiple scattering on the structure factor is shown to be separable into two parts: a mean-field part which affects only the overall scattering intensity by a constant factor, and a local-field fluctuation part, characterized by the spatial correlations of the fluctuating part of local fields, which is wave-vector dependent.

For colloidal gold aggregates[50], whose structures have been shown to exhibit the scale-invariant fractal character, the mean-field effect is shown, by using a mean-field approximation similar to that of Berry *et al.* [48], to be always negligible when the fractal dimension $d_f < 2$ (clusters grown by diffusion-limited cluster-cluster aggregation) for $ka \ll 1$, where a denotes the particle size and k the incident wave vector. When $d_f > 2$ (clusters grown by reaction-limited cluster-

cluster aggregation), the effect does become important when the particle number in the aggregates grows to $N \sim (ka)^{-d_f/(d_f-2)}$ ($\sim 10^{23}$ for incident wavelength at 4880 Å). At this stage, the cluster is geometrically opaque.

The local-field fluctuation effect is studied by exactly solving the multiple scattering equations for the local fields. We use the structural information of the computer-generated fractal clusters (whose structure has been checked to be in accord with the colloidal aggregates) as our calculational input. It is found that the correlation in the fluctuating part of local fields is small in magnitude and short-ranged in its extent for both $d_f < 2$ and $d_f > 2$ aggregates. Therefore, we conclude that multiple scattering does not mask the structural information in the scattering intensity, when $q \leq a^{-1}$. This result clears the ambiguity involved in the structure determination by using light scattering.

Dynamic field would also generate electromagnetic excitations inside a particle or collective excitations among neighboring particles. When this happens, a fraction of electromagnetic energy of the incident wave is absorbed. Since absorption depends on the local field, its characteristics would thus be sensitive to the local environments. For gold aggregates, recent experimental studies[51] indeed observed interesting characteristics, such as the double absorption peaks and enhanced depolarized scattering, that are not explainable in terms of the traditional mean-field theories, such as the Maxwell-Garnett theory, since the mean-field theories are based on the assumption of a random, isotropic distribution of neighboring particles which ignore the strong short-range anisotropic correlations inherent in a connected cluster. Furthermore, since the particles are close to each other, high-order multipole interactions are expected to be strong in these systems. While an exact calculation, comprising of all the multipole interactions and the aggregate's structure, would pose formidable calculational

difficulties, the physics of the electromagnetic coupling between the particles can be captured by considering simpler structures, such as a chain of the gold particles, that are generic building blocks of the aggregates.

In Chapter four, we study a simple model that consists of a periodic chain of cylindrical particles. Compared to other models consisting of spherical particles, this model has the advantage of being able to yield a rigorous scattering solution with relatively simple mathematics. Rigorous scattering solution of the model shows that when the incident wave is polarized along the chain direction, the chain exhibits a second, red-shifted absorption peak as distinct from the single-particle Mie resonance. The depolarized scattering also shows dramatic increase around this absorption peak frequency. Averaging over random orientations of the chain yields the double absorption peaks and the enhanced depolarized scattering that are in good accord with experimental observations.

The rest of this thesis is organized as follows: Chapter two presents a study of the general properties of the local field in random dielectrics. Local field distribution and its quantitative relationships to both the geometric and dielectric properties are examined in detail. In Chapter three, a multiple scattering formulation of light scattering from aggregated clusters is presented. The effects of multiple scattering are differentiated into a mean-field part and a local-field fluctuation part. These effects are then studied in detailed for the colloidal gold aggregates which exhibit the fractal symmetry. Chapter four addresses the issue of high-order multipole interaction on the optical absorption and scattering characteristics for aggregate structures. A rigorous solution of a simple model is present. Results obtained are compared with the experimental observations.

REFERENCES

1. N. F. Mott, *Metal-Insulator Transitions*, (Taylor and Francis, London, 1974).

2. N. F. Mott and E. A. Davis, *Electronic Process in Non-Crystalline Materials*, (Oxford University Press, London, 1979) 2nd edition.

3. *Scattering and Localization of Classical Wave in Random Media*, edited by P. Sheng, (World Scientific, Singapore, 1990), and references therein.

4. *Anderson Localization*, edited by Y. Nagaoka and H. Fukuyama, (Springer Verlag, 1982), and references therein.

5. *Fundamentals of Armophous Semiconductors*, (National Academy of Science, Washington, D.C., 1972).

6. *Physics and Chemistry of Porous Media*, edited by D. L. Johnson and P. N. Sen, (American Institute of Physics, New York, 1984).

7. *Polymer in Solar Energy Utilization*, edited by C. G. Gebelein, P. J. Williams, and R. D. Deanin, (American Chemical Society, Washington, D. C., 1983).

8. *Polymer Materials and Artificial Organs*, edited by C. G. Gebelein, (American Chemical Society, Washington, D. C., 1984).

9. see for example, C. Kittel, *Introduction for Solid State Physics*, 5th edition (Wiley & Sons, New York, 1976).

10. D. Stauffer, *Introduction to Percolation Theory* (Taylor and Francis, London, 1985).

11. B. B. Mandelbrot, *The Fractal Geometry of Nature* (Freeman, San Francisico, 1982).

12. see R. Landauer, in *Electrical Transport and Optical Properties of Inhomogeneous Media*, 1977, edited by J. C. Garland and D. B. Tanner, AIP Conference Preceeding No. 40 (American Institute of Physics, New York, 1978), P.2.

13. O. Mossotti, *Mem. math. fis. Modena*, **24**, II, 49 (1850).

14. R. Clausius, *Die Mechanische Behandlung der Electricität*, (Vieweg-Verlag, Brunswick, 1879), Vol. II.

15. H. A. Lorentz, *The Theory of Electrons*, (B. G. Teubner, Leipzig, 1909; Reprint: Dover, New York, 1952).

16. O. Wiener, *Abhandlungen der Mathematish-Physischen Klasse der Koenigl. Saechsischen Gesellschaft der Wissenschaften* **32**, 509 (1912).

17. W. L. Bragg and A. B. Pippard, *Acta. Cryst.* **6**, 865 (1953).

18. M. Pollak and M. Knotek, *J. Non-Cryst. Solids* **4**, 459 (1970).

19. M. Pollak, *Proc. R. Soc. Lond.* **A325**, 383 (1971).

20. H. A. Pohl and M. Pollak, *J. Chem. Phys.* , 66, 4031 (1977).

21. R. Landauer and J. W. F. Woo, *Phys. Rev. B* , 5 (1189), 1972.

22. J. C. Maxwell, *A Treatise on Electricity and Magnetism*, Vol. 1 (Dover, New York, 1954), P.440.

23. J. C. M. Garnett, *Philos. Trans. R. Soc. Lond.* **203**, 385 (1904).

24. J. I. Gittleman and B. Abeles, *Phys. Rev. B* , 15, 3273 (1977).

25. D. A. G. Bruggeman, *Ann. Physik (Leipz.)* **24**, 636 (1935); **24**, 665 (1935); **25**, 645 (1936).

26. see, for example, P. Sheng, in *Homogenization and Effective Moduli of Materials and Media*, edited by J. L. Ericksen, The IMA volumes in mathematics and its applications, vol. 1 (Springer-Verlag, New York, 1986).

27. G. Milton, in *Physics and Chemistry of Porous Media*, edited by D. L. Johnson and P. N. Sen, (American Institute of Physics, New York, 1984). P.66.

28. Z. Hashin and S. Strikman, *J. Appl. Phys.* **33**, 3125 (1962).

29. J. G. Kirkwood, *J. Chem. Phys.* **4**, 592 (1936).

30. J. Yvon, *Recherches sur la théorie cinétique des liquides II*, (Hermann, Paris, 1937).

31. J. de Boer, F. ran der Maesen, and C. A. tan Seldam, *Physica* **19**, 265 (1955).

32. W. F. Brown Jr., *J. Chem. Phys.* **23**, 154 (1955).

33. J. G. Kirkwood, *J. Chem. Phys.* , 5, 300 (1935); J. G. Kirkwood and E. M. Boggs, *ibid*, **10**, 392 (1942).

34. G. Stell and G. S. Rushbrooke, *Chem. Phys. Lett.* **24**, 531 (1974).

35. J. K. Percus and G. L. Yevick, *Phys. Rev.* **110**, 1 (1958).

36. B. L. Alder, J. -J. Weis and H. L. Strauss, *Phys. Rev.* **A7**, 281 (1973).

37. B. U. Felderhof, *J. Phys.* **C15**, 3943 (1982).

38. B. U. Felderhof, *J. Phys.* **C15**, 3953 (1982).

39. B. U. Felderhof, G. W. Ford, and E. G. D. Cohen, *J. Stat. Phys.* **28**, 649 (1982).

40. B. U. Felderhof, G. W. Ford, and E. G. D. Cohen, *J. Stat. Phys.* **33**, 241 (1983).

41. U. Geigenmüuer and P. Mazar, *Physica* **136A**, 316 (1986).

42. L. Onsager, *J. Am. Chem. Soc.* **58**, 1486 (1936).

43. H. Frõlich, *Theory of Dielectrics*, 2nd edition (Oxford University Press, 1958).

44. R. Zallen, *The Physics of Amorphous Solids* (Wiley, New York 1983).

45. R. W. Hellwarth, *Phys. Rev.* **152**, 152 (1966).

46. L. L. Foldy, *Phys. Rev.* **67**, 107 (1945).

47. M. Lax, *Rev. Mod. Phys.* **23**, 287 (1951).

48. M. V. Berry and I. C. Percival, *Opt. Acta.* **33**, 577 (1986).

49. Z. Chen, P. Sheng, D. A. Weitz, M. H. Lindsay, M. Lin, and P. Meakin, *Phys. Rev. B* **37**, 5232 (1988).

50. D. A. Weitz and M. Oliveria, *Phys. Rev. Lett.* **52**, 1433 (1984).

51. M. H. Lindsay, M. Y. Lin, D. A. Weitz, P. Sheng, Z. Chen, R. Klein, and P. Meakin, *Faraday Discuss. Chem. Soc.* **83**, 153 (1987).

CHAPTER 2

LOCAL-FIELD DISTRIBUTION IN RANDOM DIELECTRICS

ABSTRACT

A generalized Onsager approach is developed for the calculation of local-fields in random dielectrics. The distribution of local-fields obtained is shown to display a double-peak character in general. This unexpected behavior is explained in terms of two types of local environments defined relative to the applied field. We find the characteristics of the local-field distribution to be sensitive to the microstructure of a random medium. Two types of random structures, characterized by uniform or percolative spatial correlations, were considered. The standard deviation of the distribution is shown to be directly proportional to the product of the polarizability and a parameter that measures the local anisotropy of the medium. On the other hand, the mean of the distribution is found to be bounded below by the Lorentz local-field value, with the fractional deviation S from the lower bound proportional to the variance σ^2. The same quantity S is indentified as the correction factor to the Clausius-Mossotti relation. We demonstrate that the extended spatial correlation has a significant effect on the values of S. Implications of our results, for the effective medium theories and the optical properties of random small particle systems, are disscused.

2.1. INTRODUCTION

When an electric field $\vec{E}_0$ is applied to a dielectric medium consisting of polarizable particles, the local field[1] at a particular particle differs from $\vec{E}_0$ by an amount that is the sum of the dipole fields from all the other polarized particles. Due to the long-range nature of the dipole field, however, a straightforward summation of its contributions would yield conditionally-convergent results. In 1909, Lorentz[2] proposed the physical concept of (what has become known as) the Lorentz cavity to evaluate the local field. This classical solution of the local-field problem, together with the associated Clausius-Mossotti (CM) relation[3], may rightly be regarded as the basis for the modern theory of dielectric materials.

In spite of its overwhelming sucess, however, the Lorentz theory still left some important questions about the local field unresolved. For example, whereas the Lorentz theory predicts an unique local-field value for a given medium, yet for a random medium the diversity of local environments is expected to generate a distribution of local field values. What is the shape and quantitative characteristics of this distribution? What is the relationship between the local-field distribution and the microstructure of a random medium? Although in the past decades there have been continued theoretical studies on the effects of randomness, yet the formal nature of these investigations[4,5,6,7,8] has precluded their addressing the specific issues raised above. The physical effects of randomness on local field therefore remain today a topic to be clarified.

Another problem with the Lorentz theory is in regard to its generalization to polar media where each constituent particle not only is polarizable, but also has a permanant dipole moment $\vec{\mu}$. In such cases the simple replacement of the polarizability α by $\alpha + \mu^2/kT$ in the CM relation[9], where T is temperature and k the Boltzmann constant, are shown to result in divergent dielectric constant at fi-

nite temperatures, a phenomenon not generally observed[10,11]. In 1936, Onsager[12] resolved this problem by proposing a division of the local field into components such that the correct contribution of the permanant dipoles may be easily isolated and evaluated. Besides creating a new theory for the local field and the dielectric constant of polar materials, Onsager's approach offers the advantage of generalizability since its steps involve only well-defined boundary-value problems.

In this Chapter, we present a generalization of the Onsager approach for the calculation of local fields for a cluster of particles. This generalization is motivated by two considerations. First, only by explicitly taking into account the interaction between a particle and its neighbors is it possible to study the effects of randomness and their sensitivity to microstructures. Since the original Onsager calculation involves only one particle and its interaction with an effective-medium continuum, the purpose of our present study obviously requires an extension of the calculational tool. Second, it is well-known that a random system is generally characterized by a correlation length ξ above which the medium may be regarded as homogeneous. Therefore, in order that the calculated results may be truely representative of the system, it is necessary that we use as our calculational unit a cluster whose dimension is at least as large or larger than the correlation length. By enabling the explicit accounting of the interactions between the polarizable particles in a consistent manner, the generalized Onsager approach can thus provide a valuable tool for determining the local field distribution and its relation to the microstructure.

Our results[13] indicate that the local-field distribution is doubly-peaked in general. This unexpected behavior is explained in terms of two types of local environments defined relative to the applied field. We also find the characteristics of the local-field distribution to be sensitive to the microstructure of a

random medium. First of all, the width of the distribution as characterized by the standard deviation σ is directly proportional to the product $\alpha\eta$, where η is a parameter that measures the local anisotropy of the medium. Second, the mean of the distribution is found to be bounded below by the Lorentz local-field value, with the fractional deviation S from the lower bound proportional to the variance σ^2. The same quantity S is also indentified as the correction factor to the Clausius-Mossotti relation. For fractal or growth aggregates, the value of S is especially large, implying that for these systems the Lorentz local-field and its associated dielectric constant prediction are poor approximations to their true values.

This Chapter is organized as follows. Section 2.2 describes briefly the Onsager approach and the concept of reaction-field. This is followed by the generalization of the approach to random systems presented in Section 2.3. Sections 2.4 to 2.6 present the results of local-field distribution, its geometric, and its dielectric implications, respectively. In Section 2.7, we discuss some questions related to the generalized Onsager approach. Section 2.8 discusses implications of the local-field distribution on effective-medium theories. We conclude the Chapter by addressing further research opportunities.

2.2. ONSAGER'S REACTION-FIELD APPROACH

In an effort to resolve the difficulty of polarization catastrophy encountered in the Lorentz theory, Onsager[12] proposed in 1936 a new approach for studying the local field in polar liquids. The approach consists of following two elements: (a) a molecule with isotropic polarizability is placed inside an empty spherical cavity of radius a, and (b) the sphere is embedded in an effective dielectric continuum. The calculation of the local field is thus reduced to a simple electrostatic problem,

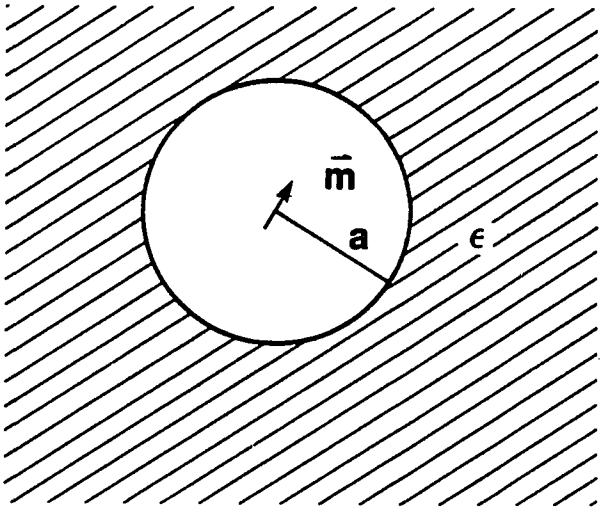

Figure 2.1 Schematic sketch of the Onsager model. The cavity size is set to the averaged molecular volume in order to recover the Lorentz local field value for non-polar molecules.

as depicted in Fig.2.1.

When an external electric field is applied to the system, the local field at the molecular position (center of the cavity) is a sum of two fields. One is due to the polarization change of the cavity wall in absence of the molecule and the other is the reaction-field arising from the additional polarization of the surrounding due to the polarized molecule. Both fields can be obtained by solving simple electrostatic boundary-value problems.

To calculate the first part of the local field we need only to solve the Laplace equation for the electric potential inside the empty cavity with an applied external field. The relevant equations and boundary conditions are:

$$\nabla^2\phi_{in} = \nabla^2\phi_{out} = 0, \tag{2.1a}$$

$$\phi_{in} = \phi_{out} \quad \text{and} \quad \frac{\partial\phi_{in}}{\partial r} = \epsilon\frac{\partial\phi_{out}}{\partial r} \qquad \text{at} \quad r = a, \tag{2.1b}$$

$$\phi_{in} \quad \text{is finite} \qquad \text{at} \quad r = 0, \tag{2.1c}$$

$$\phi_{out} \to -Er\cos\theta \qquad \text{as} \quad r \to \infty. \tag{2.1d}$$

In Eqs.(2.1), we have set the z axis in the incident wave direction. Since the problem is symmetric with respect the azimuth angle ϕ, the general solution of (2.1a), in spherical coordinate system, is

$$\phi_{in} = \sum_n \left[A_\ell r^\ell + \frac{B_\ell}{r^{\ell+1}}\right] P_\ell(\cos\theta), \tag{2.2}$$

$$\phi_{out} = \sum_n \left[C_\ell r^\ell + \frac{D_\ell}{r^{\ell+1}}\right] P_\ell(\cos\theta). \tag{2.3}$$

The coefficients A_ℓ, B_ℓ, C_ℓ, and D_ℓ are to be determined by boundary conditions (2.1b) to (2.1d). Since the boundary conditions contain only $\cos\theta$, all the coefficients with $\ell > 1$ should vanish. For the remaining ($\ell = 1$) four coefficients,

condition (2.1c) sets $B_1 = 0$ and condition (2.1d) requires $C_1 = -E$. By using boundary conditions (2.1b) yield two coupled equations for A_1 and D_1:

$$A_1 a = -Ea + D_1, \tag{2.4a}$$

$$A_1 = \epsilon \left[-E - \frac{2D_1}{a^3} \right], \tag{2.4b}$$

with the solution

$$A_1 = -\frac{3\epsilon}{2\epsilon + 1} E \quad \text{and} \quad D_1 = -\frac{\epsilon - 1}{2\epsilon + 1} Ea^3. \tag{2.5}$$

Therefore the electric potential inside the cavity is

$$\phi_{in} = -\frac{3\epsilon}{2\epsilon + 1} Er\cos\theta. \tag{2.6}$$

It is straightforward to obtain from Eq.(2.6) the cavity field $\vec{G}$ as

$$\vec{G} = -\nabla\phi_{in}|_{r=0} = \frac{3\epsilon}{2\epsilon + 1}\vec{E}. \tag{2.7}$$

The reaction-field, as coined by Onsager, can be calculated by replacing the polarized molecule back in the cavity and solving for the potential without the external field. Mathematically, it differs from Eq.(2.1) only in the boundary conditions (2.1c) and (2.1d), which are replaced by

$$\phi_{in} = \frac{m\cos\theta}{r^2} \qquad \text{as} \quad r \to 0, \tag{2.8a}$$

and

$$\phi_{out} \to 0 \qquad \text{as} \quad r \to \infty, \tag{2.8b}$$

where $\vec{m}(= \vec{\mu} + \vec{p}_{induced})$ denotes the total dipole moment of the molecule. The general solution of the potentials, is still given by Eqs.(2.2) and (2.3). However, the boundary conditions (2.8a) and (2.8b) requires $C_1 = 0$ and $B_1 = m$. By using boundary condition (2.1b) now yields

$$A_1 = \frac{2}{a^3}\frac{\epsilon - 1}{2\epsilon + 1} m \tag{2.9}$$

or

$$\phi_{in} = -\left(\frac{2}{a^3}\frac{\epsilon-1}{2\epsilon+1}mr + \frac{m}{r^2}\right)\cos\theta. \tag{2.10}$$

The reaction-field $\vec{R}$, therefore, is

$$\vec{R} = -\nabla[\phi_{in} - \phi_{\text{dipole}}]|_{r=0} = \frac{2}{a^3}\frac{\epsilon-1}{2\epsilon+1}\vec{m}. \tag{2.11}$$

Hence the local field is

$$\vec{E}_L = \vec{G} + \vec{R} = \frac{3\epsilon}{2\epsilon+1}\vec{E} + \frac{2}{a^3}\frac{\epsilon-1}{2\epsilon+1}\vec{m}. \tag{2.12}$$

The division of the local field into the cavity field and the reaction field is an important observation because $\vec{R}$ (Eq.(2.11)) is always parallel to the direction of the dipole moment. For a polar molecule with $\alpha = 0$, this field therefore will not affect the spatial orientation of the molecule since it does not exert a torque on the permanant dipole. This has dramatic consequences for the predicted dielectric behavior of polar liquids as was clearly shown in Onsager's paper[12]. In particular, the problem of polarization catastrophe is absent in Onsager's formulation.

The gist of Onsager's approach is the realization that a dipole will always experiences a reaction-field arising from the polarization of its neighbors by the dipole itself. Replacement of the surrounding neighbors by an effective-medium turns the calculation of the reaction-field into a well defined boundary-value problem. It is this aspect that makes the approach mathematically generalizable.

2.3. GENERALIZED ONSAGER'S APPROACH

A random medium is characterized by a spatial correlation length ξ which is typical of the size of the inhomogeneities in the medium. The medium may be regarded as homogeneous on scales larger than the correlation length, but is inhomogeneous on scales less than ξ. The physical properties of a medium are

known to be influenced by the nature of the correlation[14]. To take into account explicitly this microstructure in our calculation of local fields, we must therefore use a cluster of particles whose dimension is as large or larger than the correlation length. Therefore, we introduce a spherical cavity with a radius $a \geq \xi$ and replace the medium outside the cavity by an effective-dielectic continuum with a dielectric constant ϵ to be determined self-consistently. Since the interactions between the particles inside the cavity are treated exactly, the effect of microstructure is thus included.

For the N particles inside the cavity, the local field at each particle is a sum of four contributions. First, there is the cavity field $\vec{G}(\vec{r}_i)$, which is the same for every particle. Then there is the reaction-field $\vec{R}(\vec{r}_i, \vec{r}_i)$ due to the polarization by the particle itself. In contrast to the Onsager theory, the position of the particle is not aways at the cavity center. In addition to these two contributions, there is the dipolar fields $\vec{D}(\vec{r}_i, \vec{r}_j)$ produced by all the other particles in the cavity. This contribution is absent in Onsager's theory since he considered only one particle. The last contribution is the reaction-fields $\vec{R}(\vec{r}_i, \vec{r}_j)$ due to all the other particles. Therefore

$$\vec{E}_L(\vec{r}_i) = \vec{G} + \sum_{j \neq i}^{N} \vec{D}(\vec{r}_i, \vec{r}_j) + \sum_{j=1}^{N} \vec{R}(\vec{r}_i, \vec{r}_j). \tag{2.13}$$

Eq.(2.13) represents a group of equations for the local fields which must be solved simultaneously.

To complete the formulation, we need a relation to determine the dielectric constant of the effective-medium self-consistently. Since the system is homogeneous over the scale larger than the correlation length, we may consider the medium as composed of clusters of size $a \geq \xi$. The medium dielectric constant ϵ can then be determined from the coherent-potential approximation[15] of vanishing

average forward-scattering amplitude. In the static limit ($\lambda \to \infty$), this condition reduces to the requirement that the averaged dipole moments of the cavity equals zero.

$$< \text{ cavity dipole moment } >= 0, \tag{2.14}$$

where the symbole <> denotes configurational average. Equations (2.13) and (2.14) constitute the generalization of the Onsager approach.

For non-polar systems whoes constituents can be approximated by isotropic point dipoles, the dipolar field $\vec{D}(\vec{r}_i, \vec{r}_j)$ may be written as

$$\vec{D}(\vec{r}_i, \vec{r}_j) = \frac{3\vec{r}_{ij}\vec{r}_{ij} - r_{ij}^2 \overleftrightarrow{I}}{r_{ij}^5} \cdot \vec{m} \equiv \overleftrightarrow{T}_{ij} \cdot \vec{m}, \tag{2.15}$$

where $\vec{r}_{ij} = \vec{r}_i - \vec{r}_j$ and $r_{ij} = |\vec{r}_{ij}|$. The reaction-field $\vec{R}(\vec{r}_i, \vec{r}_j)$, with arbitrary $\vec{r}_i$ and $\vec{r}_j$, and the electric potential outside the cavity can be obtained by solving an electrostatic boundary-value problem to be discussed as follows.

To derive the $\vec{R}(\vec{r}_i, \vec{r}_j)$, we first consider electric field at $\vec{r}$ produced by a dipole $\vec{p}$ at $\vec{r}_j$ in vacuum. The electric potential ϕ_0 satisfies the Possion's equation:

$$\nabla^2 \phi_0(\vec{r}) = -4\pi\rho(\vec{r}), \tag{2.16}$$

where $\rho(\vec{r})$ is the free charge density. In terms of Green's function, the general solution of Eq.(2.16) is

$$\phi_0(\vec{r}) = \int_{V\to\infty} \rho(\vec{r}')G(\vec{r}, \vec{r}')d^3\vec{r}', \tag{2.17}$$

where the Green's function $G(\vec{r}, \vec{r}')$ is given by

$$G(\vec{r}, \vec{r}') = \frac{1}{|\vec{r} - \vec{r}'|} = 4\pi \sum_{\ell=0}^{\infty} \sum_{m=-\ell}^{\ell} \frac{1}{2\ell+1} \frac{r_<^\ell}{r_>^{\ell+1}} Y_{\ell m}^*(\theta', \phi') Y_{\ell m}(\theta, \phi). \tag{2.18}$$

Here $r_< = \min(r', r)$ and $r_> = \max(r', r)$, $Y_{\ell m}(\theta, \phi)$ is the normalized spherical harmonic function. For a polarizable medium with polarization strength $\vec{P}$, $\rho(\vec{r}) = -\nabla \cdot \vec{P}$. Therefore

$$\rho(\vec{r}) = -\nabla \cdot (\vec{p}\delta(\vec{r} - \vec{r}_j)) = -\vec{p} \cdot \nabla\delta(\vec{r} - \vec{r}_j). \tag{2.19}$$

By substituting Eq.(2.19) into Eq.(2.17) yields the electric potential in region $r > r_j$:

$$\phi_0(\vec{r}) = \sum_{\ell=0}^{\infty} \sum_{m=-\ell}^{\ell} C_{\ell m}(\vec{r}_j) \frac{1}{r^{\ell+1}} Y_{\ell m}(\theta, \phi), \tag{2.20}$$

with

$$C_{\ell m}(\vec{r}_j) = -\vec{p} \cdot \left[\frac{4\pi}{2\ell + 1} \int \nabla\delta(\vec{r} - \vec{r}_j) r^{\ell} Y^*_{\ell m}(\theta, \phi) d^3 r \right]. \tag{2.21}$$

By noticing the identity

$$[\nabla\delta(\vec{r} - \vec{r}_j)]g(\vec{r}) = \nabla[\delta(\vec{r} - \vec{r}_j)g(\vec{r})] - \delta(\vec{r} - \vec{r}_j)[\nabla g(\vec{r})], \tag{2.22}$$

the integral of Eq.(2.21) can be simplified if we let $g(\vec{r})$ denotes $r^{\ell} Y^*_{\ell m}(\theta, \phi)$. Then the integration of the first term $\nabla[\delta(\vec{r} - \vec{r}_j)g(\vec{r})]$ vanishes for $\vec{r}_j \neq 0$. Integration of the second term of Eq.(2.22) simply replace the argument of $g(\vec{r})$ by $\vec{r}_j$, a consequence of the δ-function. Therefore

$$C_{\ell m}(\vec{r}_j) = -\frac{4\pi}{2\ell + 1} \vec{p} \cdot \nabla[r_j^{\ell} Y^*_{\ell m}(\theta_j, \phi_j)]. \tag{2.23}$$

Now let us place the dipole $\vec{p}$ at $\vec{r}_j$ inside a cavity of radius a. The electric potentials inside ϕ_{in} and outside ϕ_{out} the cavity satisfy the Laplace equation:

$$\nabla^2 \phi_{in}(\vec{r}) = 0, \qquad \text{for} \quad r_j < r < a, \tag{2.24}$$

$$\nabla^2 \phi_{out}(\vec{r}) = 0, \qquad \text{for} \quad r > a. \tag{2.25}$$

Their general solution is in the form of

$$\phi_{in}(\vec{r}) = \sum_{\ell=0}^{\infty} \sum_{m=-\ell}^{\ell} (A_{\ell m} r^{\ell} + B_{\ell m} r^{-\ell-1}) Y_{\ell m}(\theta, \phi), \tag{2.26}$$

$$\phi_{out}(\vec{r}) = \sum_{\ell=0}^{\infty} \sum_{m=-\ell}^{\ell} (C_{\ell m} r^{\ell} + D_{\ell m} r^{-\ell-1}) Y_{\ell m}(\theta, \phi), \tag{2.27}$$

where $A_{\ell m}$, $B_{\ell m}$, $C_{\ell m}$, and $D_{\ell m}$ coefficients to be determined by the following boundary conditions:

$$\phi_{in}(\vec{r}) = \phi_{out}(\vec{r}), \qquad \text{at} \quad r = a, \tag{2.28a}$$

$$\frac{\partial \phi_{in}(\vec{r})}{\partial r} = \epsilon \frac{\partial \phi_{out}(\vec{r})}{\partial r}, \qquad \text{at} \quad r = a, \tag{2.28b}$$

$$\phi_{out}(\vec{r}) \to 0, \qquad \text{for} \quad r \to \infty, \tag{2.28c}$$

$$\phi_{in}(\vec{r}) = \phi_{out}(\vec{r}) = \phi_0(\vec{r}), \qquad \text{when} \quad \epsilon = 1. \tag{2.28d}$$

Boundary condition (2.28d) simply state that when the cavity is absent ($\epsilon = 1$) the electrical potentials should be identical to the solution of the dipole in the vacuum, Eq.(2.20). The boundary conditions (2.28b) to (2.28d) completely determine the expansion coefficients, and the solutions are

$$\phi_{in}(\vec{r}) = \sum_{\ell=0}^{\infty} \sum_{m=-\ell}^{\ell} [-\frac{(\epsilon-1)(\ell+1)}{\ell+(\ell+1)\epsilon} a^{-2\ell-} r^{\ell} + r^{-\ell-1}] C_{\ell m}(\vec{r_j}) Y_{\ell m}(\theta, \phi), \tag{2.29}$$

and

$$\phi_{out}(\vec{r}) = \sum_{\ell=0}^{\infty} \sum_{m=-\ell}^{\ell} \frac{(2\ell+1)}{\ell+(\ell+1)\epsilon} r^{-\ell-1} C_{\ell m}(\vec{r_j}) Y_{\ell m}(\theta, \phi), \tag{2.30}$$

where $C_{\ell m}(\vec{r_j})$ is given by Eq.(2.23). The part of the potential in ϕ_{in} that arises from the polarization of the outside medium by the dipole is simply the difference of ϕ_{in} and the dipolar field ϕ_0 in vacuum, i.e.

$$\begin{aligned} \phi_R(\vec{r}) &= \phi_{in}(\vec{r}) - \phi_0(\vec{r}) \\ &= -\sum_{\ell=0}^{\infty} \sum_{m=-\ell}^{\ell} \frac{(\epsilon-1)(\ell+1)}{\ell+(\ell+1)\epsilon} a^{-2\ell-1} r^{\ell} C_{\ell m}(\vec{r_j}) Y_{\ell m}(\theta, \phi). \end{aligned} \tag{2.31}$$

So the reaction-field at $\vec{r}$ is

$$\begin{aligned}\vec{R}(\vec{r},\vec{r}_j) &= -\nabla\phi_R(\vec{r}) \\ &= \sum_{\ell=0}^{\infty}\sum_{m=-\ell}^{\ell}\frac{(\epsilon-1)(\ell+1)}{\ell+(\ell+1)\epsilon}a^{-2\ell-1}C_{\ell m}(\vec{r}_j)\nabla[r^\ell Y_{\ell m}(\theta,\phi)] \\ &= \alpha\sum_{\ell=0}^{\infty}\sum_{m=-\ell}^{\ell}c_{\ell m}(\epsilon)[\vec{q}^*(\ell,m,\vec{r}_j)\cdot\vec{p}]\vec{q}(\ell,m,\vec{r}),\end{aligned} \tag{2.32}$$

where

$$\vec{q}(\ell,m,\vec{r}_i) = \vec{\nabla}[(\frac{|\vec{r}_i|}{a})^\ell Y_{\ell m}(\theta_i,\phi_i)], \tag{2.33}$$

$$c_{\ell m}(\epsilon) = \frac{4\pi}{2\ell+1}\,\frac{(\epsilon-1)(\ell+1)}{\ell+(\ell+1)\epsilon}\,\frac{1}{a}. \tag{2.34}$$

Since there is no free charge in region $0 \le r \le r_j$, the above solution of reaction-field is also valid in this region.

Substituting Eq.(2.32) into Eq.(2.13), we obtain explicit equations for the local fields,

$$\vec{E}_L(\vec{r}_i) = \frac{3\epsilon}{2\epsilon+1}\vec{E}(\vec{r}_i) + \sum_{j=1}^{N}\overleftrightarrow{S}(\vec{r}_i,\vec{r}_j,\epsilon)\bullet\vec{E}_L(\vec{r}_j), \tag{2.35}$$

where $\vec{E}$ is the macroscopic field, ρ is the number density of the dipoles, and $\vec{p} = \alpha\vec{E}_L$. The scattering matrix $\overleftrightarrow{S}$ in Eq.(2.35) includes both the reaction-field and the dipolar field:

$$S_{\mu\nu}(\vec{r}_i,\vec{r}_j,\epsilon) = r_{\mu\nu}(\vec{r}_i,\vec{r}_j,\epsilon) + d_{\mu\nu}(\vec{r}_i,\vec{r}_j)(1-\delta_{ij}) \tag{2.36}$$

with

$$r_{\mu\nu}(\vec{r}_i,\vec{r}_j,\epsilon) = \alpha\sum_{\ell=0}^{\infty}\sum_{m=-\ell}^{\ell}c_{\ell m}(\epsilon)[\vec{q}(\ell,m,\vec{r}_i)]_\mu[\vec{q}(\ell,m,\vec{r}_j)]^*_\nu, \tag{2.37}$$

$$d_{\mu\nu}(\vec{r}_i,\vec{r}_j) = \alpha\frac{3(\vec{r}_i-\vec{r}_j)_\mu(\vec{r}_i-\vec{r}_j)_\nu - |\vec{r}_i-\vec{r}_j|^2\delta_{\mu\nu}}{|\vec{r}_i-\vec{r}_j|^5}. \tag{2.38}$$

Here $\mu, \nu = 1, 2, 3$, denote the three Cartisian components of the field, and δ_{ij} is the Kronecker delta function.

To calculate the total dipole moment of the cavity, let us look for the total electric potential ϕ^T_{out} outside the cavity when there is an external field applied to the medium. In this case there are two more contributions to ϕ^T_{out}, in addition to ϕ_{out} of Eq.(2.30) obtained above. One is the external field itself and the other is due to the polarization of the cavity by the applied field. The later contribution is equivalent to a dipole field. Therefore,

$$\phi^T_{out}(\vec{r}) = \phi_{out}(\vec{r}) - Er\cos\theta - \frac{\epsilon - 1}{2\epsilon + 1} Ea^3 \frac{\cos\theta}{r^2}, \tag{2.39}$$

when there is only one dipole inside the cavity. For N particles inside the cavity, we obtain

$$\phi^T_{out}(\vec{r}) = \sum_{j=1}^{N} \phi_{out}(\vec{r}, \vec{r}_j) - Er\cos\theta - \frac{\epsilon - 1}{2\epsilon + 1} Ea^3 \frac{\cos\theta}{r^2}, \tag{2.40}$$

in which the local fields are given by the solution of Eq.(2.35). The total dipole moment d of the cavity thus is

$$d = -\frac{\epsilon - 1}{2\epsilon + 1} Ea^3 + \frac{3}{2\epsilon + 1} \sum_{j=1}^{N} C_{1m}(\vec{r}_j) \tag{2.41}$$

Substituting Eq.(2.41) into Eq.(2.14), yields

$$\frac{\epsilon - 1}{4\pi} = \rho\alpha < \frac{1}{N} \sum_{i=1}^{N} \vec{E}_L(\vec{r}_i) \cdot \vec{E}/E^2 >, \tag{2.42}$$

A closer examination of Eq.(2.38) reveals that it is identical to the constitutive relation in the electromagnetic theory[16], $P = (\epsilon - 1)/4\pi E$, since P, by definition, is the dipole moment per unit volume, i.e. $P \equiv \rho < p >= \rho\alpha < (1/N) \sum_i^N \alpha E_L >$.

Equations (2.35) and (2.42) are the basic equations of generalized Onsager approach for non-polar media. Together, they represent $3N + 1$ simultaneous equations. To obtain the local field and the dielectric constant ϵ, we first assume an initial trial dielectric constant from the CM relation to solve the $3N$ simultaneous equations Eq.(2.35) for the local fields. With the calculated local field values, a new dielectric constant ϵ is obtained from Eq.(2.42). This new ϵ is substituted back into Eq.(2.35), and the above process is repeated until consistency is obtained. This usually takes $3 - 8$ iterations. As the polarizability decreases, fewer iteration steps are needed for convergence.

With the local fields calculated for each configuration as described above, the calculation is repeated for many configurations and the configuration averaged value of local field is then used to get a dielectric constant from Eq.(2.42). Using this dielectric constant as input, we solve for local field once again. Such iteration is continued until the averaged local field is consistent with the dielectric constant. Usually 2-3 such iteration steps are sufficient.

Since the cavity is only a contraption of our model, for particles lying close to the cavity wall their local fields would be distorted by the discontinuous change in the geometric environment. To reduce this boundary effect, we introduce a transitional region around the cavity wall: if $a - \delta \leq |\vec{r}_i| \leq a + \delta$, where δ is on the order of one nearest-neighbor distance, then particle i is assigned the averaged local-field value at each iteration stage. It should be noted that we have created a region even outside the cavity wall. These particles interact with the particles inside sphere of $r \leq a - \delta$ depending on whether they are inside or outside the cavity boundary. For a particle outside the cavity but inside the boundary region, it interacts with the inside particles via only the dipolar field. For a particle inside the cavity boundary, however, it interacts with not only the dipolar field but also

the reaction-field. The local field values of the particles in the transitional region are excluded in our statistical analysis of the local-field distributions. With this prescription, our calculation correctly reproduce the results of Onsager's for a single particle in a cavity and that of Lorentz's for a cubic lattice consists of even 27 particles. The local field distribution in the later case is sharply peaked at the Lorentz local-field value as would be expected.

2.4. RANDOM SYSTEM CHARACTERIZATION

Two types of random media are considered. One is denoted as the uniform random medium. In such media, every position $\vec{r}$ in space is occupied with the same probability, and the pair correlation length ξ is proportional to $\rho^{-1/3}$, where ρ is the number density of the particles. The other is the much studied percolative random structures[17], where the particles are required to be connected. Here the correlation length ξ is known to vary as $\xi \sim (p - p_c)^{-\nu}$, for p close to the percolation threshold p_c. The exponent ν is close to $4/3$ for $3d$ site percolation. For $p \sim 1$, ξ is on the order of the averaged nearest-neighbor distance and the system is similar to an uniform random medium. For $p \to p_c$, ξ diverges and the system exhibits fractal symmetry[18]. The local environments in this limit are expected to be more anisotropic than that of an uniform random medium. It is therefore interesting to compare the local-field distribution characteristics between these two media. Since the cluster size is limited by the computer capacity, our calculations can only be performed for p not too close to p_c. Nonetheless, results of such calculations already demonstrate behavior which is distinct from that of uniform random media.

The positions of our random point particles are generated on a simple cubic lattice. Effects from the underlying lattice will be discussed later. To generate

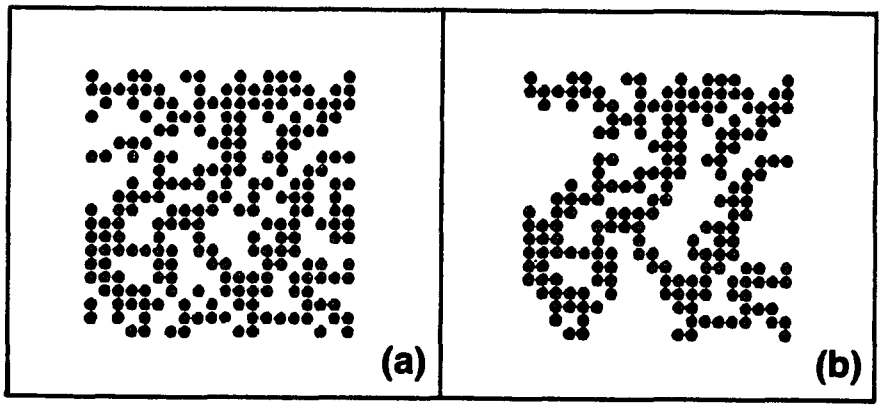

Figure 2.2 (a) A two dimensional sample of an uniform random system with particle density $\rho = 0.6$. (b) Connected part of system (a). It is clear from the plot that the local environmant of (b) is more anisotropic than the uniform system (a).

an uniform random medium, we start with a fully occupied lattice and randomly take out particles until a desired number density of the remaining is reached (a $2d$ sample with $\rho = 0.60$ is shown in Fig.2.2a). The percolative random structure is obtained by further taking out the isolated clusters from an otherwise uniform random medium, preserving only the connected part (Fig.2.2b is obtained by retaining the connected structure of Fig.2.2a). To guarantee a connected structure, the occupation probability p used to obtain the uniform random medium must be greater than the percolation threshold ($p_c = 0.331$ for 3d site percolation; and $p_c = 0.591$ for the 2d case). It should be noted the $p = \rho$ for the uniform random medium but $\rho \neq p$ for the percolative structures. In fact, $\rho \rightarrow 0$ as $p \rightarrow p_c$. By examining figures 2.2a and 2.2b, it is appearant that the local environment in a percolative structure is more anisotropic than that of the uniform random medium.

2.5. LOCAL-FIELD DISTRIBUTION

Figure 2.3 displays some of our calculated local-field distributions Figures 2.3a-2.3c are for uniform random systems with three different particle number densities. Figure 2.3d is a typical plot for a percolative random structure (with a number density 0.261 to be compared with figure 2.3c). It is clear that the distribution exhibits double-peak* character in general. The single peak of Figure 2.4b is interpretable as the merging of two peaks. The relative peak strength is noted to depend strongly on the number density in the uniform random system. For the local field components perpendicular to the applied field, the distribution is found generally to be Gaussian like with a small distribution width on the

* Since the local field is calculated on occupied site only and the polarizable particle has no internal states such as that for the Ising spin the double-peak character here should be distinguished from those model behaviors which originated from different types of sites or internal states.

Figure 2.3 Local-field distribution as a function of $E_{\|}/E_L$. (a)-(c) are for uniform random medium with different densities. (d) is for a random percolative structure. Number of the particles used to obtain each distribution is: (a) 2593, (b) 3117, (c) 3103, and (d) 5613.

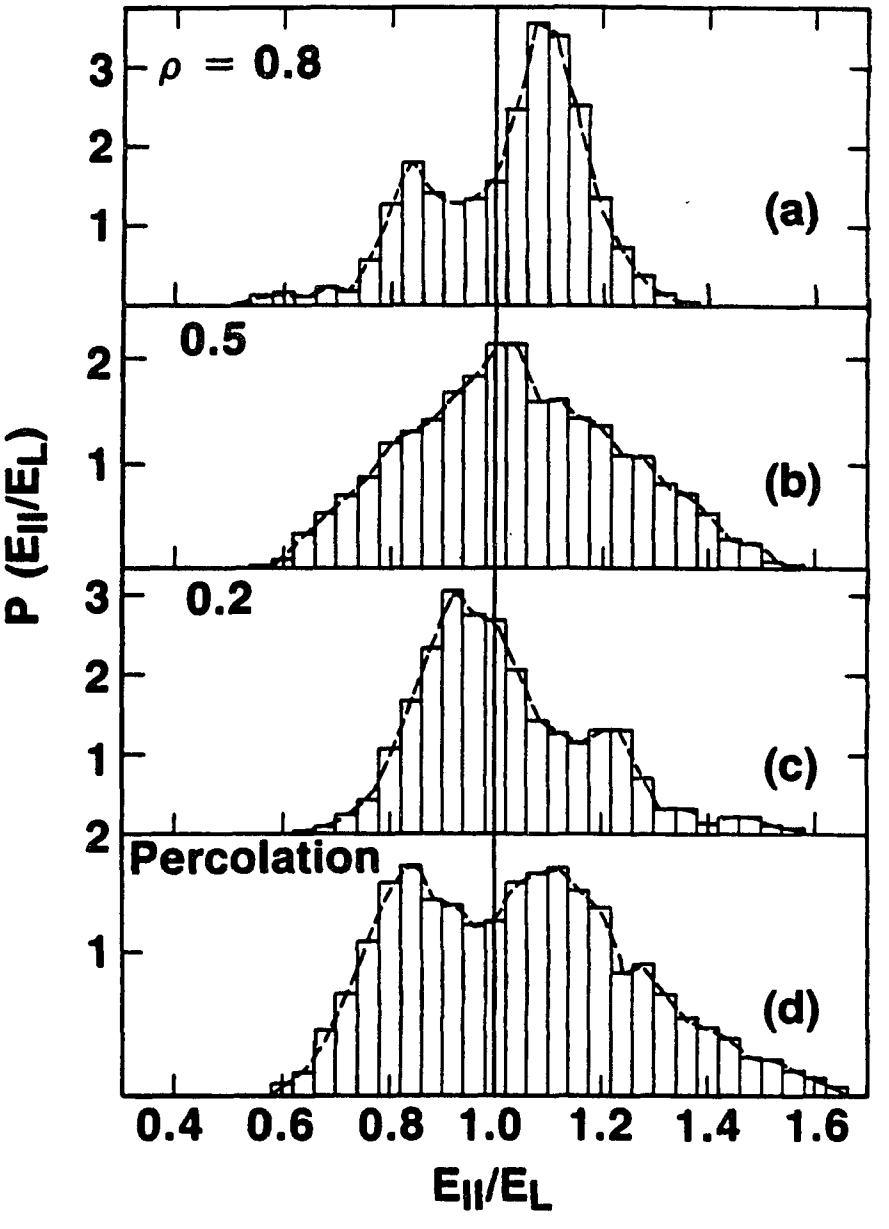
ρ = 0.8
(a)
0.5
(b)
0.2
(c)
Percolation
(d)
P (E||/EL)
E||/EL
0.4
0.6
0.8
1.0
1.2
1.4
1.6

Figure 2.4 Illustration of the local-field distribution for three different polarizabilities. The medium is uniformly random with a number density of 0.2.

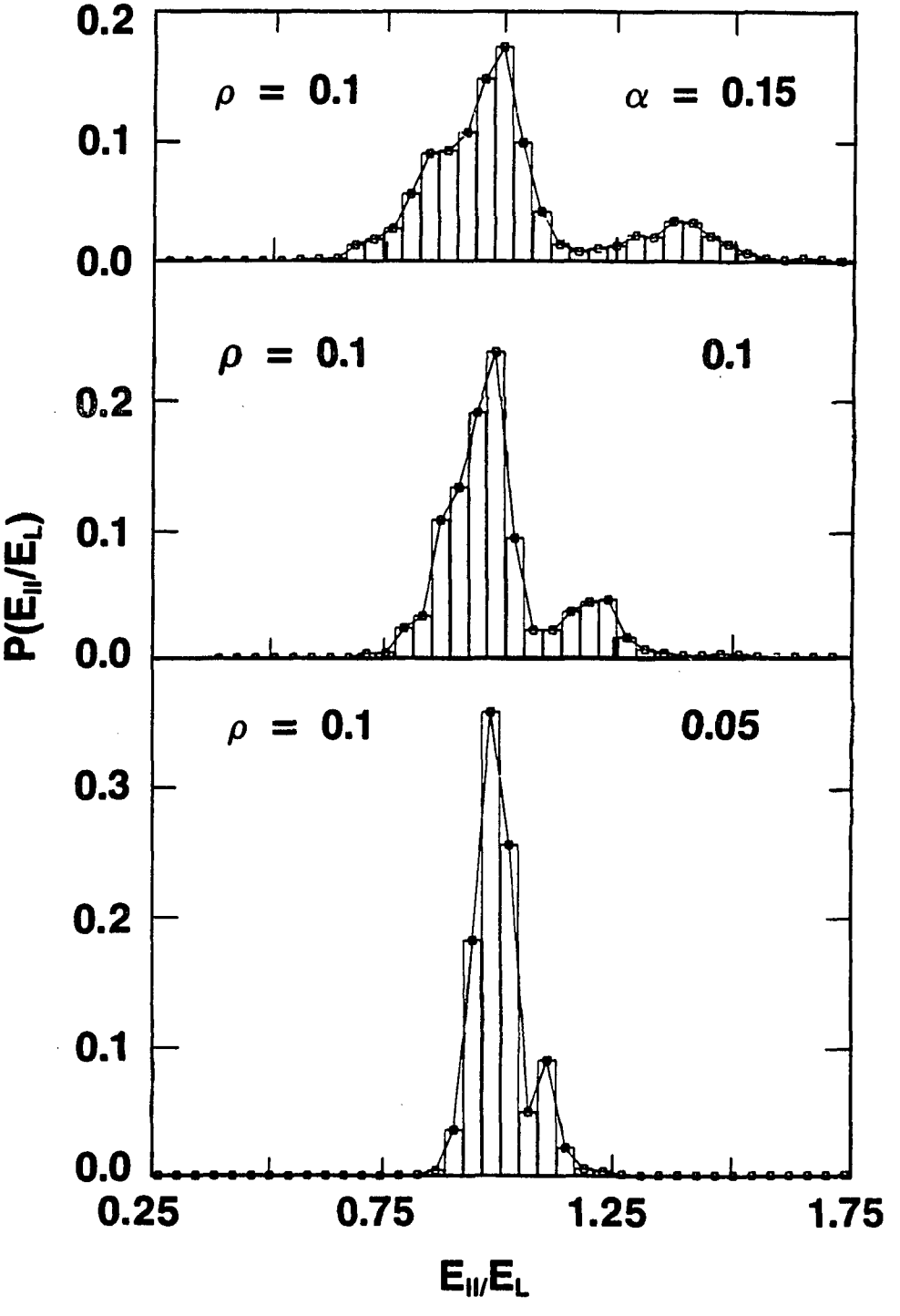
0.2
0.1
0.0
ρ = 0.1
α = 0.15
ρ = 0.1
0.1
0.2
0.1
0.0
ρ = 0.1
0.05
0.3
0.2
0.1
0.0
P(E_II/E_L)
0.25
0.75
1.25
1.75
E_II/E_L

order of $0.01E$. At a fixed number density, the separation between the two peaks is noted to depend on the particle polarizability. Such dependence is illustrated in Fig.2.4 for $\rho = 0.2$ uniform random medium with three different polarizabilities. As the polarizability increases, the peak separation and therefore the distribution width also increases.

The unexpected double-peak character of the local field distribution can be qualitatively understood by considering the nearest-neighbor interactions. For a typical particle (denoted as O in Fig.2.5) in the system, it has six possible nearest-neighbor sites. When an external electric field (along $\hat{z}$ direction) is applied to the system, it not only induces a dipole moment at each occupied nearest-neighbor site but also separates the six possible sites into two groups: group-I consists of two sites on the axis parallel to $\hat{z}$ through the site O, and group-II consists of four other sites in the plane perpendicular to $\hat{z}$. A dipole polarized along $+\hat{z}$ in a group-II site produces an electric field $-(1/2)\hat{z}$ at O (the polarizability, lattice constant, and the applied field strength are assumed to be 1 for convenience), which is different from the value $1\hat{z}$ for a dipole in a group-I site. The double-peak character in the distribution of local field values is therefore seen to be associated with the existence of two types of local environments relative to the applid field direction. For instance, a local configuration with only the sites in the group-I sites occupied will result in an electric field at O larger than the averaged, whereas in the case where nearest-neighbor configurations consist of occupied sites only in the perpendicular plane, the local field value will be less than the averaged. In general, nearest-neighbor configurations consist of occupied sites from both groups. The probability of occurance of the nearest-neighbor configurations and their associated local field values at O can be enumerated exactly. Suppose the occupation probability of each site is p, then the probability to have n sites ($n \leq 2$)

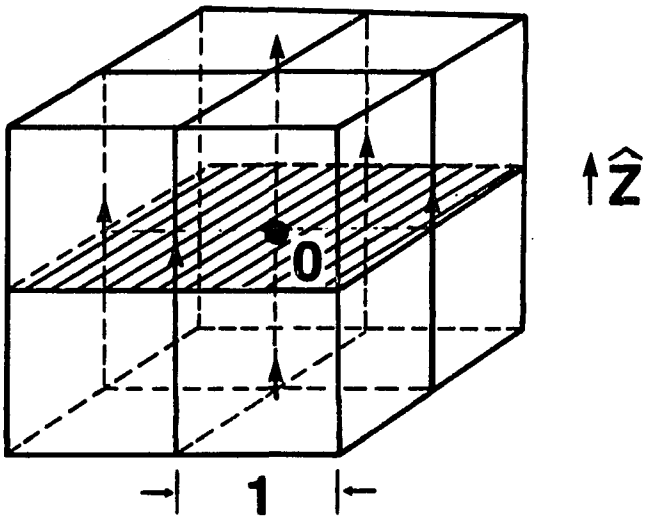

Figure 2.5 Illustration of a occupied site with its nearest-neighbores on a simple cubic lattice.

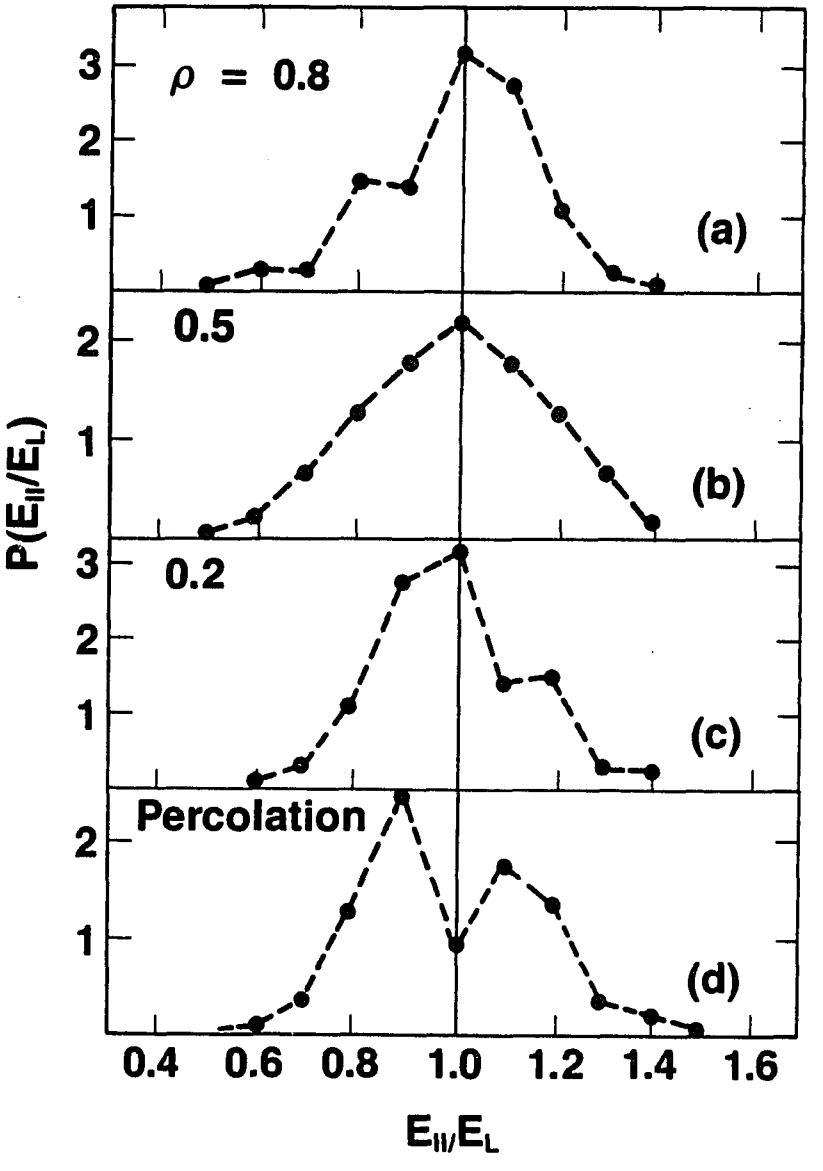

Figure 2.6 Probabilistic distribution of local fields calculated within the nearest-neighbor approximation. Good qualitative agreement with Fig.2.3 is clearly seen.

in group-I and m sites ($m \leq 4$) in group-II occupied is $p^{n+m}(1-p)^{6-n-m}$. The total number of the configurations with n dipoles in group-I and m dipoles in group-II is $C_2^n C_4^m$, where $C_\ell^k = \ell!/(\ell-k)!$. Since each configuration (n, m) produces the local field $E = (n - m/2)$ at O, the probability to have this field value at O is given by

$$P(E) = C_2^n C_4^m p^{n+m}(1-p)^{6-(n+m)}. \tag{2.43}$$

Here E denotes the deviation from the mean local-field value.

In Fig.2.6 we show a plot of $P(E)$ given by Eq.(2.43) for three occupation probabilities corresponding to those shown in Fig.2.4. There is a clear qualitative correspondence with the calculated double-peak distributions. In the $p = 0.5$ case the single peak is indeed seen to be the merging of the two peaks.

While the nearest-neighbor approximation is not sufficient to describe the percolative structures, a crude estimation can be made by subtracting from Eq.(2.43) the term corresponding to the configuration that all nearest-neighbor sites are empty since in percolative structures all particles are connected to their neighbors. Figure.2.6d does indicate the pronounced double peak character and the accompanying increase in the distribution width as observed in Fig.2.4d. Since the local field value $E = n - m/2$ depends linearly on α, Eq.(2.43) also predicts that the separation between the two peaks depends linearly on the polarizability. Our calculated results show that whereas at $\alpha < 0.1$ (in unit of lattice constant cubed) the peak separation is indeed linear in α, for $\alpha > 0.1$ the separation increases faster than linear. The discrepancy arises from the non-linear many-body electromagnetic interaction that tends to increase the effective polarizability. This will be discussed in Section 2.6.

2.6. THE SECOND MOMENT OF THE DISTRIBUTION

Discussion of last section suggests that the distribution width is sensitive to the microstructure of the system as well as to the particle polarizability. To quantify such relationships, we first define a quantity that measures the degree of local anisotropy of a random medium. For a random medium, we notice that the deviation from the Lorentz local-field value can be attributed to the field of dipoles inside the Lorentz cavity. A first order estimate for the magnitude of the deviation may therefore be obtained from the parameter

$$\eta = < | \sum_{j \neq i} \vec{D}(\vec{r}_i, \vec{r}_j) |^2 >^{1/2}, \tag{2.44}$$

where the dipole field $\vec{D}$ at i is calculated by assuming that the dipole at every occupied sites is given by a unit vector $\hat{z}^*$ and the summation is over all occupied sites $\vec{r}_j$ in a sufficiently large spherical cavity (so that the values of η converges) centered at an arbitrary site r_i. From symmetry, we know that η is zero for a cubic or spherical environment as assumed in the Lorentz formula, and $\eta \neq 0$ in general for random systems. Therefore η may be regarded as a geometric parameter that measures the local anisotropy in the dipolar sense. In Fig.2.7, the η parameter is plotted as a function of number density ρ for both the uniform and percolative random systems. At large densities, difference between the two random systems is small, and η exhibits the same behavior for both. As ρ decreases, the requirement for the particles to be connected makes the local structure of the percolative system much more anisotropic than the uniform case. This increased local anisotropy is reflected in the increased value of η.

In Fig.2.8, the normalized standard deviation of the distribution, $\sigma = < (E_{\|} / < E_L >)^2 - 1 >^{1/2}$, is plotted versus the η parameter for different samples.

* Note while this assumption is inconsistent with the actual situation, but the η parameter can nevertheless be attributed a geometric meaning.

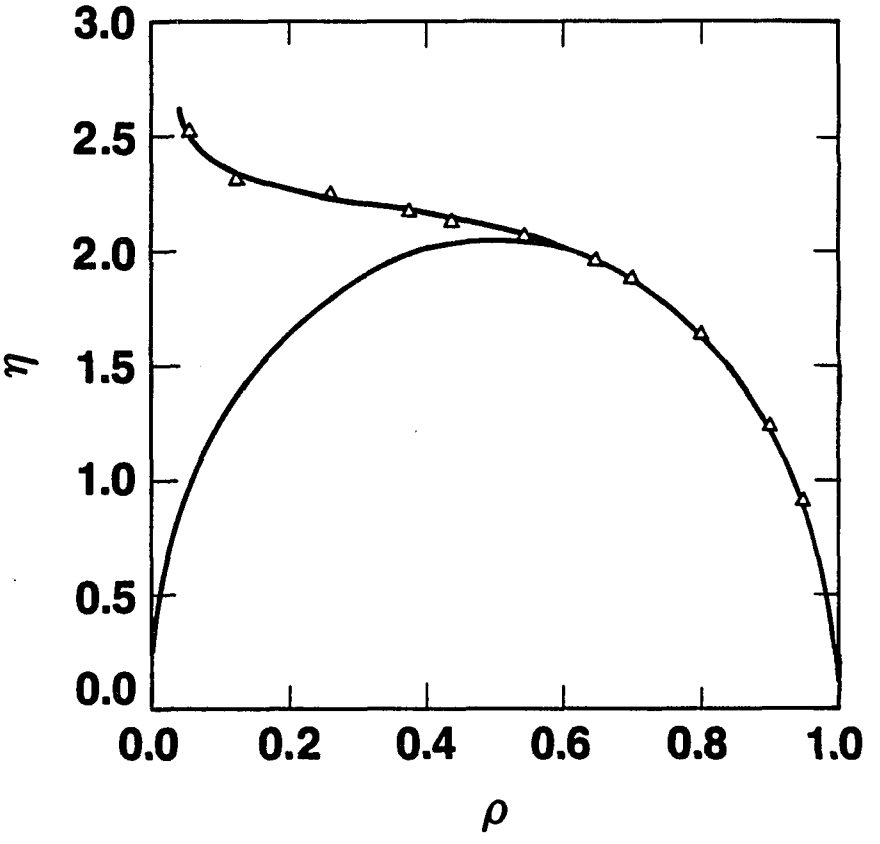

Figure 2.7 Density dependence of the local anisotropic parameter η for both the uniform and the percolative random media. The difference in the degree of local anisotropy between these two kind of systems is demonstrated by the η parameter in the low density region.

Figure 2.8 Standard deviation of the local-field distribution for three different polarizabilities plotted as a function of η defined in the text. Solid triangles denote the results for percolative structures where each point is the average over 3000-6000 particles; all other data points are for uniform random systems with each point averaged over 1500-3000 particles. The solid lines are the least-square fit to the equation $\sigma = a + b\eta$.

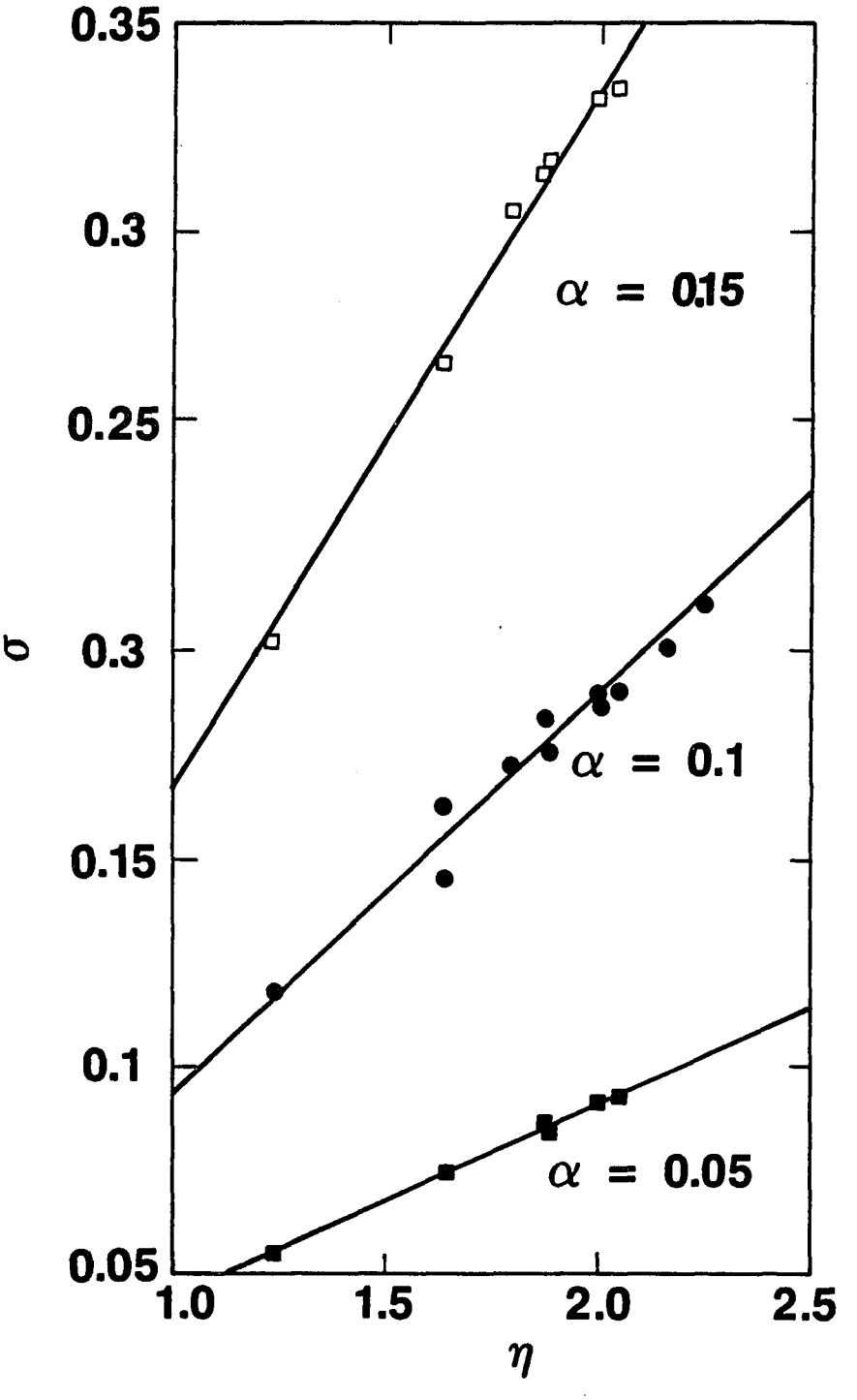
0.35
0.3
0.25
0.3
0.15
0.1
0.05
σ
α = 0.15
α = 0.1
α = 0.05
1.0
1.5
2.0
2.5
η

Three different polarizabilities, $\alpha = 0.05, 0.1, 0.15$, are used in the calculation so that the α dependence can be explored. In each case, a least-square fit by the equation $\sigma = a + b(\alpha)\eta$ yeilds an excellent linear relation between the σ and the η:

$$\sigma = b(\alpha)\eta, \tag{2.45}$$

with $a \sim 10^{-2} - 10^{-3}$, i.e. the intercept is close to 0. The coefficients $b(\alpha)$ are found to be 0.909α, 0.94α and 1.12α for α =0.05, 0.1, and 0.15, respectively. Unlike the predicted linear dependence by the nearest-neighbor analysis, $b(\alpha)$ is seen to have slight non-linear dependence on α. This nonlinearity is a result of the many-body interaction that tends to enhance the polarizability α of each particle. Equation (2.45) therefore states that distribution width as measured by the standard deviation of the local field is directly proportational to the procduct of the polarizability, the η parameter that measures the degree of local anisotropy of the random structure, and an enhencement factor for α resulting from many-body interactions.

2.7. THE FIRST MOMENT OF THE DISTRIBUTION

In this section, we examine the behavior of the mean of the local field distribution and its relation to the macroscopic dielectric properties of random media.

The relation between the dielectric constant ϵ and the mean of the local field $< E_L >$ is expressed by Eq.(2.42). For comparison, let us express $< E_L >= E_{\text{Lorentz}} + (< E_L > - E_{\text{Lorentz}}) = E_{\text{Lorentz}} + \triangle E$. Equation (2.42) can be rewritten as

$$\begin{aligned} \frac{\epsilon - 1}{4\pi} &= \rho\alpha[E_{\text{Lorentz}} + \triangle E] \\ &= \rho\alpha E_{\text{Lorentz}}[1 + \frac{\triangle E}{E_{\text{Lorentz}}}]. \end{aligned} \tag{2.46}$$

By defining $E_{\text{Lorentz}} = (\epsilon + 2)/3$ in units of the average macroscopic field and substituting it into Eq.(2.46), an equation for the dielectric constant ϵ is obtained:

$$\frac{\epsilon - 1}{\epsilon + 2} = \frac{4\pi}{3}\rho\alpha(1 + S), \tag{2.47}$$

where $S = \triangle E/E_{\text{Lorentz}}$ is the correction factor to the CM relation. For a fully occupied simple cubic lattice, $S = 0$, and the CM relation is rigorously valid.

Before we show the results of S for random systems, we note that Eq.(2.47) is indeed in the form of Kirkwood-Yvon (KY) theory derived by using formal statistical mechanics. In the KY theory S is expressed in terms of the integrals over the many-body correlation functions:

$$S = \alpha^2\Big[8\pi\rho\int g_2(r)r^{-4}dr + 2\rho^2\int[g_3(r,s) - g_2(r)g_2(s)]r^{-3}s^{-3}P_2(\cos\theta)d^3rd^3s\Big] + O(\alpha^3), \tag{2.48}$$

where g_2 and g_3 are pair and three-body correlation functions, $P_2(\cos\theta)$ is the second order Legendre polyernomials, and θ is the angle between r and s. Even in its leading order correction, one already encounters the three-body correlation functions. The simplifying superposition approximation[19] used to express g_3 as products of g_2's will be seen to severly limit the accuracy in the evaluation of S. We wish to show that, to order α^2, the correction $S^{(2)}$ is directly related to the η parameter as defined in Section 2.6. To see this connection[20], we take the origin of r and s in Eq.(2.48) to be at the center of a spherical sample. The integral of the $g_2(r)g_2(s)$ term then makes no contribution to $S^{(2)}$ and the second integral in Eq.(2.48) can be written as

$$\alpha^2 < \hat{z}\cdot\sum_{j\neq k}\overleftrightarrow{T}_{ij}\cdot\overleftrightarrow{T}_{ik}\cdot\hat{z} >, \tag{2.49}$$

where $\overleftrightarrow{T}_{ij}$ is the dipolar tensor defined in Eq.(2.15) and $\hat{z}$ is the unit vector of the applied electric field. The first integral in Eq.(2.48) can also be written in terms of the dipolar tensor as

$$\alpha^2 < \hat{z} \cdot \sum_j \overleftrightarrow{T}_{ij} \cdot \overleftrightarrow{T}_{ij} \cdot \hat{z} > . \tag{2.50}$$

By adding (2.49) to (2.50), we have

$$S^{(2)} = \alpha^2 < \hat{z} \cdot (\sum_j \overleftrightarrow{T}_{ij}) \cdot (\sum_k \overleftrightarrow{T}_{ik}) \cdot \hat{z} >= \alpha^2 \eta^2 \geq 0. \tag{2.51}$$

Therefore $S^{(2)}$ can be obtained by the result of direct Monte Carlo calculation of η presented in Section 2.6, thus avoiding the calculation of correlation functions. (Alder et. al.[21] had performed such a calculation at only one density $\rho = 0.884$).

Since our calculations are carried out on a lattice, comparison of our results with those in the literatures requires the removal of the lattice effect. To this end, one defines[7] a constant $\beta^2 = (2\pi/3)B\alpha^2$, where

$$B = \int e^{-\phi_{ij}/kT} r_{ij}^{-4} dr_{ij}. \tag{2.52}$$

In Eq.(2.52), ϕ_{ij} is the interaction potential between particles i and j, k is Boltzmann constant and T denotes temperature. For a system of hard spheres, $\phi_{ij} = 0$ for $r_{ij} > r_0$ and $\phi_{ij} = \infty$ for $r_{ij} \leq r_0$, where r_0 is the radius of a sphere. By substituting this ϕ_{ij} into Eq.(2.52) and carrying out the integration yields $B = 8\pi/3$ for the system of hard spheres. The same integration is also performed for point particles on the simple cubic lattice. In this case, the integration is replaced by summation,

$$B =< \sum_j \hat{z} \cdot \overleftrightarrow{T}_{ij} \cdot \overleftrightarrow{T}_{ji} \cdot \hat{z} >, \tag{2.53}$$

which yields $B = 16.8$, about twice of the value calculated for the hard sphere system. Division of S by β^2 removes the leading-order dependence on α and the underlying lattice and makes possible direct comparison with the KY theory.

In Fig.2.9 the Monte Carlo results of $S^{(2)}/\beta^2$ for both the uniform and the percolative random systems are plotted as a function of ρ in solid lines. Values of S/β^2, calculated from the local field distribution with three different polarizabilities, are plotted in symbols. Kirkwood's analytic result for a system of low-density hard spheres is also plotted (dots dashed line) for comparison. The good agreement of $S^{(2)}$ with the calculated values of S demonstrates that $S^{(2)}$ is the major fraction of S[8]. Several points should be noted from Fig.2.9. First, in all our calculations $S \geq 0$. This is consistent with the KY results since the $S^{(2)}$ given by Eq.(2.51) is non-negative. In a different context, Hellwarth[22] has also shown that the ϵ calculated from the CM relation is in fact a lower bound for the dielectric constant, which implies $S \geq 0$. A curious implication of the fact $< E_L > \geq E_{\text{Lorentz}}$ is that if an initially simple cubic material is randomized, then the net absorption of the material would increase because the mean of the local fields does not average to the same value as before but would always increase. Furthermore, for two materials with the same density, the material with more string-like structures (such as a fractal aggregate) would yield bigger absorption since the $S^{(2)} \propto \eta^2$, and η is a measure of local anisotropy. It follows that the S of a percolative random system is always larger or equals to that of the uniform random system at any fixed density. Second, for the kirkwood's analytic solution of $S^{(2)}$, the agreement with our numerical calculation is indeed excellent at low densities for uniform random systems. At high densities and for percolative random structures, the Kirkwood solution differs significantly from both the calculated S and the Monte Carlo results of $S^{(2)}$, since the analytic solution utilizing the superposition approximation. We therefore conclude that in percolative random structures the superposition approximation is not accurate even at low densities.

The effect of extended spatial correlation in a random system is clearly visible

Figure 2.9 Correction to the Clausius-Mossotti relation plotted as a function of the particle number density. Symbols (except the open squares) represent the results obtained using the generalized Onsager approach with the same statistics as that for Fig.2.8. Solid triangles are for percolative random structures. Solid lines denote the fit to Monte Carlo results of $S^{(2)}$ from the KY theory where each point is the average of 30,000-100,000 particles. In the simulation of percolative random structures (open squares), the correlation length, in descending order, are (in unit of lattice constant): 176, 23, 6.4, 3.4, 2.3, 1.5, and 1.1. Solid dots connected by solid line represent the analytic result of Kirkwood.

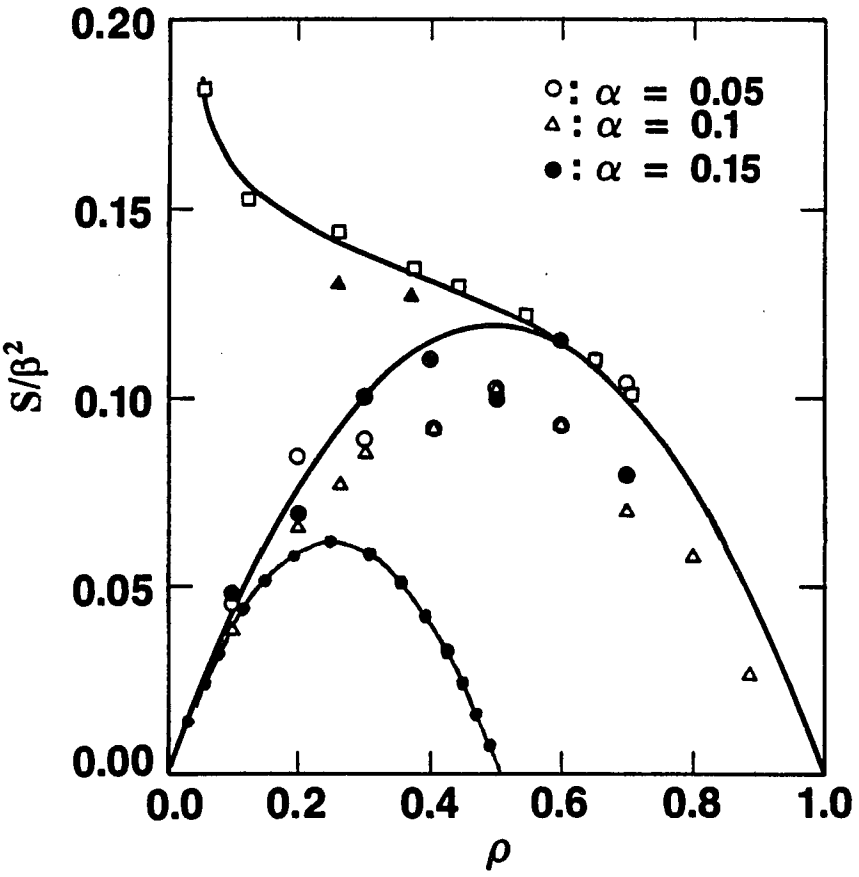
0.20
0.15
0.10
0.05
0.00
S/β²
○: α = 0.05
△: α = 0.1
●: α = 0.15
0.0
0.2
0.4
0.6
0.8
1.0
ρ

through the behavior of the correction factor as a function of density. Whereas the uniform random medium has the maximum CM correction at $\rho = 0.5$, the percolative structure with extended structural correlations shows monotonic increase in the value of S as the correlation length increases. A finite limiting value of S is predicted for $\rho = 0$ (and $\xi \to \infty$), which would be that of a percolation cluster. A upper bound of this limiting value is calculated from a straight infinite chain of dipoles, which yields $S^{(2)}_{max}/\beta^2 \leq 0.35$. Since this increase in S at low densities arises from increased local anisotropy, we expect the local field distribution for aggregates or growth structures to have large variance. The Lorentz local-field value would be therefore a poor approximation in these systems. Through the relations $S \simeq S^{(2)} = \alpha^2\eta^2$ and $\sigma \propto \alpha\eta$, we also conclude that $S \propto \sigma$. That is, if the width of the distribution is zero, then $< E_L >$ must be equal to E_{Lorentz}. As $< E_L >$ increases away from E_{Lorentz}, the distribution width increase correspondly. We have systematically checked the α dependence of S and found it not strictly quadratic at large α values. This is consistent with the earlier observation about the distribution width dependence of α.

2.8. EFFECTS OF UNDERLYING LATTICE AND FINITE PARTICLE SIZE

Since our random systems are generated on simple cubic lattice, one may first ask whether our results would be affected by the orientation of the applied $\vec{E}$ field relative to the lattice. For simple cubic lattice, it is easy to see that the orientation should have no effect because we can always decompose the applied field into components that are parallel to the lattice axes. Since the problem is linear for the electric field, we can apply the superposition principle. The equivalence of the three lattice axis directions implies that the resultant statistical properties to

be indentical to what we have obtained. But suppose now we consider a different lattice, how much the distribution characteristics will be affected by the underlying lattice? To answer this question, we first note that the applied field direction constitute a special direction for each local configuration in a random structure. In relation to this special direction, there can be two types of local environments for a given particle. One type of local environment has more particles near the axis passing through the particle along the applied field direction than near the plane perpendicular to the field direction. These local configurations produce local field values above the mean. The other type of the local environment has more particles near the plane perpendicular to the field direction, which yields values less than the mean. Unless the local environment is perfectly spherical or cubic, the distribution of the local field values will always be different from the δ-function. We therefore expect that double-peak character to be generic to random dielectrics. However, since the separation (or width σ) between two peaks depends on α, the two peaks may not always be visible at low α-values. In Fig.2.10, we plotted the local-field distributions calculated for random systems with $\rho = 0.2$ generated on BCC lattice. Two different polarizabilities are used. While the distribution for $\alpha = 0.1$ shows almost a single peak, the two peaks becomes visibly separated when α is increased to 0.15.

The local field distributions shown in Sections 2.5, 2.6, and 2.7 are all calculated with point dipoles. While the assumption of point dipole is often a good approximation at the microscopic level and for macroscopic particles which are widely separated, effect of finite particle size could become important as the particle separation decrease so that high-order multipole interactions become comparable to the dipolar interaction. Since a straightforward inclusion of the multipole-interaction effect may pose formidable calculatioal difficulties, we suggest that

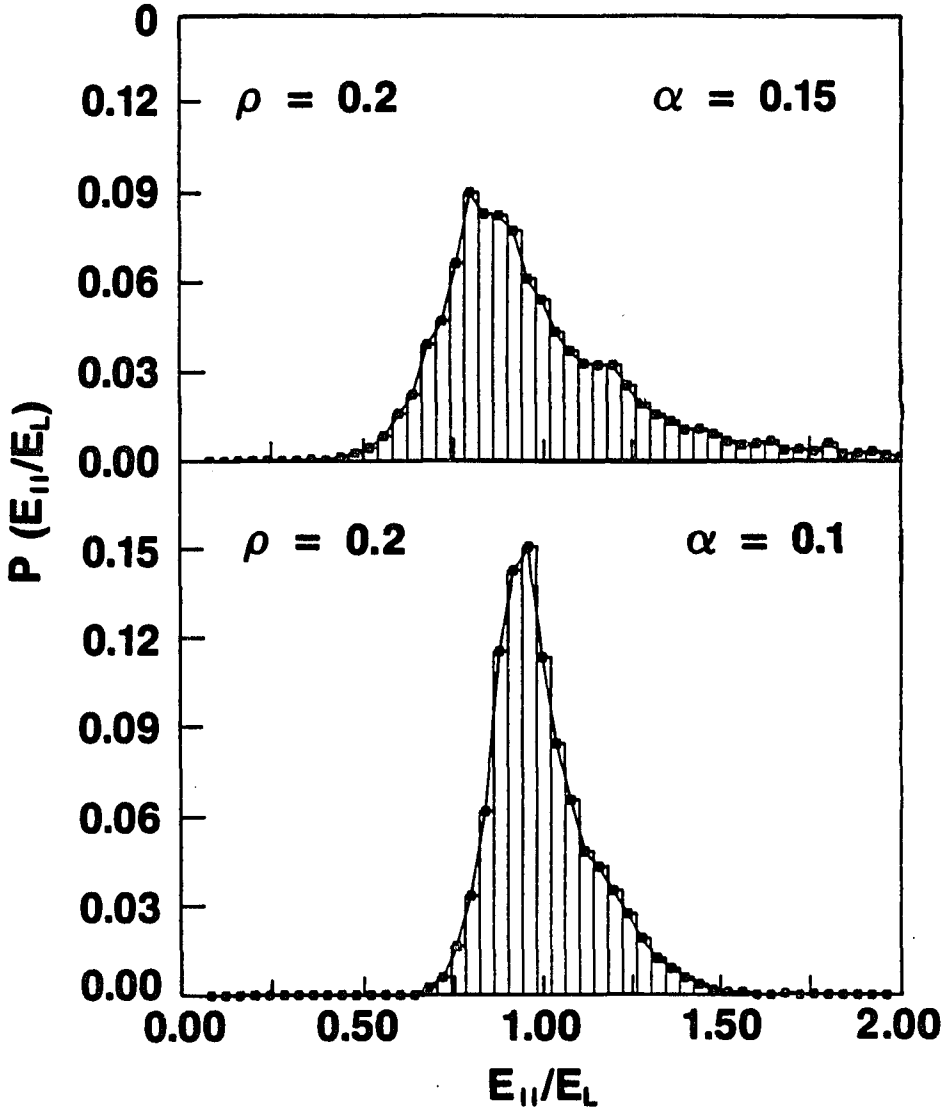

Figure 2.10 Local-field distributions for an uniform random medium, generated on BCC lattice, plotted as a function of $E\|/E_L$. Figure (a) is obtained with the particle polarizability $\alpha = 0.15$. In Figure (b), $\alpha = 0.1$. As α increases, the two peak character of the distribution starts to emerge.

the problem may be made tractable by dividing it into two steps. Since multipole interaction is short-ranged as compared to the dipole interaction, one may regard the short-range high-order multipole interaction as having the net effect of renormalizing the vacuum polarizability of a particle to a new value that is more appropriate for its local environment. The resultant α could be a tensoral quantity. An approximate solution to the local-field problem for finite-sized particles may now be obtained by treating the particles again as point-like particles but with the renormalized polarizability.

2.9 CORRECTION TO EFFECTIVE MEDIUM THEORIES

In Section III, we have seen that fluctuations of local fields in random systems, as characterized by their distribution function, are very sensitive to the microstructure of the system. For a percolative random medium the Lorentz local field and its prediction on the dielectric constant are by no means accurate. Since a random system in general possesses correlated structure at scale less than ξ, the effective-medium theories widely used to predict the dielectric behaviors may have to be modified to incorporate such statistical effect of microstructure.

For illustration, let us take the widely used Maxwell-Garnett theory as an example. The Maxwell-Garnett formula can be derived in many equivalent ways with the assumption of a homogeneous local environment. The traditional derivation is to substitute the electrostatic polarizability $\alpha = r_0^3(\epsilon_m - 1)/(\epsilon_m + 2)$ for a spherical particle, where ϵ_m is the dielectric constant of the particle and r_0 its radius, into the CM relation. This yields the Maxwell-Garnett formula

$$\frac{\epsilon - 1}{\epsilon + 2} = f\frac{\epsilon_m - 1}{\epsilon_m + 2}, \tag{2.54}$$

where $f = (4\pi/3)\rho r_0^3$ is the volume fraction of the particle inclusion. Equation (2.54) has been used as the basic equation for the description of optical properties

of composite. The assumption of homogeneous local environment in the CM relation obviously neglects the microstructure and the local field fluctuations in a random system.

These effects can now be included by using our equation (2.47). By using the same electrostatic polarizability of the particle inclusion, Eq.(2.47) can be written as

$$\frac{\epsilon - 1}{\epsilon + 2} = f(1 + S(f, \alpha, \xi))\frac{\epsilon_m - 1}{\epsilon_m + 2}. \tag{2.55}$$

We thus get an extension of the Maxwell-Garnett formula which can be served as the effective medium theory for aggregated or fractal structures.

2.10 CONCLUDING REMARKS

We have presented a direct extension of the Lorentz theory of local field to random dielectrics. Quantitative relationships between the local-field distribution characteristics and the geometric and dielectric properties of a random system are obtained. It would be very interesting to see an analytic theory for the distribution functions. Such a theory would necessarily have to incorporate the effects of the microstructure as seen from our results. Also, we would like to note that the predicted correlation between S and σ is experimentally verifiable, for example, by comparing the broadening of spectral lines in a gas due to the Stark effect with the deviation of the dielectric constant from the CM value[23].

While our results are obtained for non-polar systems, the formulation may be further developed to treat polar systems. In this case, however, numerical calculation needs to have an efficient Monte Carlo algorithm to handle the thermodynamics. A set of new phenomena, such as a spin-glass-like state, is anticipated. Investigations in this direction is currently underway.

REFERENCES

1. see for example, C. Kittel, *Introduction for Solid State Physics*, 5th edition (Wiley & Sons, New York, 1976), p. 399.

2. H. A. Lorentz, *The Theory of Electrons* (B. G. Teubner, Leipzig, 1909; Reprint: Dover, New York, 1952).

3. see R. Landauer, in *Electrical Transport and Optical Properties of Inhomogeneous Media*, edited by J. C. Garland and D. B. Tanner, AIP Conference Preceeding No. 40 (American Institute of Physics, New York, 1978), P.2.

4. J. G. Kirkwood, *J. Chem. Phys.* **4**, 592 (1936).

5. J. Yvon, *Recherches sur la théorie cinétique des liquides II* (Hermann, Paris, 1937).

6. W. F. Brown Jr., *J. Chem. Phys.* **23**, 154 (1955).

7. J. de Boer, F. ran der Maesen, and C. A. tan Seldam, *Physica* **19**, 265 (1955).

8. U. Geigenmüuer and P. Mazar, *Physica* **136A**, 316 (1986).

9. P. Debye, *Polar molecules* (The Chemical Catalog Company, Inc., New York, 1929), P.27.

10. H. Frõlich, *Theory of Dielectrics*, 2nd edition (Oxford University Press, 1958).

11. Van Vleck, *J. Chem. Phys.* **5**, 320 (1937); **5**, 556 (1937).

12. L. Onsager, *J. Am. Chem. Soc.* **58**, 1486 (1936).

13. P. Sheng and Z. Chen, *Phys. Rev. Lett.* **60**, 227 (1988).

14. R. Zallen, *The Physics of Amorphous Solids* (Wiley, New York, 1983).

15. see, for example, P. Sheng, in *Homogenization and Effective Moduli of Materials and Media*, edited by J. L. Ericksen, The IMA volumes in mathematics and its applications, vol. 1 (Springer-Verlag, New York, 1986).

16. J. D. Jackson, *Classical Electrodynamics*, 2nd edition (Wiley & Sons, New York, 1975).

17. D. Stauffer, *Introduction to Percolation Theory* (Taylor and Francis, London, 1985).

18. B. B. Mandelbrot, *The Fractal Geometry of Nature* (Freeman, San Francisico, 1982).

19. J. G. Kirkwood, *J. Chem. Phys.* , 5, 300 (1935); J. G. Kirkwood and E. M. Boggs, *ibid*, **10**, 392 (1942).

20. G. Stell and G. S. Rushbrooke, *Chem. Phys. Lett.* **24**, 531 (1974).

21. B. L. Alder, J. -J. Weis and H. L. Strauss, *Phys. Rev.* **A7**, 281 (1973).

22. R. W. Hellwarth, *Phys. Rev.* **152**, 152 (1966).

23. We wish to thank the referee of our Phys. Rev. Lett. (Ref.13) for this idea.

CHAPTER 3

OPTICS OF RANDOM FRACTAL CLUSTERS: EFFECTS OF MULTIPLE SCATTERING

ABSTRACT

The use of light scattering as a structure probe is generally justified on the basis of single scattering assumption. For systems whose constituents are strong scatterers, this naturally raises a fundamental question: Will the multiple scattering mask the structural information contained in the scattered light intensity? In this Chapter, we calculate the scattering fields by using Ewald's method and show that the effects of multiple scattering are separable into two parts: a mean-field part related to the index of refraction and a local-field fluctuation part, characterized by the spatial correlation function of the fluctuating local fields, which would give a wave-vector dependent correction to the single scattering result. The mean-field effect is found to be always negligible for clusters with fractal dimension d_f less than two and becomes important for $d_f > 2$ when the number of particles in the cluster exceeds $(ka)^{-d_f/(d_f-2)}$, where a is the particle size and k is the incident wave-vector. Contrary to intiuitive expections, analysis of local field fluctuations shows that multiple scattering dose not mask the q dependence of the scattering for $q \leq a^{-1}$, even when $d_f > 2$ so that the cluster is geometrically opaque.

3.1. INTRODUCTION

An understanding of the optical properties of particulate aggregates is of great importance in many diverse areas of science and technology. Examples of current interest include the absorption and scattering of light by interplanetary and interstellar dust[1,2], the optical effects of air and water pollution, radiative transport of energy in fires[3], the nuclear-winter scenario[4], and industrial processes[5,6]. Of essential importance in determining the optical properties of such aggregates is a detailed knowledge of their structure. Considerable progress has been achieved recently, with the realization that aggregates often possess scale-invariant structures[7,8]. Indeed, light scattering has been widely used to determine the fractal dimension, d_f, of aggregates[9,10,11], since the structure factor $S(q) \sim q^{-d_f}$ in the Born approximation, where q is the scattering vector. However, light may be multiply scattered in aggregates and this multiple scattering process will inevitably invalidates the single scattering assumption made in the Born approximation. This raises a fundamental question: Will the multiple scattering mask the structural information contained in the scattering intensity? On the other hand, the finite size of the particles and the connected nature of the aggregate structures naturally raise the importance of high-mutiple interactions. This short-ranged correlation poses an additional challenge to the study of the optical properties of aggregates. In this Chapter, we will focus our attention on the structural implications of multiple scattering. The effects that arising from the short-range correlation of the aggregates, such as absorption and depolarized scattering, will be the subject of the following Chapter.

Multiple scattering of light has been an subject of much study. Its effect on the fractal correlation, however, is only addressed recently by Berry and Percival[4] for dielectric clusters, and by Chen *et al.* [12] for metallic aggregates. Using a mean-

field approximation, Berry *et al.* estimated the importance of multiple scattering in different coagulation stage of a fractal cluster. While they found some interesting correlations between the importance of multiple scattering and the fractal dimension and cluster-size, the effects of multiple scattering on the structural determination can not be answered within the mean-field approximation. In Ref.(12), we examined this effect by using the computer-generated fractal clusters. The q-dependence of multiple scattering was analyzed in terms of the spatial correlation function of local fields. It is found that multiple scattering does not affect the q-dependence of the scattering intensity.

In this Chapter, we present an general multiple scattering formulation, based on Ewald's self-consistent field method[13], for the scattering fields. We show that the effects of multiple scattering are separable into two parts: a mean-field part that affects only the magnitude of the scattering intensity and a local-field fluctuation part which contains a q-dependent correction to the static structure factor. The mean-field effect is shown to be related to the results of Berry *et al.* , and is found that it is always negligible when the fractal dimension $d_f < 2$ and $ka \ll 1$, where k is the incident wave-vector and a is the particle size. When $d_f > 2$, it does become important as the aggregation process preceeds to the stage that the number of particles in the aggregate is about $(ka)^{-d_f/(d_f-2)}$. The local-field fluctuation effect is characterized by the spatial correlation of the fluctuating part of local fields, which is shown to be both short-ranged and small in magnitude. Therefore the q dependence of the scattering intensity is not altered by multiple scattering in general. Within this formulation, the effect of collective excitation that usually present in the metallic aggregates is also explored. It is found that the q-dependence of the scattering in $q > \ell_0^{-1}$, where ℓ_0 describes the spatial extent of the collective excitation mode, is affected by the collective excitation,

in agreement with experimental observations.

This Chapter is organized as follows: Section 3.2 briefly summaries the structural properties of the colloidal gold aggregates. The concept of fractal and its structural implications are introduced. In Section 3.3, the nature of the electromagnetic interactions between two neighboring gold spheres is discussed. Section 3.4 presents a multiple scattering formulation for the calculation of light scattering intensity, with the effects of multiple scattering being differentiated into a mean-field part and a local-field fluctuation part. In Section 3.5, we show that the mean-field effect resembles the results of Berry *et al.* and the relevant results are rederived. Numerical results and discussions of the local-field fluctuation effect are presented in Section 3.6. Section 3.7 summaries our main results and discusses their experimental implications.

3.2. CLUSTER STATISTICS

An electron micrograph of a typical gold colloidal aggregate is shown in Fig.3.1. The aggregate, embedded in water solution, is comprised of small gold spheres with a radius of about 75 Å. Extensive analysis[14] has shown that the tenuous, sparse structure of the aggregates exhibits fractal symmetry[15], i.e. the *average* number of particles in a spherical cavity of radius R obeys the following scaling relation:

$$N(R) = \text{constant } (\frac{R}{a})^{d_f}, \tag{3.1}$$

where the proportionality constant is on the order of unit. Unlike the case of Euclidean geometry, the scaling exponent, d_f, may be a non-integer ($\sim$ 1.8 for aggregates formed by diffusion-limited aggregation; $\sim$ 2.1 for those formed by reaction-limited aggregation). Such non-integral exponents are a common manifestation for a wide class of naturally occuring phenomena and objects, and

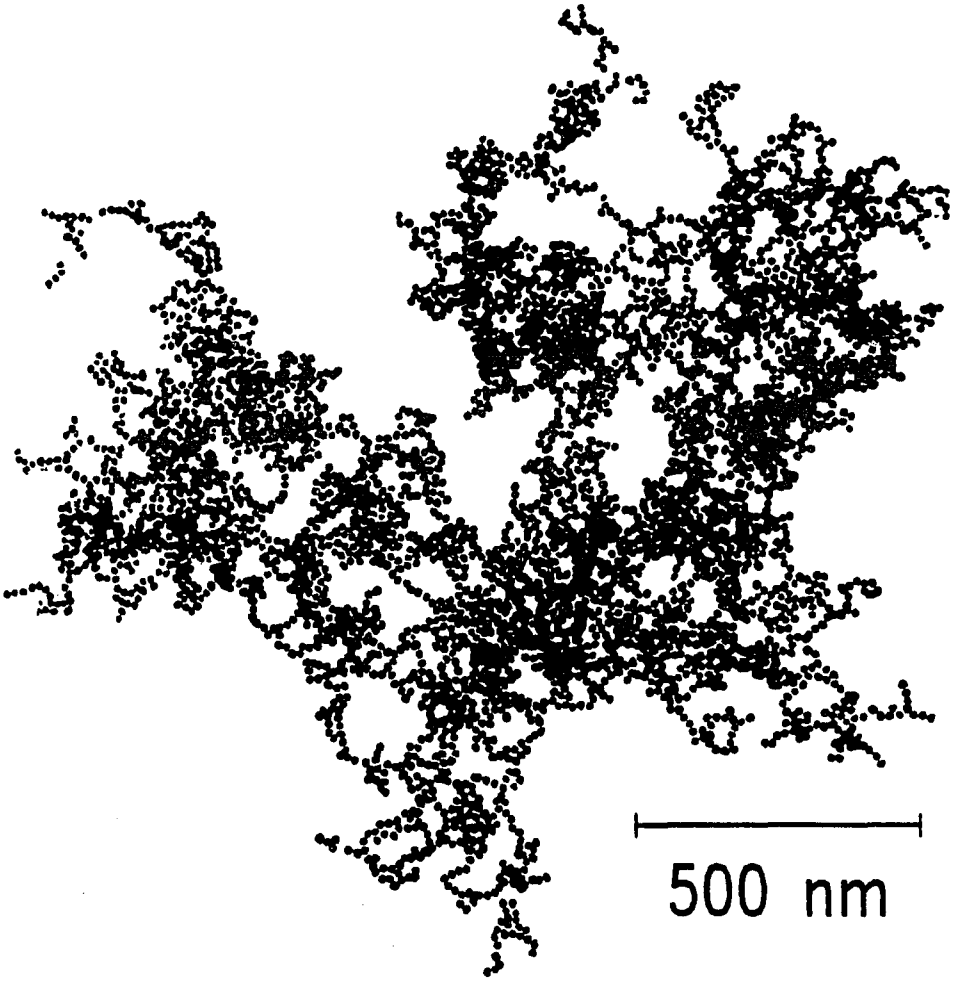

Figure 3.1 An electron micrograph of a typical gold colloidal aggregate. Each gold particle has a radius of about 75 Å. The aggregates have been shown to exhibit the fractal symmetry with a fractal dimension $d_f = 1.8$. (courtesy of D. Weitz and M. Lin).

Mandelbrot has coined the term "fractal" to denote this particular kind of dilatational symmetry. The exponent d_f, known as fractal dimension, may be viewed as characterizing the sparseness of the object's structure.

A more complete characterization of the aggregates' structure is obtained by specifying the many-body density correlation functions of an aggregate, i.e.

$$< \rho(0)\rho(r_1)\rho(r_2)\ldots\rho(r_n) >,$$

where $\rho(r_i)$ denotes the density at r_i and will be set to 1 at the center of each gold sphere and 0 elsewhere. The fractal symmetry is then reflected in the following scale transformation:

$$< \rho(0)\rho(\lambda r_1)\rho(\lambda r_2)\ldots\rho(\lambda r_n) >= \lambda^{A(n)} < \rho(0)\rho(r_1)\rho(r_2)\ldots\rho(r_n) >, \qquad (3.2)$$

which ensures that the structure is scale-invariant. The powers $A(n)$ are system-dependent constants. For the density-density (two-body) correlation function, solution of Eq.(3.2) yields

$$< \rho(0)\rho(r) >= br^{A(1)}, \qquad (3.3)$$

where $b =< \rho(0)\rho(0) >$.

The system-dependent exponent $A(1)$ is directly related to the fractal dimension d_f, since the total mass (or total particle number in our definition of $\rho(r)$) in the spherical region of radius R is

$$\begin{aligned} N(R) &= \int_0^R < \rho(0)\rho(r) > 4\pi r^2 dr \\ &= 4\pi b \int_0^r r^{A(1)+2} dr \\ &= cR^{A(1)+3}, \end{aligned} \qquad (3.4)$$

where $c = 4\pi b/(A(1)+3)$. Comparing Eq.(3.4) with Eq.(3.1) immediately yields

$$A(1) = d_f - 3, \tag{3.5}$$

It should be noted that an implicit assumption is made in Eq.(3.1) and Eq.(3.3) that the aggregates have infinite size. This, however, can never be realized in the real world. Therefore the fractal symmetry is always restricted to some size region, $a < r < R_g$, where a is the diameter of the gold sphere and R_g is a upper cut-off scale which is chosen as the radius of gyration of the aggregate cluster in our calculations. The effect of an upper cutoff on the density-density correlation function $C(r)$ can be modeled by a function f depending only on the variable r/R_g:

$$\begin{aligned} C(r) &\equiv < \rho(0)\rho(r) > \\ &= br^{d_f-d} f(r/R_g), \end{aligned} \tag{3.6}$$

where d is the Euclidean dimension. For mathematical convenience, we chose an exponential form for f,

$$f(r/R_g) = e^{-\gamma r/R_g}. \tag{3.7}$$

The constant γ is to be determined by the normalization condition

$$\int C(x)x^2 dx = 1. \tag{3.8}$$

The incorporation of finite cluster-size in the calculation is crucial in order to correctly interpret the experimental results. For in experiments one always measures the results from samples containing many clusters with varying sizes. A meaningful comparison between model calculations and experiments can only be achieved by properly taking into account the information of the cluster-size distribution of the aggregated clusters. We will come back to this point in Section 3.6.

Figure 3.2 A two dimensional projection of a fractal cluster simulated by Meakin. The cluster contains 1000 particles with a fractal dimension about 1.8. It exhibits a clear visual resemblance to Figure 3.1. (courtesy of P. Meakin).

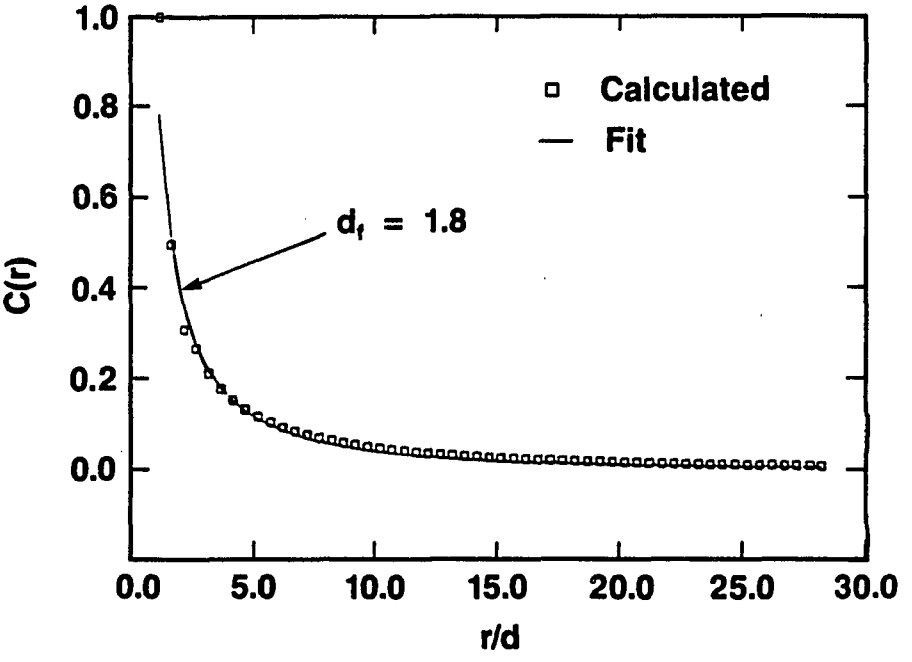

Figure 3.3 Density-density correlation function of the 1000-particle computer-generated fractal cluster. It exhibits an excellent power-law behavior. A fit to equation (3.6) in the text yields a fractal dimension 1.8.

The aggregates' structure has been simulated on computer by Meakin *et al.*[16] Figure 3.2 shows a two-dimensional projection of a typical cluster (1000 particles) simulated by diffusion-limited cluster-cluster aggregation algorithm. It closely resembles the experimental one shown in Fig.3.1. Besides the visual resemblance, it is also easy to calculate the fractal dimension, the pair correlation function, etc. from the simulated particle coordinates. Figure 3.3 shows the averaged pair correlation function for 1000-clusters. It exhibits an excellent power-law behavior. A fit of the data to Eq.(3.6) yields a fractal dimension 1.8 which agrees well with the experimental aggregates. Since the information about the three-dimensional particle coordinates is difficult to obtain experimentally for real aggregates, we will use the computer-generated fractal clusters as our calculational input.

3.3. INTERACTION BETWEEN NEIGHBORING PARTICLES

Since the gold particles in the aggregates (see Fig.3.1) are in physical contact with their nearest-neighbors, it is necessary to first assess the nature of the electromagnetic interaction among the neighboring gold particles. Between two touching metal spheres, there is an electrical resistance R of the contact and a capacitance C between the spheres. As illustrated in Fig.3.4, the total complex impedance z at frequency ω can be written as

$$\frac{1}{z} = \frac{1}{R} + j\omega C, \tag{3.9a}$$

or

$$z = \frac{R}{\sqrt{1+(\omega RC)^2}} e^{j\tan^{-1}(\omega RC)} = \begin{cases} R, & \omega RC \ll 1, \\ \frac{1}{j\omega C}, & \omega RC \gg 1, \end{cases} \tag{3.9b}$$

where $j = \sqrt{-1}$. It is clear from Eq.(3.9b) that if $\omega RC \gg 1$, z behaves like a capacitor and the two touching spheres are capacitively coupled; on the other hand, if $\omega RC \ll 1$, the spheres are resistively coupled.

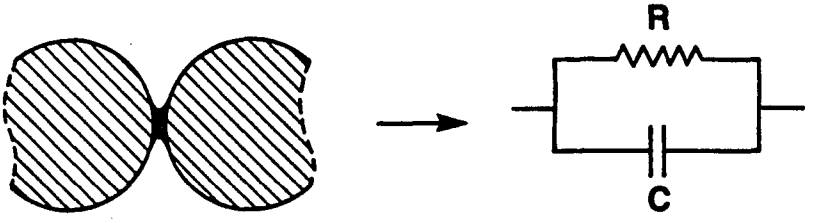

Figure 3.4 The contact between two metal spheres consists of an electric resistance R and a capacitance C. The total impedance at frequency ω, is obtained from the circuit illustrated in the plot.

For our aggregates, the width w of the contact-bond is seen from Fig.3.1 to be at most a few angstroms. Since this constriction is substantially less than the bulk mean free path ℓ of the electrons ($\sim 300\mathring{A}$ for bulk gold at room temperature), the effective resistance between the particles is expected to be increased substantially from the bulk due to the constriction at the contact. If we account for this increase by treating the contact constriction as a parallel scattering channel, then

$$\frac{\rho}{\rho_0} = \frac{\ell^{-1} + w^{-1}}{\ell^{-1}} = (1 + \ell/w), \tag{3.10}$$

where ρ_0 is the bulk resistivity. The resistance R of the contact would then be $R \sim \rho\ell/w^2$. For the capacitance, we note that the capacitance of two touching conducting spheres is $d \ln 2$, where d is the diameter of the spheres. Using $w \sim 0.03d$ ($\sim 5\mathring{A}$), we get $\omega RC \sim 10^2 \gg 1$ at optical frequencies. Therefore the coupling between the particles is predominantly capacitive in nature.

The fact that the gold particles are resistively separated affords some degree of simplification in the problem. However, since the strength of the capacitive coupling is determined by all multipole interactions between the neighboring particles, a complete calculation, comprising of all these interactions and the aggregates' structure, would still pose formidable calculational difficulties. We propose the following approximation scheme. Since the high-order multipole interactions are short-ranged compared to the dipole-dipole interaction, we may view the net high-order multipole interactions as renormalizing the polarizability of each particle. Due to the string-like local structure of the aggregates, the renormalized polarizability $\overleftrightarrow{\alpha}\ (\omega, \vec{q})$ is characterized by uniaxial symmetry with $\alpha_{zz} = \alpha_1$, $\alpha_{xx} = \alpha_{yy} = \alpha_2$, and $\alpha_{xy} = \alpha_{xz} = \alpha_{yz} = 0$ in the coordinate system where the z-axis coincides with the local chain axis. Using this $\overleftrightarrow{\alpha}$, the scattering property of an aggregate may then be calculated by treating each particle as a polarizable

point dipole. Quantitative derivation of the renormalized polarizability $\overleftrightarrow{\alpha}$ is given in the Appendix A.

3.4. MULTIPLE SCATTERING FORMULATION

To examine the multiple scattering effects, we use Ewald's self-consistent field method[13] in which the local exciting field at each particle site, including multiple scattering to all orders, is obtained exactly. Let $\vec{E}(\vec{r}_i)$ and $\vec{H}(\vec{r}_i)$ denote the local electric and magnetic field at site $\vec{r}_i$, then

$$\vec{E}(\vec{r}_i) = \vec{E}_0 + \sum_{j \neq i} \vec{E}_{ij}, \tag{3.11a}$$

$$\vec{H}(\vec{r}_i) = \vec{H}_0 + \sum_{j \neq i} \vec{H}_{ij}, \tag{3.11b}$$

where $\vec{E}_0$ ($\vec{H}_0$) is the electric (magnetic) vector of the incident wave, $\vec{E}_{ij}$ ($\vec{H}_{ij}$) is the electric (magnetic) field at site i produced by a particle at site j. For point dipoles,

$$\vec{E}_{ij} = \nabla \times \nabla \times \frac{\vec{p}(t - r_{ij}/c)}{r_{ij}}, \tag{3.12a}$$

$$\vec{H}_{ij} = \frac{1}{c} \nabla \times \frac{\frac{d}{dt}\vec{p}(t - r_{ij}/c)}{r_{ij}}, \tag{3.12b}$$

where r_{ij} denotes the distance between sites i and j, and c the speed of light. The curl operation is with respect to the position vector $\vec{r}_i$. We have omitted in Eq.(3.12) the contribution of magnetic dipoles because it is a factor of $\sim 1/c$ smaller than the electric dipole. However, the retardation effects are fully included. By substituting Eqs.(3.12) into (3.11) and using $\vec{p}_j = \overleftrightarrow{\alpha}_j \cdot \vec{E}(\vec{r}_j)$, we have

$$\vec{E}(\vec{r}_i) = \vec{E}_0 + \sum_{i \neq j} \nabla \times \nabla \times \frac{\overleftrightarrow{\alpha}_j \cdot \vec{E}(\vec{r}_j, t - r_{ij}/c)}{r_{ij}}, \tag{3.13a}$$

$$\vec{H}(\vec{r}_i) = \vec{H}_0 + \frac{1}{c}\sum_{i\neq j} \nabla \times \frac{\overleftrightarrow{\alpha}_j \cdot \frac{d}{dt}\vec{E}(\vec{r}_j, t - r_{ij}/c)}{r_{ij}}, \tag{3.13b}$$

Eqs.(3.13) completely describe the interaction between the incident light and the aggregates. In the continuum limit, it is essentially equivalent to Maxwell's equations[17].

Solution of Eq.(3.13a) determines the local electric fields. These can then be used to obtain magnetic fields from Eq.(3.13b). For an incident plane wave $\vec{E}_0 = \hat{e}_0 \exp(i\vec{k}_0 \cdot \vec{r}_i)$, where $\vec{k}_0$ is the incident wave vector, $\hat{e}_0$ is a unit vector, Eq.(3.13a) becomes

$$\vec{E}(\vec{r}_i) = \hat{e}_0 e^{i\vec{k}_0\cdot\vec{r}_i} + k_0^2 \sum_{j\neq i}^{N} \left[C^{(1)}(i,j)\vec{p}(\vec{r}_i) + C^{(2)}(i,j)[\vec{p}(\vec{r}_j)\cdot\vec{r}_{ij}]\vec{r}_{ij} \right] \frac{e^{ik_0 r_{ij}}}{r_{ij}}, \tag{3.14}$$

where

$$C^{(1)}(i,j) = 1 + \frac{i}{k_0 r_{ij}} - \frac{1}{(k_0 r_{ij})^2}, \tag{3.15a}$$

and

$$C^{(2)}(i,j) = \frac{1}{r_{ij}^2}\left[-1 - \frac{3i}{k_0 r_{ij}} + \frac{1}{(k_0 r_{ij})^2} \right]. \tag{3.15b}$$

By defining the multiple scattering coefficients $\vec{e}_j$ as

$$\vec{E}(\vec{r}_j) = \vec{e}_j e^{i\vec{k}_0\cdot\vec{r}_j}, \tag{3.16}$$

Eq.(3.14) is simplified as

$$\vec{e}_i = \hat{e}_0 + k_0^2 \sum_{j\neq i}^{N} \left[C^{(1)}(i,j)\ \overleftrightarrow{\alpha}_j \cdot \vec{e}_j + C^{(2)}(i,j)[(\overleftrightarrow{\alpha}_j \cdot \vec{e}_j)\cdot\vec{r}_{ij}]\vec{r}_{ij} \right] \frac{e^{ik_0 r_{ij} - i\vec{k}_0\cdot\vec{r}_{ij}}}{r_{ij}}, \tag{3.17}$$

where

$$i, j = 1,\ 2,\ 3,\ \ldots,\ N.$$

Eq.(3.17)* is a set of $3N$ equations whose simultaneous solution determines the amplitude of local field at each particle position. In the case of Born approximation, the multiple scattering contributions (second term of the right-hand-side) is set to zero so that $\vec{e}_i = \hat{e}_0$ for all i. For an understanding of the multiple scattering effects, we need exact solutions of Eq.(3.17).

The scattered intensity at an observation point O far away from an aggregate can be obtained by summing the contributions from all the dipoles. From Eq.(3.14), the total scattering field at O is

$$\vec{E}_s = k_0^2 \sum_{j=1}^{N} \left[C^{(1)}(O,j)\vec{p}(\vec{r}_j) + C^{(2)}(O,j)[\vec{p}(\vec{r}_j)\cdot\vec{r}_{Oj}]\vec{r}_{Oj} \right] \frac{e^{ik_0 r_{Oj}}}{r_{Oj}}. \qquad (3.18)$$

Since

$$\vec{r}_{Oj} = r - \hat{n}\cdot\vec{r}_j, \qquad \text{for} \quad r >> r_j, \qquad (3.19)$$

where r denotes the distance between the point O and the origin and $\hat{n}$ the directional unit vector of r. Taking the limit of $r \gg \max\{r_j\}$ and substituting Eq.(3.19) in Eq.(3.18) yields

$$\vec{E}_s \cong \vec{f}(\vec{k}_s, \vec{k}_0)\, \frac{e^{ikr}}{r}, \qquad (3.20)$$

where

$$\vec{f}(\vec{k}_s, \vec{k}_0) = \sum_{j=1}^{N} \left[[\vec{k}_s \times (\overleftrightarrow{\alpha}_j \cdot \vec{e}_j)] \times \vec{k}_s \right] e^{i\vec{q}\cdot\vec{r}_j}. \qquad (3.21)$$

Here $\vec{k}_s = k_0\hat{n}$ specifies the propogation direction of the scattering wave. The vector $\vec{q}$ is the scattering wave vector and equals to $\vec{k}_0 - \vec{k}_s \equiv 2k_0 \sin\frac{\theta}{2}$, where θ denotes the angle between $\vec{k}_0$ and $\vec{k}_s$.

* For isotropic polarizabilities, this equation is noted to be equivalent to the Eq.(64) of Berry *et al.* [4] who takes the unitarity-preserving weak-scattering approximation to the exact Mie theory.

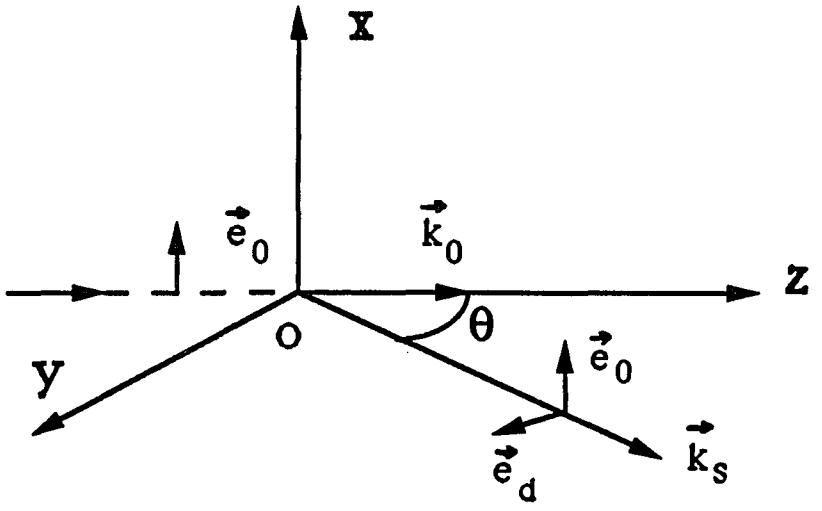

Figure 3.5 Illustration of the coordinate system used in the text. The incident wave, polarized ($\vec{e}_0$) in the x direction, propogates along the z direction. Polarized scattering arises from the scattering field component parallel to $\vec{e}_0$, and the depoalrized scattering is from the component parallel to $\vec{e}_d$.

If we define the direction of the incident light as the z-direction, the direction of the incident electric field, $\hat{e}_0$, as the x-direction, and the yoz plane as the scattering plane as illustrated in Fig.3.5, then the differential scattering cross-section for both polarized and depolarzed scatterings* is

$$(\frac{d\sigma}{d\Omega})_{1,2} = k_0^4 |\vec{e}_{0,d} \cdot \vec{f}(\vec{k}_s, \vec{k}_0)|^2$$

$$= k_0^4 |\vec{e}_{0,d} \cdot \sum_j \overleftrightarrow{\alpha}_j \cdot \vec{e}_j e^{i\vec{q}\cdot\vec{r}_j}|^2, \tag{3.22}$$

where $\vec{e}_d$ is the unit vector in the scattering plane yoz perpendicular to $\vec{k}_s$. By averaging Eq.(3.22) over cluster configurations and using the definition of delta-function yield

$$< (\frac{d\sigma}{d\Omega})_{1,2} >= k_0^4 N \int g_{1,2}(\vec{r}) e^{i\vec{q}\cdot\vec{r}} d^3r, \tag{3.23}$$

where

$$g_1(\vec{r}) = \frac{1}{N} < \sum_{i,j}^{N} \delta(\vec{r} - \vec{r}_{ij}) \tilde{p}_x(\vec{r} + \vec{r}_j) \tilde{p}_x^*(\vec{r}_j) >, \tag{3.24}$$

$$g_2(\vec{r}) = \frac{1}{N} < \sum_{i,j}^{N} \delta(\vec{r} - \vec{r}_{ij}) [\tilde{p}_y(\vec{r} + \vec{r}_j) \cos\theta - \tilde{p}_z(\vec{r} + \vec{r}_j) \sin\theta]$$

$$\times [\tilde{p}_y^*(\vec{r}_j) \cos\theta - \tilde{p}_z^*(\vec{r}_j) \sin\theta] > . \tag{3.25}$$

Here <> denotes configurational averaging, and $\tilde{p}_{x,y,z}(\vec{r}_j) = (\overleftrightarrow{\alpha}_j \cdot \vec{e}_j)_{x,y,z}$. For isotropic polarizability, $\tilde{p}$ corresponds to local field (normalized by the incident field) multiplied by the polarizability. Therefore $g_1(\vec{r})$ and $g_2(\vec{r})$ denote, in general, the spatial correlation functions of local fields.

---

* By polarized scattering we mean the scattering that arises from the component $(\hat{e}_0 \cdot \vec{E}_s)$ of the scattering fields which is parallel to the incident-field polarization direction $(\hat{e}_0)$; the depolarized scattering arises from the components polarized in the scattering plane (yoz) and perpendicular to $\vec{k}_s$.

To gain some intuitive feeling of g_1 and g_2, let us first examine the consequences of Eqs.(3.24) and (3.25) in the single scattering limit. For isotropic polarizability, it means

$$\tilde{p}_x(\vec{r}_j) = \alpha\delta(\vec{r}_j)\hat{e}_0, \quad \text{and} \quad \tilde{p}_y(\vec{r}_j) = \tilde{p}_z(\vec{r}_j) = 0. \tag{3.26}$$

Substituting Eq.(3.26) into Eqs.(2.24) and (3.25), we have

$$g_1(\vec{r}) = \frac{1}{N}\alpha^2 < \sum_{i,j}^{N} \delta(\vec{r} - \vec{r}_{ij})\rho(\vec{r} + \vec{r}_j)\rho(\vec{r}_j) > \equiv \alpha^2 C(r), \tag{3.27}$$

and $g_2 = 0$. This yields the well-known results that (1) polarized scattering gives the structure factor, Fourier transform of of density-density correlation, and (2) there is no depolarized scattering in the Born approximation, i.e. g_2 reflects purely the consequence of multiple scattering. Note, however, even in the single scattering limit there could be depolarized scattering if the polarizability is anisotropic. Also, the polarized scattering would deviate from the simple structure factor if $\overleftrightarrow{\alpha}$ is also spatial dependent.

In general, if we write the amplitude of the dipole moment $\tilde{p}_x$ as a sum of its mean value and a fluctuating part,

$$\tilde{p}_x(\vec{r}_i) = m_x + \Delta_x(\vec{r}_i), \tag{3.28}$$

where

$$< \Delta_x(\vec{r}_i) >= 0, \tag{3.29}$$

then g_1 can be seperated into two parts. Namely,

$$g_1(r) = |m_x|^2 C(r) + F_1(r), \tag{3.30}$$

with

$$F_1(r) = \frac{1}{N} < \sum_{i,j}^{N} \delta(\vec{r} - \vec{r}_{ij})\Delta_x(\vec{r} + \vec{r}_j)\Delta_x^*(\vec{r}_j) > . \tag{3.31}$$

Equation (3.30) tells us that beyond single scattering, effect of multiple scattering is a sum of two parts: a mean-field part $|m_x|^2$ and a local field fluctuation part characterized by the spatial correlation of the fluctuating part of the local fields. Since $|m_x|^2$ affects just the magnitude of the density-density correlation function, it only changes the overall scattering intensity by a constant factor. The deviation of the q-dependence of the scattering intensity from the static structure factor is accounted for by $F_1(r)$. The same procedure can also be applied to g_2. However, the general expectation that $|m_{y,z}|^2 \sim 0$ and that there is no correlation in $F_2(r)$ beyond nearest-neighbors, would immediately predict that the depolarized scattering is small and is almost independent of q. We now address the effects of $|m_x|^2$ and $F_1(r)$ in more detail.

3.5. MEAN-FIELD EFFECT

Let us first examine the mean-field aspect of the multiple scattering effects. To do this, we start with the Eq.(3.17) for the multiple scattering coefficients. The main complication for a mean-field analysis is the spatial dependent $\overleftrightarrow{\alpha}_j$ in Eq.(3.17). For simplicity, we consider the isotropic α case. In the mean-field level, this is justified on the ground that when the incident light does not excite a collective mode between the neighboring particles, $\overleftrightarrow{\alpha}$ is indeed close to being isotropic. At the collective excitation frequency, however, the neighboring particles are coupled coherently so that the approximation is expected to break down. In this case, if the coherently excited particles on a chain segment are considered as a new entity then the new system may be treated by using a renormalized isotropic polarizability appropriate to the particles in the coherent region.

For isotropic α, if we dot both sides of Eq.(3.17) by $\hat{e}_0$ and sum the result

over all particles, then

$$\sum_i^N \vec{e}_i \cdot \hat{e}_0 = N + k_0^2 \alpha \sum_i^N \sum_{j \neq i}^N \Big[C^{(1)}(i,j) \vec{e}_j \cdot \hat{e}_0 + C^{(2)}(i,j) [\vec{e}_j \cdot \vec{r}_{ij}] \vec{r}_{ij} \cdot \hat{e}_0 \Big] \frac{e^{ik_0 r_{ij} - i\vec{k}_0 \cdot \vec{r}_{ij}}}{r_{ij}}. \tag{3.32}$$

Since the mean of local field coefficients $M \equiv < \frac{1}{N} \sum_i^N \vec{e}_i \cdot \hat{e}_0 >$, we obtain from Eq.(3.32)

$$M = 1 + k_0^2 \alpha \frac{1}{N} \sum_i^N \sum_{j \neq i}^N < \Big[C^{(1)}(i,j) \vec{e}_j \cdot \hat{e}_0 + C^{(2)}(i,j) [\vec{e}_j \cdot \vec{r}_{ij}] \vec{r}_{ij} \cdot \hat{e}_0 \Big] \frac{e^{ik_0 r_{ij} - i\vec{k}_0 \cdot \vec{r}_{ij}}}{r_{ij}}. \tag{3.33}$$

Now let us introduce the mean-field approximation by setting $\vec{e}_i = M \hat{e}_0$. Then Eq.(3.33) becomes

$$M = 1 + k_0^3 \alpha M (N-1) P, \tag{3.34}$$

where

$$P \equiv < \frac{e^{ikr_{ij}}}{k_0 r_{ij}} cos \vec{k}_0 \cdot \vec{r}_{ij} \{ (C^{(1)}(i,j) + C^{(2)}(i,j)) (\hat{n}_{ij} \cdot \hat{e}_0)^2 \} > . \tag{3.35}$$

Here $\hat{n}_{ij} \equiv \vec{r}_{ij} / |\vec{r}_{ij}|$. In fact, Eqs.(3.34) and (3.35) are equvialent to the Eqs.(67) and (68) of Berry *et al.* [4].

The quantity M is related to the m_x by $m_x = \alpha M$ for the isotropic polarizability case. For anisotropic polarizability, we expect that m_x and M to have the same qualitative behavior, because the local-chain orientation in the aggregates is isotropic. Therefore the dependence of m_x on the fractal dimension and cluster-size can be explored following Ref.(4). In the rest of this section, we rederive some of the mean-field results for the colloidal aggregates.

From Eq.(3.34) we immediately obtain M as

$$M = [1 - (N-1)k_0^2 \alpha P]^{-1}. \tag{3.36}$$

By using the density-density correlation function of Eq.(3.6), P can be expressed as

$$P = \frac{1}{k_0^2 R^2} \int_0^\infty dx\, x^2 C(x) \frac{e^{iX}}{x^2} \left\{ \left[1 - \frac{2}{X^2} + \frac{3}{X^4} + \frac{i}{X}(1 - \frac{3}{X^2}) \right] \right.$$
$$\left. \times \sin X + \frac{1}{X}(1 - \frac{3}{X^2} + \frac{3i}{X}) \cos X \right\}, \tag{3.37}$$

where $X = k_0 R x$, and $R = (N/a)^{1/D}$ is the linear size of the cluster. The dependence on the initial polarization $\hat{e}_0$ is eliminated because of the isotropy of the cluster statistics. Since the term in the bracket vanishes like X as $X \to 0$, the integral is convergent. If we express the sine and cosine function in terms of the exponentials, i.e.

$$\sin X = \frac{e^{iX} - e^{-iX}}{2i}, \tag{3.38}$$

and

$$\cos X = \frac{e^{iX} + e^{-iX}}{2}, \tag{3.39}$$

the integrals of Eq.(3.37) can be reduced to the sum of the following two integral formulae:

$$I^{(n)} = \frac{1}{(k_0 R)^n} \int_0^\infty x^{(D-2-n)-1} e^{-(\gamma - i2k_0 R)x}\, dx,$$
$$= \frac{2^n}{Z^n} \frac{1}{\gamma^{D-2}(1 - iZ)^{D-2-n}} \Gamma(D-2-n), \tag{3.40}$$

and

$$J^{(n)} = \frac{1}{(k_0 R)^n} \int_0^\infty x^{(D-2-n)-1} e^{-\gamma x}\, dx,$$
$$= \frac{2^n}{Z^n} \frac{1}{\gamma^{D-2}} \Gamma(D-2-n), \tag{3.41}$$

where $Z = 2k_0R/\gamma$ and the Γ-function obey the following recursion relation when its argument is negative,

$$\Gamma(x) = \frac{\Gamma(x+1)}{x}, \qquad \text{for} \quad x < 0. \tag{3.42}$$

Therefore

$$\begin{aligned} P &= \frac{b}{2(k_0R)^2}\left\{\left[-iI^{(0)} + 2I^{(1)} + 5iI^{(2)} - 6I^{(3)} - 3iI^{(4)}\right]\right. \\ &\quad \left. + i\left[J^{(0} + J^{(2)} + 3J^{(4)}\right]\right\} \\ &= \frac{b\Gamma(d_f)}{2(d_f-1)Z^2\gamma^{d_f}}\left\{(1+Z^2)^{1-d_f/2}e^{i(d_f-2)\tan^{-1}Z}\left[\frac{A_1}{Z} + \frac{A_3}{Z^3}\right.\right. \\ &\quad \left.\left. + i(B_0 + \frac{B_2}{Z^2} + \frac{B_4}{Z^4})\right] + i\left[C_0 + \frac{C_2}{Z^2} + \frac{C_4}{Z^4}\right]\right\}. \end{aligned} \tag{3.43}$$

The coefficients $A_{1,3}$, $B_{0,2,4}$, and $C_{0,2,4}$ in Eq.(3.43) are constants depending only on the fractal dimension d_f and are given in Appendix B.

With the quantity P evaluated above, the mean-field effects of multiple scattering can be obtained by analyzing the quantity $Nk_0^3|\alpha P|$ in Eq.(3.36), since multiple scattering can be neglected only when

$$Nk_0^3|\alpha P| \ll 1. \tag{3.44}$$

For small clusters, i.e. $k_0R \ll 1$ or $Z \ll 1$ in Eq.(3.43). By using series expansion for $(1+Z^2)^{1-d_f/2}$ and $e^{i(d_f-2)\tan^{-1}Z}$, we obtain

$$|Nk_0^3\alpha P| \sim (ka)^{3-d_f}(kR)^{d_f} \ll 1. \tag{3.45}$$

Therefore the multiple scattering is not important for small clusters as expected.

For large clusters, i.e. $k_0R \gg 1$, the limiting value of Eq.(3.43) depends on the value of fractal dimension d_f as follows:

$$|Nk_0^3\alpha P| \approx \frac{\Gamma(d_f)}{2(d_f-1)\gamma^{-d_f}}\frac{k^3\alpha}{4Z^2}NZ^{2-d_f}B_0 \sim (ka)^{3-d_f}, \qquad \text{for} \quad d_f < 2, \quad (3.46)$$

and

$$|Nk_0^3\alpha P| \approx \frac{\Gamma(d_f)}{2(d_f-1)\gamma^{-d_f}}\frac{k^3\alpha}{4Z^2}NC_0 \sim kaN^{1-2/d_f}. \qquad \text{for} \quad d_f > 2, \quad (3.47)$$

In obtaining Eqs.(3.46) and (3.47), we have used the formula of polarizability, $\alpha = [(\epsilon-1)/(\epsilon+2)]a^3$, for small spheres of radius a.

Notice $|Nk_0^3\alpha P|$ is independent of the particle number N in the case $d_f < 2$. Therefore for small particle aggregates, multiple scattering (on the mean field) can always be neglected. For $d_f > 2$ multiple scattering becomes important when $N \sim (ka)^{-d_f/(d_f-2)}$, (or when $R \sim (ka)^{-1/(d_f-2)}$). For the gold colloidal aggregates of $d_f = 2.1$ (reaction-limited aggregation), it means only when the aggregation reach the stage $N \sim 10^{23}$, multiple scattering becomes to affect the m_x.

3.6. EFFECT OF LOCAL-FIELD FLUCTUATIONS

The mean-field analysis of the previous section has shown some interesting dependence of the multiple scattering on the fractal dimension and the size of fractal clusters. In this section, the effects on the q-dependence of the scattering intensity is analyzed by examining the correlation in the fluctuating part of local fields:

$$F_1(r) = \frac{1}{N} < \sum_{i\neq j}^{N} \delta(\vec{r}-\vec{r}_{ij})\Delta_x(\vec{r}+\vec{r}_j)\Delta_x^*(\vec{r}_j) > . \qquad (3.48)$$

To obtain the statistics of Δ_x's, we use computer-generated fractal clusters as our particle position input and solve Eq.(3.17) exactly by using a linear-equation-solver routine.

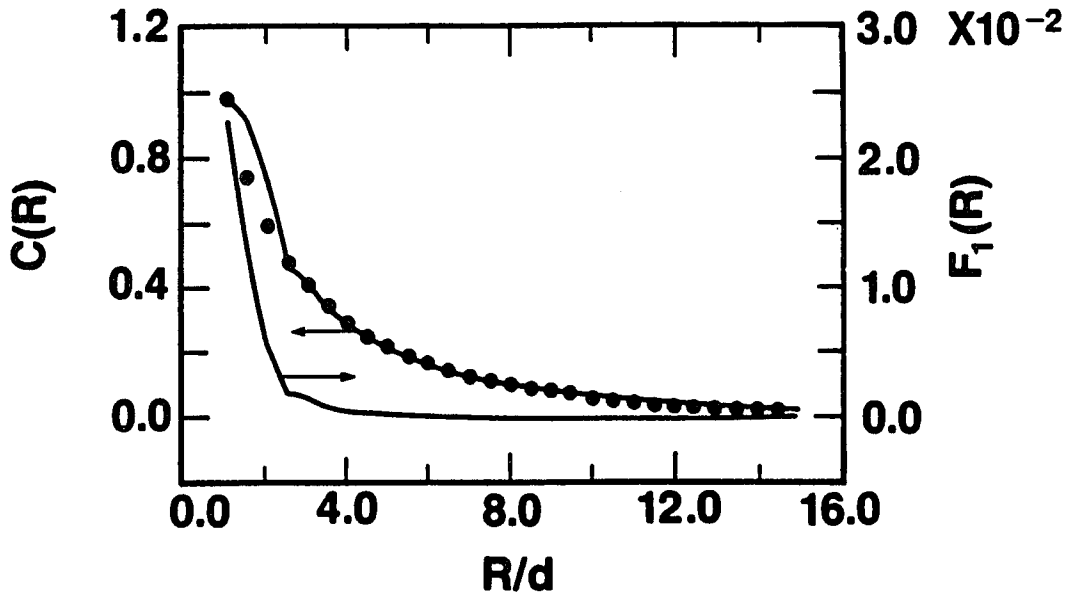

Figure 3.6a $C(r)$ and $F_1(r)$ plotted as a function of r/d for fractal clusters with $d_f = 1.8$. Here d is the diameter of the gold sphere. Dots are the Fourier transform of the calculated scattering intensity. It is clearly shown that $F_1(r)$ is both small in magnitude and short-ranged in spatial extent as compared to $C(r)$.

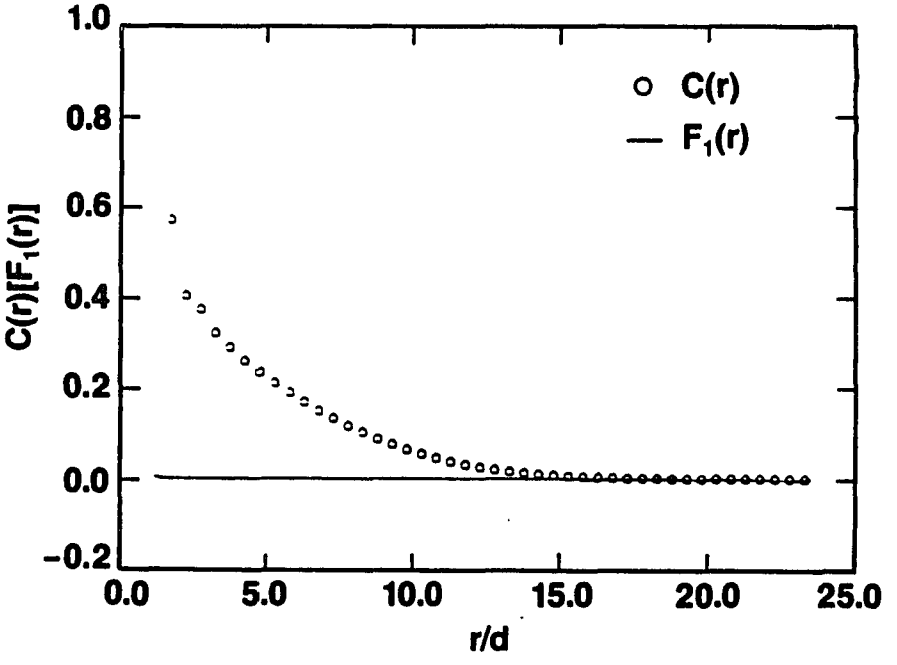

Figure 3.6b $C(r)$ and $F_1(r)$ plotted as a function of r/d for fractal clusters with $d_f = 2.5$. Here d is the diameter of the gold sphere. Again, $F_1(r)$ is both small in magnitude and short-ranged in spatial extent as compared to $C(r)$ for these clusters.

Before going to present our numerical results, some properties of $F_1(r)$ should first be noted. First, as we noted in Section 3.4 if there is no multiple scattering, then all $\Delta_x(\vec{r}_i) = 0$, and $F_1(r)$ vanish. In this case, we recover the result of the Born (or single scattering) approximation. Second, if Δ_x's assume white-noise like random values, i.e. $< \Delta_i \Delta_j >= \eta \delta_{ij}$, then the Fourier transform of $F_1(r)$ would be independent of the q vector. Third, in the case that $F_1(r)$ do exhibit nontrivial correlation, the effect on the q dependence is dictated by the magnitude of the correlation η, f.g. if $\eta \ll |m_x|^2$ then the multiple scattering would still be negligible.

In Fig.3.6a, $C(r)$ and $F_1(r)$, calculated for a typical set of clusters (with 300 particles), with incident light wave-length $\lambda = 4880$ Å, are plotted as a function of r/d, where d is the diameter of a gold particle. $C(r)$ displays a power-law fall-off, $(r/d)^{d_f-3}$, as expected. By contrast, $F_1(r)$ is both small in magnitude (even though $|\Delta_x|$ is non-negligible) and short-ranged in nature, with a width comparable to d. Thus the Fourier transform of $F_1(r)$ produces only a very small constant in $S(q)$ for $q \leq 1/d$. The solid points shown in Fig.3.6a are the Fourier transform of $S(q)$ calculated directly using Eq.(3.22) and the local fields. It is in excellent accord with $C(r)$, with an indiscernable contribution from $F_1(r)$. In Fig.3.6b, similar results are present for the fractal clusters simulated using single-particle diffusion limited aggregation, which have a fractal dimension $d_f = 2.5 > 2$. In this case the cluster is geometrically opaque if its size is large. In both cases, $F_1(r)$ is small in magnitude and short-ranged in its extend. From these results, we conclude that the effects of multiple scattering only alter the magnitude of the scattering but not its form when $S(q) \sim q^{-d_f}$. Despite the fact that the calculation is performed on 300-particle clusters, we note from the plots that $F_1(r)$ is independent of cluster size, a fact which can immediately be deduced

from the short-ranged nature of $F_1(r)$. Thus, in our calculations, we have already reached the large-size limit for $F_1(r)$, and further increase in cluster size will have no effect on either the spatial extent, or the magnitude of $F_1(r)$ compared to $C(r)$. The physical origin of the above conclusion presumably arises from the fact that multiple scattering completely scrambles any structural information in $S(q)$, as evidenced by the lack of correlations for $\Delta_x(r)$.

It should be pointed out that the above conclusions are drawn strictly for the configurationally averaged properties. For a specific cluster configuration relative to the incident light, difference between the multiple scattering result and the single scattering result does exist. In Fig.3.7 we compare the differential scattering cross section calculated with the single scattering approximation for a single configuration. In the small q regime, the incident wave probes only an effective medium, apart from a constant factor (determined by the $|m_x|^2$), and the difference is small as expected. As q increase, the incident light starts to probe the structure of the cluster. Deviations between the exact calculation, which includes the multiple scattering,and the single scattering approximation emerges. It is also appearant from the plot that the fractal scaling itself is an orientationally and configurationally averaged behavior for fractal aggregates.

The depolarized scattering, characterized by $F_2(r)$, is purely a result of multiple scattering. We found that $\Delta_\perp$'s to have random values distributed uniformly between [-1,1] with a mean value close to zero for $\lambda = 4880$ Å. The Fourier transform of $F_2(r)$ should therefore yield depolarized scattering almost independent of q. This prediction is indeed verified by experiments as illustrated in Fig.3.8, where both the calculated the experimentally measured depolarized scattering intensity display almost no q dependence over all measurable q values.

However, there exists a fundamental difference between the metallic aggre-

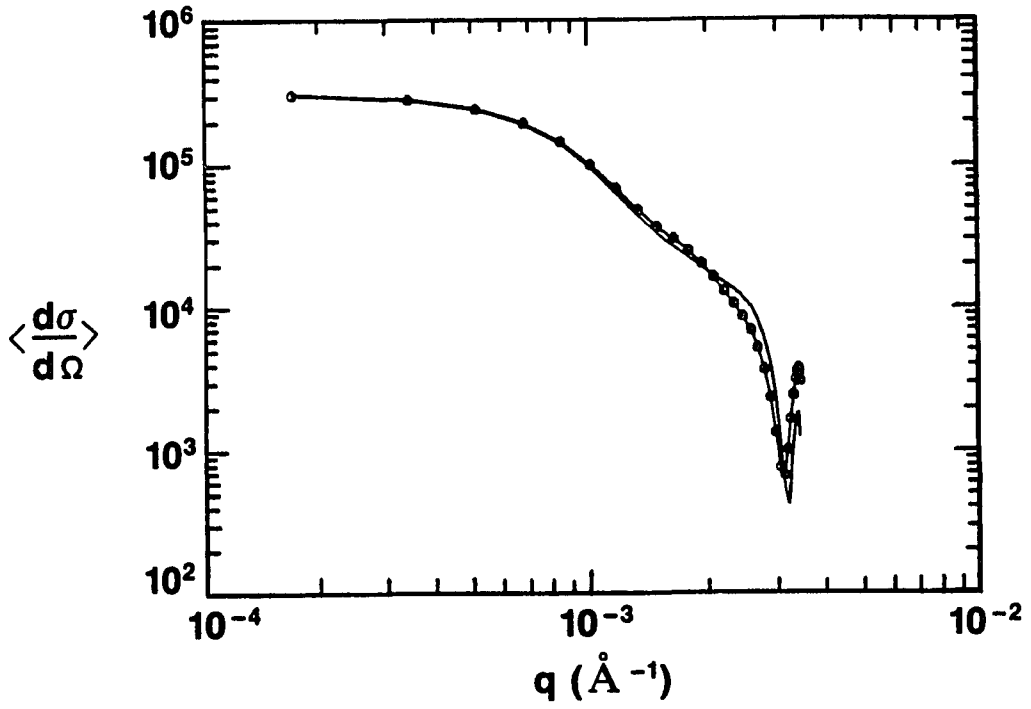

Figure 3.7 Log-log plot of the scattering intensity for a single cluster obtained by both the exact calculation and the Born approximation. Two points should be noted here. First, while the multiple scattering is shown to has negligible effect on the q-dependence of the scattering intensity after averaging, differences do exist for individual configurations. Second, the fractal scaling itself is strictly an averaged behavior.

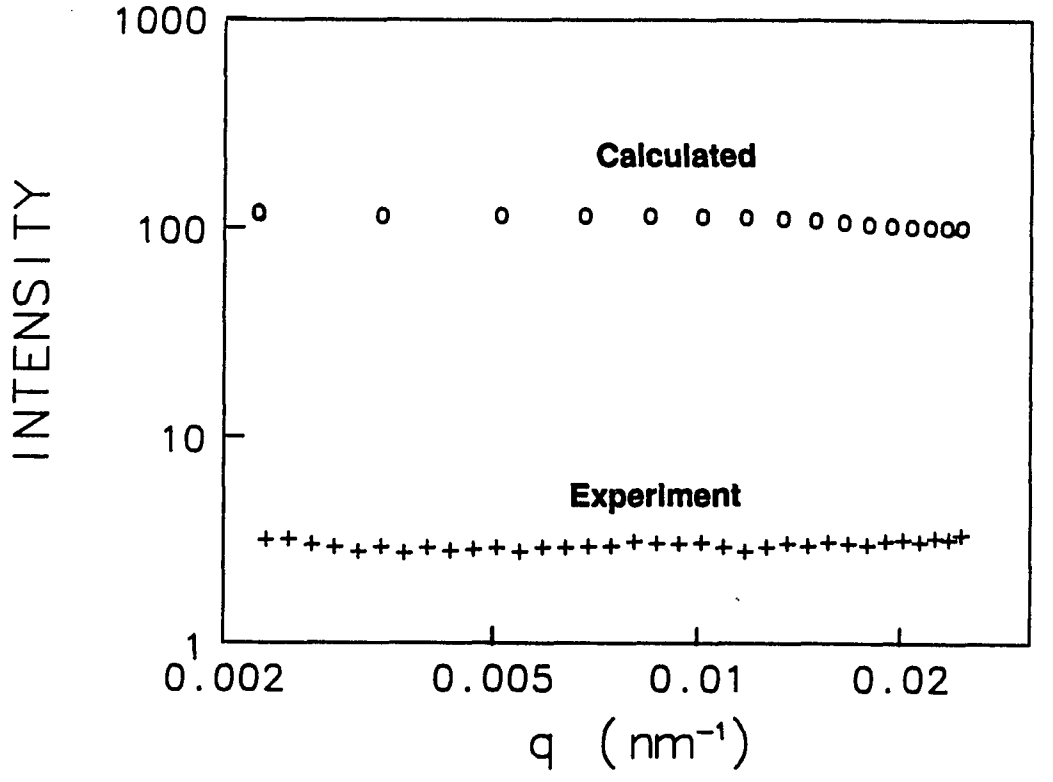

Figure 3.8 Log-log plot of the depolarized scattering intensity from both the exact calculation and experiments. The calculation agrees well the experimental result, both showing an almost q independent behavior. For the purpose of illustration, the unit of the intensity used in the plot is arbitrary.

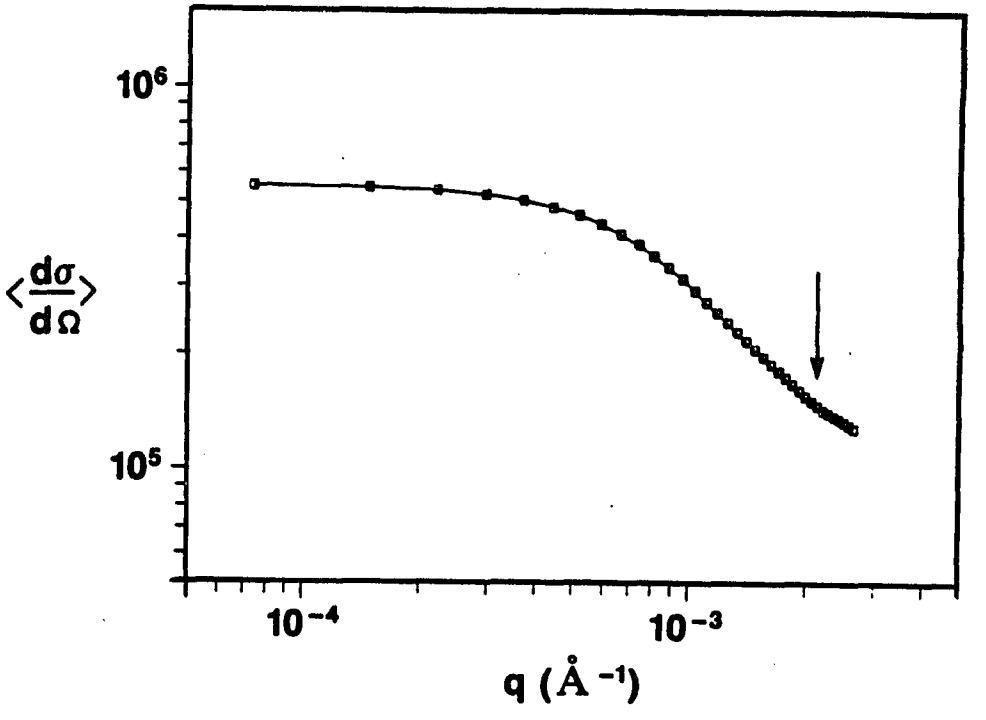

Figure 3.9 Log-log plot of the scattering intensity calculated for 300-particle clusters with incident wavelength $\lambda = 6300$ Å, at which a collective excitation was observed experimentally. At large wave-vectors, deviation of the scattering intensity from the power-law scaling is shown in the plot. This deviation has also been observed experimentally.

gates and that of a dielectric cluster, i.e. a metal particle has a Mie resonance frequency. When two metallic particles are brought together, a collective resonance, red-shifted from the original single-particle Mie resonance can result[18]. At the collective excitation frequency, a new length scale ℓ_0, which describes the spatial extent of the collective mode emerges. The appearance of ℓ_0 thus will mask out the fractal correlation in region $r < \ell_0$. Physically, since the aggregates have locally chain-like structure, the effect of collective excitation could be thought of as changing the form factor of a spherical particle to that of a cylindrical one. In Fig.3.9, we plotted the configurational averaged scattering intensity as a function of q calculated by using a $\overleftrightarrow{\alpha}$ determined at $\lambda = 6300$ Å, where a collective excitation is observed experimentally[19]. It is seen that the scattering intensity shows a small tail at large q's. This tail was also observed experimentally[20]. An exact comparison of the calculation with the experiments, however, requires the calculation on large enough clusters. Effort in this aspect is currently underway. Nontheless, the calculation suggests that the high-order multipole interaction may have significant scattering effects at the collective excitation frequency.

3.7. SUMMARY

In summary, we have present a multiple scattering formulation for the light scattering from an aggregated fractal cluster. The effects of multiple scattering on the scattering intensity is differentiated into two parts: a mean-field part which affects only the over-all magnitude of the scattering intensity and a local-field fluctuation part, characterized by the correlation function of the fluctuating part of local fields, which contains a wave-vector dependent correction to the single scattering result.

By using a mean-field analysis similar to that of Berry *et al.* [4] we have shown

that the mean-field effect is always negligible for clusters with fractal dimension d_f less than two and $ka \ll 1$. For $d_f > 2$, multiple scattering becomes important as the aggregation preceeds until the number of particles in the aggregate is comparable to $\sim (ka)^{-d_f/(d_f-2)}$.

The effects of local-field fluctuation is analyzed by using the exact solution of local-field coefficients for the computer-generated fractal clusters. We found the correlation in fluctuating local fields is small in magnitude and short-ranged in its extent for both $d_f < 2$ and $d_f > 2$. Therefore multiple scattering does not mask the structural information in the scattering intensity for $q \leq a^{-1}$, where a is on the order of the particle diameter. It suggests that light scattering technique is an accurate tool for determining d_f of fractal clusters.

It is cautioned, however, from our analysis of the polarizability $\overleftrightarrow{\alpha}$ that for metallic aggregates there exist a collective excitation mode due to the electromagnetic interaction between the the neighboring particles. At this collective excitation frequency, a new length scale ℓ_0 that describes the spatial extent of the excitation mode emerges. In this region, fractal correlation no longer exists. Both calculation and experiments found that the q-dependence of the scattering intensity starts to deviate form the simple scaling $S(q) \sim q^{-d_f}$, for $q > \ell_0^{-1}$. Therefore, for the purpose of determining d_f one has to avoid to work near the collective excitation frequency.

Appendix A

In this Appendix, we derive the anisotropic polarizability $\overleftrightarrow{\alpha}_i$ used in our calculation. Because of the string-like structures of the aggregates, we consider each gold particle as being embedded in a locally chain-like environment. Since the electromagnetic coupling between neighboring particles is distinctively different for incident polarizations in and perpendicular to the chain axis, (see discussions in Chapter 4), we expect $\overleftrightarrow{\alpha}_i$ to have uniaxial symmetry, i.e. $\alpha_{zz} = \alpha_1$, $\alpha_{xx} = \alpha_{yy} = \alpha_2$, and $\alpha_{xy} = \alpha_{xz} = \alpha_{yz} = 0$ in the coordinate system where the z axis coincides with the local chain axis.

The values of α_1 and α_2 are derived from the rigorous solutions of a periodic chain of cylindrical particles (to be discussed in Chapter 4). By comparing the scattering field of the rigorous solution to that of a chain of polarizable point dipoles for the two different polarization configurations, the ratio α_1/α_2 is deduced as follows.

From Chapter 4, the scattering field from a chain of cylinders (for a normal incidence wave $\vec{E}_i$) at $r \to \infty$ is

$$\vec{E}_s = k_0 \sum_n \left[-ia_{n0}\vec{e}_\phi + b_{n0}\vec{e}_z\right] \sqrt{\frac{2}{\pi k_0 r}} e^{ik_0 r} e^{in\phi - n\pi/2} e^{-i\pi/4}, \qquad \text{(A.1)}$$

where a_{n0} and b_{n0} are the expansion coefficients, and the chain axis is chosen as the z axis (Fig.4.1). For $\vec{E}_i || \vec{e}_z$, we take from (A.1) the scattering field component

$$E_{sz}^{(||)} = k_0 \sum_n b_{n0}^{(||)} e^{in\phi - n\pi/2} \sqrt{\frac{2}{\pi k_0 r}} e^{ik_0 r} e^{-i\pi/4}, \qquad \text{(A.2)}$$

and for $\vec{E}_i || \vec{e}_y \perp \vec{e}_z$, we take

$$E_{sy}^{(\perp)} = ik_0 \sum_n a_{n0}^{(\perp)} e^{in\phi - n\pi/2} \sqrt{\frac{2}{\pi k_0 r}} e^{ik_0 r} e^{-i\pi/4}. \qquad \text{(A.3)}$$

Let us denote the ratio of these two scattering field components as Y

$$Y = \frac{\vec{E}_{sz}^{(||)}}{\vec{E}_{sy}^{(\perp)}}. \tag{A.4}$$

For a infinite chain of polarizable point dipoles, the corresponding ratio, denoted as Y', is

$$Y' = \frac{\alpha_1 E_{||}}{\alpha_2 E_{\perp}} \frac{\sum_j [1 - (\vec{e}_z \cdot \hat{n}_j)^2] \frac{e^{ik_0 r_j}}{r_j}}{\sum_j [1 - (\vec{e}_y \cdot \hat{n}_j)^2] \frac{e^{ik_0 r_j}}{r_j}} \tag{A.5}$$

where α_1 (α_2) is the polarizability corresponding to the incident polarization in (perpendicular to) the chain axis. $E_{||}$ and $E_{\perp}$ are the local field at each point dipole for the two incident polarizations and are given by

$$E_{||(\perp)} = \frac{E_0}{1 - A_{||(\perp)} \alpha_{1(2)}}, \tag{A.6}$$

where E_0 is the amplitude of the incident field,

$$A_{||} = 2 \sum_j^{\infty} \left[\frac{2}{j^3} - \frac{2ik_0}{j^2} \right] e^{ik_0 j}, \tag{A.7a}$$

and

$$A_{\perp} = 2 \sum_j^{\infty} \left[\frac{-1}{j^3} + \frac{ik_0}{j^2} + \frac{k_0^2}{j} \right] e^{ik_0 j}. \tag{A.7b}$$

Here we have normalized the separation distance between two neighboring particles to unit.

By equating Eq.(A.4) and Eq.(A.5) and solving the corresponding equation, we obtain

$$\frac{\alpha_1}{\alpha_2} = \frac{Y\beta}{1 - A_{\perp}\alpha_2 + A_{||}\alpha_2 Y}, \tag{A.8}$$

where

$$\beta = \frac{\sum_j [1 - (\vec{e}_z \cdot \hat{n}_j)^2] \frac{e^{ik_0 r_j}}{r_j}}{\sum_j [1 - (\vec{e}_y \cdot \hat{n}_j)^2] \frac{e^{ik_0 r_j}}{r_j}}. \tag{A.9}$$

Since the particles are almost decoupled when the incident polarization is perpendicular to the chain axis, α_2 may be chosen to be the isotropic polarizability of a single gold sphere. Therefore, α_1 is completely determined by Eq.(A.8).

In the laboratory reference frame, $\overleftrightarrow{\alpha}_j$ will be given by a full second-rank tensor as follows:

$$\overleftrightarrow{\alpha}_j = \alpha_2 \begin{pmatrix} 1 & 0 & 0 \\ 0 & 1 & 0 \\ 0 & 0 & 1 \end{pmatrix} + (\alpha_1 - \alpha_2) \begin{pmatrix} a_x^2 & a_x a_y & a_x a_z \\ a_y a_x & a_y^2 & a_y a_z \\ a_z a_x & a_z a_y & a_z^3 \end{pmatrix}, \tag{A.10}$$

where $a_{x,y,z}$'s specify the direction $\vec{l}_j$ of the local chain axis at particle j

$$\vec{l}_j = a_x \vec{e}_x + a_y \vec{e}_y + a_z \vec{e}_z. \tag{A.11}$$

Appendix B

The coefficients $A_{1,3}$, $B_{0,2,4}$, and $C_{0,2,4}$ of Eq.(3.43) in the text are given as follows:

$$A_1 = -\frac{4}{d_f-3} + \frac{4}{d_f-4} + \frac{8}{d_f-5} - \frac{8}{d_f-6}, \tag{B.1}$$

$$A_3 = -\frac{8}{d_f-3} + \frac{24}{d_f-4} - \frac{24}{d_f-5} + \frac{8}{d_f-6}, \tag{B.2}$$

$$B_0 = -\frac{1}{d_f-2} + \frac{2}{d_f-4} - \frac{2}{d_f-6}, \tag{B.3}$$

$$B_2 = -\frac{2}{d_f-2} + \frac{4}{d_f-3} + \frac{10}{d_f-4} - \frac{24}{d_f-5} + \frac{12}{d_f-6}, \tag{B.4}$$

$$B_4 = -\frac{2}{d_f-2} + \frac{8}{d_f-3} - \frac{12}{d_f-4} + \frac{8}{d_f-5} - \frac{6}{d_f-6}, \tag{B.5}$$

$$C_0 = \frac{1}{d_f-2}, \tag{B.6}$$

$$C_2 = \frac{2}{d_f-2} - \frac{4}{d_f-3} + \frac{2}{d_f-4}, \tag{B.7}$$

$$C_4 = \frac{2}{d_f-2} - \frac{8}{d_f-3} + \frac{12}{d_f-4} - \frac{8}{d_f-5} + \frac{6}{d_f-6}. \tag{B.8}$$

REFERENCES

1. W. M. Purcell, C. K. Pennypackw, *The Astrophysical Journal* **186**, 705 (1973).

2. B. Donn (unpublished).

3. J. DeRis, *Seventeenth Symposium (International) on Combustion* (Combustion Institute, Pittsburg, PA, 1978), P.1103.

4. M. V. Berry and I. C. Percival, *Opt. Acta.* **33**, 577 (1986).

5. T. C. Patton, *Paint Flow and Pigment Dispersion* (Wiley-Interscience, New York, 1979).

6. S. W. Billmeyer and M. Saltzman, *Principles of Color Technology* (Wiley, New York, 1967).

7. *Kinetics of Aggregation and Gelation*, edited by F. Family and D. P. Landau (Elsevier, Amsterdam, 1984).

8. D. A. Weitz and M. Oliveria, *Phys. Rev. Lett.* **52**, 1433 (1984).

9. D. W. Schaefer, J. E. Martin, P. Wiltzius, and D. S. Cannell, *Phys. Rev. Lett.* **52**, 2371 (1984).

10. D. A. Weitz, J. S. Huang, M. Y. Lin, and J. Sung, *Phys. Rev. Lett.* **54**, 1416 (1985).

11. M. Matsushita, K. Sumida, and Y. Sawada, *J. Phys. Soc. Jpn.* **54**, 2786 (1985).

12. Z. Chen, P. Sheng, D. A. Weitz, M. H. Lindsay, M. Lin, and P. Meakin, *Phys. Rev. B* **37**, 5232 (1988).

13. M. Lax, *Rev. Mod. Phys.* **23**, 287 (1951).

14. D. A. Weitz, M. Y. Lin, J. S. Huang, T. A. Witten, S. K. Sinha, J. S. Geljner, and R. C. Ball, in *Scaling Phenomena in Disordered Systems*, Vol. 133 of *NATO Advanced Study Institute Conference, Series B*, edited by R. Pynn and A. Skjeltorp (Plenum, New York, 1985).

15. B. B. Mandelbrot, *The Fractal Geometry of Nature* (Freeman, San Francisico, 1982).

16. P. Meakin, *Phys. Lett.* **107A**, 269 (1985).

17. M. Born and E. Wolf, *Principles of Optics*, (Pergamon Press, Oxford, 1975), 5th edition, P. 100.

18. Z. Chen and P. Sheng, *Phys. Rev. B* , 39, 9816 (1989).

19. M. H. Lindsay, M. Y. Lin, D. A. Weitz, P. Sheng, Z. Chen, R. Klein, and P. Meakin, *Faraday Discuss. Chem. Soc.* **83**, 153 (1987).

20. D. A. Weitz, Private communication.

CHAPTER 4

OPTICS OF RANDOM FRACTAL CLUSTERS: EFFECTS OF HIGH-ORDER MULTIPOLE INTERACTION

ABSTRACT

Recent experimental studies on the optical properties of gold colloidal aggregates have found intersting characteristics, such as the double absorption peaks and enhanced depolarized scattering, that are not explainable in terms of the traditional mean-field theories. Based on the observation that the aggregate clusters have a locally chain-like structure of touching spheres, a simple model for the calculation of their absorption and scattering characteritics is proposed that consists of a randomly-oriented chain of cylindrical particles under the excitation of an electromagnetic field. The consideration of cylindrical geometry considerably simplifies the mathematics while retaining the essential physics of capacitive coupling between the particles. In the optical frequency regime, rigorous scattering solution for the model shows that besides the single-particle Mie resonance, there exists a low frequency collective excitation arising from the anisotropic, high-multipole interactions between the metal particles. It results in a second absorption peak whose peak position is controlled by the capacitive coupling between adjacent particles. Both the polarized and the depolarized scattering also show accompanying increases at the collective excitation frequency. Good agreement is found between the calculated results and the experimental observation.

4.1. INTRODUCTION

In Chapter 3, we have addressed the important question of the effects of multiple scattering on the structure factor of the aggregated clusters and found that the dominant effect of multiple scattering is reflected in the mean-field index of refraction of the clusters and therefore does not mask the q dependence of the scattering. However, it was noted that traditional mean-field treatments, such as the Maxwell-Garnett theory[1], do not adequately describe the absorption of the clusters since they are based on the random, isotropic distribution of neighboring particles and thus ignore the strong short-range anisotropic correlations inherent in a connected cluster. For metallic clusters, a mean-field approach will therefore not be able to account for the experimental observations[2] such as the appearance of a second, red-shifted, absorption peak (other than the Mie-resonance peak), or the large degree of depolarized scattering. We suggest that a more appropriate approach for these properties is through the calculation of the effective polarizability of small chain-like structures as seen from the TEM pictures (see Fig.3.1) of these clusters[3], subjected to an averaged field determined by the mean-field index of refraction.

It is shown in Chapter three that the gold spheres in the aggregates are capacitively coupled. Therefore, the absorption characteristics are determined by the multipole interactions between the connected neighboring particles. Based on the observation that the aggregates have locally chain-like structures, we study in this Chapter a simple model of periodic chain of cylindrical metallic segments under the excitation of an electromagnetic field. The consideration of the cylindrical geometry is intended to keep the mathematics tractable but, nonetherless, reflect the essential physics of the capacitive coupling between the particles. An alternative approach would be to consider the scattering solution for two or more touching

spheres[4,5,6,7,8]. Howerer, the mathematics would then be significantly complex. One may view the net effect of our model calculation as the renormalization of the metal-particle polarizability α due to the high-multipole interactions with the neighbors. The renormalized α would be a tensorial quantity with uniaxial symmetry, where the symmetry axis coincides with the local chain axis. Rigorous scattering solution[9] shows that when the incident wave is poalrized along the symmetry direction, the renormalized α exhibits a second, red-shifted absorption peak as distinct from the single-particle Mie resonance. The depolarized scattering also shows dramatic increase around this absorption peak frequency. Averaging over random orientations of the chain yields the double absorption peaks and the enhanced depolarized scattering that are in good agreement with experimental observations.

This Chapter is organized as follows: Section 4.2 presents the formulation of our solution approach for the periodic chain of cylindrical particles. This is followed by a discussion of numerical results and their comparison with experiments in Section 4.3. Section 4.4 summarize our main results with remarks noting some problems in our approach as well as further research apportunities.

4.2. RIGOROUS SCATTERING SOLUTION

Our goal in this Section is to present a relatively straightforward, but rigorous, solution of Maxwell's equations for a periodic chain of cylindrical particles illuminated by an incident plane wave $\vec{E}_I = \vec{E}_0 \exp(j\vec{k}_0 \cdot \vec{r} - j\omega t)$, where $\vec{k}_0$ is the wave vector, ω is the fequency, and t is the time. The chain is embedded in a matrix with a dielectric constant ϵ_0. As shown in Fig.4.1, the length of each cylindrical segment is denoted by L and the radius of the cross-section by a. If the separation between two adjacent cylinders is d, then the periodicity

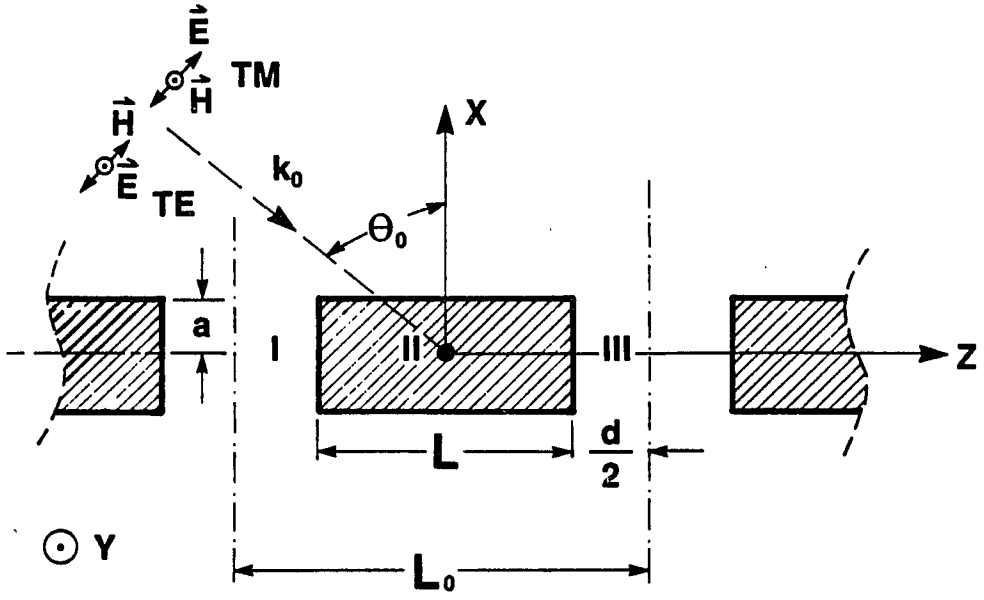

Figure 4.1 Sketch of a portion of the periodic chain of cylinders. Parameters for the cylinders are radius a, length L, separation d, and periodicity L_0. The cylindrical coordinate system is chosen such that the $r\phi$ plane coincides with the xy pland and the counterclockwise direction represents the positive direction of $\hat{e}_\phi$. In the TM (TE) mode the electric field is polarized in (perpendicular to) the incident plane xz.

is $L_0 = L + d$. The dielectric constant of the particles is denoted by $\epsilon(\omega)$, and the magnetic susceptibility $\mu \equiv 1$. Instead of following the traditional approach, i.e. solving the Maxwell equations in each homogeneous region and matching the boundary conditions at interfaces, we employ the periodicity in the problem to construct an eigenvalue problem for the electromagnetic field in the $r \leq a$ region. The electromagnetic field in the $r \leq a$ region is then expanded in terms of these eigenfields, each of which now rigorously satisfies the boundary conditions at internal periodic interfaces. The expansion coefficients of these excited fields, as well as the scattering waves, are then determined by matching the boundary conditions at the single interface $r = a$.

4.2.1. General solutions of Maxwell equations

In a linear, isotropic, and homogeneous medium, the sourceless time harmonic electromagnetic fields satisfy the following equations:

$$\nabla^2 \vec{E} + k^2 \vec{E} = 0, \tag{4.1a}$$

$$\nabla^2 \vec{H} + k^2 \vec{H} = 0, \tag{4.1b}$$

$$\nabla \cdot \vec{E} = 0, \tag{4.1c}$$

$$\nabla \cdot \vec{H} = 0, \tag{4.1d}$$

where $\vec{E}$ and $\vec{H}$ are the spatial-dependent electric- and magnetic-field vectors, respectively, and k is the propagation wave vector obeying the dispersion relation $k^2 = \omega^2 \epsilon_0$. Here ϵ_0 is the dielectric constant of the medium. The $\vec{E}$ and $\vec{H}$ are related to each other by

$$\nabla \times \vec{E} = j\omega \vec{H}, \tag{4.2a}$$

$$\nabla \times \vec{H} = -j\omega \epsilon_0 \vec{E}. \tag{4.2b}$$

It is straightforward to show[10] that Eq.(4.1) can be satisfied by the function $\vec{M}$ and $\vec{N}$, where

$$\vec{M} = \nabla \times (\vec{c}\psi), \tag{4.3a}$$

$$\vec{N} = \nabla \times \vec{M}/k, \tag{4.3b}$$

$\vec{c}$ is a arbitrary constant vector, and ψ is a scalar function satisfying the scalar Helmholtz equation

$$\nabla^2\psi + k^2\psi = 0. \tag{4.4}$$

The vector functions $\vec{M}$ and $\vec{N}$, generally denoted as vector harmonics, therefore have all the required properties of the electromagnetic fields. The form of the generating function ψ is dictated by the symmetry of the problem. For cylindrical symmetry,

$$\psi_n(r,\phi,z) = R_n(\rho)e^{jn\phi}e^{jhz}, \tag{4.5}$$

where $R_n(\rho)$ is a Bessel function of order n, h is a separation constant to be determined, and $\rho = r(k^2 - h^2)^{1/2}$. The vector harmonics $\vec{M}$, $\vec{N}$ are obtained from Eq. (4.2) and by letting $\vec{c} = \hat{e}_z$:

$$\vec{M}_n = \left[jn\mu\frac{R_n(\rho)}{\rho}\hat{e}_r - uR_n'(\rho)\hat{e}_\phi\right]e^{jn\phi}e^{jhz}, \tag{4.6a}$$

$$\vec{N}_n = \frac{u}{k}\left[ihR_n'(\rho)\hat{e}_r - hn\frac{R_n(\rho)}{\rho}\hat{e}_\phi + uR_n(\rho)\hat{e}_z\right]e^{jn\phi}e^{jhz}, \tag{4.6b}$$

where $u = (k^2 - h^2)^{1/2}$. $\vec{M}_n$ and $\vec{N}_n$ obtained above are noted to be orthogonal:

$$\int_0^{2\pi}\vec{M}_n\cdot\vec{M}_m^*d\phi = \int_0^{2\pi}\vec{N}_n\cdot\vec{N}_m^*d\phi = \int_0^{2\pi}\vec{M}_n\cdot\vec{N}_m^*d\phi = 0, \qquad \text{for} \quad (n \neq m), \tag{4.7}$$

where the asterisk represents complex conjugation.

4.2.2. Expansion of Incident Field

The incident wave can now be expanded in terms of the above vector harmonics with $R_n(\rho)$ and h determined as follows. For the incident waves, we distinguish between two polarizations as shown in Fig.4.1. In case (1) an incident wave is polarized in the incident plane, denoted as the TM mode, and in case (2) the wave is polarized perpendicular to the incident plane, denoted as the TE mode. An arbitrary incident wave can be decomposed into a linear combination of these two independent cases.

In case (1), we write the E field of the incident wave as

$$\vec{E}_I^{(1)} = (\sin\theta_0 \hat{e}_x + \cos\theta_0 \hat{e}_z)\, E_0 e^{-jk_0(x\cos\theta_0 - z\sin\theta_0)}. \tag{4.8}$$

Since $\vec{E}_I$ is finite at $r = 0$, $R_n(\rho)$ in Eq.(4.6) must be Bessel function of the first kind, $J_n(\rho)$. It is clear from Eq.(4.8) that the z dependence of the incident wave is explicitly contained in the phase factor, and therefore the separation constant h should be equal to $k_0 \sin\theta_0$. The generating function for the incident wave is thus

$$\psi_n^{(I)}(r,\phi,z) = J_n(k_0 r\cos\theta_0) e^{jn\phi} e^{jk_0 z\sin\theta_0}. \tag{4.9}$$

Expanding Eq.(4.8) in terms of the vector harmonics that are generated by $\psi_n^{(I)}$, we write

$$\vec{E}_I^{(1)} = \sum_n [A_n \vec{M}_n^{(I)} + B_n \vec{N}_n^{(I)}]. \tag{4.10}$$

Using the orthogonality relation Eq.(4.7), we obtain, after some lengthy algebra,

$$A_n = 0 \qquad \text{and} \qquad B_n = E_n \equiv \frac{(-j)^n E_0}{k_0 \cos\theta_0}. \tag{4.11}$$

Therefore

$$\vec{E}_I^{(1)} = \sum_n E_n \vec{N}_n^{(I)}, \tag{4.12}$$

$$\vec{H}_I^{(1)} = \frac{1}{jk_0}\nabla \times \vec{E}_I^{(1)} = -j\sum_n E_n \vec{M}_n^{(I)}, \tag{4.13}$$

In case (2), $\vec{E}_I$ is polarized in the y direction. The expansion in terms of the same vector harmonics yield $\vec{E}_I^{(2)} = \vec{H}_I^{(1)}$ and $\vec{H}_I^{(2)} = -\vec{E}_I^{(1)}$.

4.2.3. Expansion of Scattering Field

For the scattered waves, since they are propagating outward from $r = a$, $R_n(\rho)$ must be Henkel functions of first kind, $H_n^{(1)}(\rho)$, for which $H_n^{(1)}(\rho) \to (2/\pi\rho)^{-1/2}e^{j(\rho - n\pi/2 - \pi/4)}$ as $\rho \to \infty$. Apart from a z-dependent incident-wave phase factor, the scattering waves must be periodic in z in order to fit the boundary conditions at $r = a$. That means h has the form of

$$\gamma_m = k_0 \sin\theta_0 + \frac{2\pi m}{L_0}, \quad m = 0, \pm 1, \pm 2, \ldots, \tag{4.14}$$

The generating function for scattering waves are therefore

$$\psi_{nm}^{(s)} = H_n^{(1)}(\rho)e^{jn\phi}e^{j\gamma_m z}, \tag{4.15}$$

with $\rho = r(k_0^2 - \gamma_m^2)^{1/2}$. Expansion in terms of the vector harmonics yields

$$\vec{E}_s = \sum_n \sum_m \left[a_m^n \vec{M}_{nm}^{(s)} + b_m^n \vec{N}_{nm}^{(s)}\right], \tag{4.16a}$$

$$\vec{H}_s = -j\sum_n \sum_m \left[a_m^n \vec{N}_{nm}^{(s)} + b_m^n \vec{M}_{nm}^{(s)}\right], \tag{4.16b}$$

where $\vec{M}_{nm}^{(s)}$ and $\vec{N}_{nm}^{(s)}$ are vector harmonics generated by Eq.(4.15). The expansion coefficients in Eq.(4.16) are to be determined by fitting the electromagnetic boundary conditions at the interface $r = a$ with field configurations inside the region $r \leq a$.

4.2.4. Expansion of Fields in Region $r \leq a$:

Eigenfunctions of Electromagnetic Field

Since our system is piecewise homogeneous along the z direction in the region $r \leq a$, the traditional solution approach would require additional boundary-condition fitting at periodic interfaces. However, that can be avoided by utilizing the periodicity in the problem to construct an eigenvalue problem[11] and to obtain the corresponding eigenfields in analytic form. These eigenfunctions of the electromagnetic fields, which automatically satisfy all internal interface boundary conditions, thus provide a basis for the expanding arbitrary field configurations in this region.

To construct the eigenvalue problem, we first write $\psi(r,\phi,z) = R(r)\Phi(\phi)Z(z)$ for Eq.(4.4). The three separated equations then are

$$\frac{d^2\Phi(\phi)}{d\phi^2} + n^2\Phi(\phi) = 0, \tag{4.17}$$

$$\frac{d^2Z(z)}{dz^2} + (k^2 - \Lambda^2)Z(z) = 0, \tag{4.18}$$

$$\rho^2\frac{d^2R(\rho)}{d\rho^2} + \rho\frac{dR(\rho)}{d\rho} + (\rho^2 - n^2)R(\rho) = 0, \tag{4.19}$$

In Eq.(4.19), $\rho = \Lambda r$. The first separation constant n determines the order of the Bessel function of Eq.(4.19). The second separation constant Λ is chosen such that it remains the same for different homogeneous regions, thus enabling us to construct an eigenvalue problem for the field. Eq.(4.19) is just the Bessel equation. Since the fields must be finite at $r = 0$, the generating function should be the form of

$$\psi_n^{(e,o)}(r,\phi,z) = J_n(\Lambda r)e^{jn\phi}\begin{Bmatrix}\cos(hz)\\ \sin(hz)\end{Bmatrix} \tag{4.20}$$

where $h = (k^2 - \Lambda^2)^{1/2}$, and the superscripts (o) and (e) denote the odd and even functions in the variable z, respectively. The corresponding vector harmonics are

$$\vec{M}_n^{(e,o)} = \left[jn\Lambda \frac{J_n(\Lambda r)}{\Lambda r}\hat{e}_r - \Lambda J_n'(\Lambda r)\hat{e}_\phi \right] e^{jn\phi} \begin{Bmatrix} \cos(hz) \\ \sin(hz) \end{Bmatrix} \tag{4.21}$$

and $\vec{N}_n = \nabla \times \vec{M}_n / k$. It is helpful to note here that with the cylindrical symmetry, there are only two simple field configurations. One is the TM mode in which the $\vec{H}$ field is perpendicular to the chain axis, i.e., $H_z = 0$, and the other is the TE mode in which the $\vec{E}$ field is perpendicular to the chain axis, i.e., $E_z = 0$. In general, a field is expressible as a linear combination of both field configurations. In the following, we discuss the TM-mode field configuuration in detail. Results for the TE mode are similar to that of TM mode and will be pointed out along with our discussions. For the TM mode, since the $\vec{N}$ function obtained from Eq.(4.6b) has an nonvanishing z component, the appropriate vector harmonics for a general expansion of $\vec{H}$ must only be $\vec{M}_n$. That means

$$\vec{H}_n^i = A_n^i \vec{M}_n^{(e)}(i) + B_n^i \vec{M}_n^{(o)}(i), \tag{4.22}$$

where A_n^i and B_n^i are expansion coefficients to be determined later. Here i is the index that labels the paramaters and functions pertaining to the three homogeneous regions I, II, and III as shown in Fig.4.1. Substituting Eq.(4.21) into Eq.(4.22) gives

$$\vec{H}_n^i = (U_n \hat{e}_r - V_n \hat{e}_\phi) e^{jn\phi} Z_i(h_i z), \tag{4.23}$$

$$\begin{aligned} \vec{E}_n^i &= \frac{1}{-jk_0\epsilon_i} \nabla \times \vec{H}_n^i \\ &= \frac{-1}{jk_0\epsilon_i} [h_i(V_n \hat{e}_r + U_n \hat{e}_\phi) Z_i'(h_i z) \\ &\qquad + W_n Z_i(h_i z)\hat{e}_z] e^{jn\phi} \end{aligned} \tag{4.24}$$

where the terms with the z variable are combined into a single function

$$Z_i(h_i z) = A_n^i \cos(h_i z) + B_n^i \sin(h_i z), \tag{4.25}$$

with

$$U_n = jn\Lambda\frac{J_n(\rho)}{\rho}, \qquad V_n = \Lambda\frac{d}{d\rho}J_n(\rho), \qquad W_n = \Lambda^2 J_n(\rho), \tag{4.26}$$

and $h_i = (\epsilon_i k_0^2 - \Lambda^2)^{1/2}$. Z_i' in Eq.(4.24) denotes the derivative of Z_i with respect to the argument $h_i z$.

With Eq.(4.23) and Eq.(4.24), the transverse (ϕ, r) component of the fields can be arranged as a one-dimensional array in the order as show in Eq.(4.27). it is easy to verify that within each homogeneous region the value of the array at a plane $z = z$ is related to that at plane $z = z + \ell$ by a simple transfer matrix T_i, i.e.,

$$\begin{pmatrix} H^i_{nr}(z+\ell) \\ E^i_{n\phi}(z+\ell) \\ H^i_{n\phi}(z+\ell) \\ E^i_{nr}(z+\ell) \end{pmatrix} = T_i(\ell) \begin{pmatrix} H^i_{nr}(z) \\ E^i_{n\phi}(z) \\ H^i_{n\phi}(z) \\ E^i_{nr}(z) \end{pmatrix}, \tag{4.27}$$

where the matrix $T_i(\ell)$ dependens only on the separation distance ℓ of the two planes and is given by

$$\begin{pmatrix} \cos(h_i\ell) & -j\frac{k_0\epsilon_i}{h_i}\sin(h_i\ell) & 0 & 0 \\ -j\frac{h_i}{k_0\epsilon_i}\sin(h_i\ell) & \cos(h_i\ell) & 0 & 0 \\ 0 & 0 & \cos(h_i\ell) & j\frac{k_0\epsilon_i}{h_i}\sin(h_i\ell) \\ 0 & 0 & j\frac{h_i}{k_0\epsilon_i}\sin(h_i\ell) & \cos(h_i\ell) \end{pmatrix}$$

The benefit of this construction is due to the fact that the transverse field at interfaces $z = \pm L/2$ are continuous as required by the electromagnetic boundary conditions. Thus the transverse fields at different regions can be related to each other by a single matrix through the interface. Denoting the array in Eq.(4.27) at the plane z by $\vec{f}(z)$, we have

$$\vec{f}(L_0/2) = T_{III}(d/2) \times T_{II}(L) \times T_I(d/2)\vec{f}(-L_0/2). \tag{4.28}$$

In Eq.(4.28) the distance between the two planes is one complete period and the periodicity requires that the field value at these two planes differ by only a phase factor of the incident wave, $e^{jk_0L_0\sin\theta_0}$, i.e.,

$$\vec{f}(L_0/2) = e^{jk_0L_0\sin\theta_0}\vec{f}(-L_0/2). \tag{4.29}$$

Combining with Eq.(4.28), that means

$$(T - Ie^{jk_0L_0\sin\theta_0})\vec{f}(-L_0/2) = 0, \tag{4.30}$$

where we have denoted the matrix product $T_{III} \times T_{II} \times T_I$ in Eq.(4.30) by T and the unit matrix by I. In order for Eq.(4.30) to have an nontrivial solution, it is required that

$$\det(T - Ie^{jk_0L_0sin\theta_0}) = 0, \tag{4.31}$$

where det denotes the determinant. With a little algebra, Eq.(4.31) can be rewritten in the following simple form:

$$\cos(k_0L_0\sin\theta_0) - \cos(h_2L)\cos(h_1d) + \frac{1}{2}\left(\tau\,\frac{h_1}{h_2} + \frac{1}{\tau}\,\frac{h_2}{h_1}\right)\sin(h_2L)\sin(h_1d) = 0, \tag{4.32}$$

where $\tau = \epsilon$.

Since h_1 and h_2 contain the separation constant Λ^2, the solutions of Eq.(4.32) determine the complete set of eigenvalues $\{\Lambda_\mu^h\}$, where the subscript μ labels the eigenvalues and the superscript h denotes the TM mode. For each eigenvalue we obtain from Eq.(4.30) a corresponding eigenvector $\vec{f}(-L_0/2)$. The expansion coefficients $\{A_n^i(\mu), B_n^i(\mu)\}$ of Eq.(4.22) are then obtained from this eigenvector through Eq.(4.28). In their explicit form, the complete eigenfunctions of the TM mode are as follows:

$$\vec{\mathcal{H}}_h(n,\Lambda_\mu^h) = \left[jn\Lambda_\mu^h \frac{J_n(\Lambda_\mu^h r)}{\Lambda_\mu^h r}\hat{e}_r - \Lambda_\mu^h \frac{d}{d(\Lambda_\mu^h r)} J_n(\Lambda_\mu^h r)\hat{e}_\phi \right] e^{jn\phi}$$

$$\times \begin{cases} [A_n^I(\mu)\cos(h_1 z) + B_n^I(\mu)\sin(h_1 z)] & (-L_0/2 \le z < -L/2)\ ; \\ [A_n^{II}(\mu)\cos(h_2 z) + B_n^{II}(\mu)\sin(h_2 z)] & (|z| \le L/2); \\ [A_n^{III}(\mu)\cos(h_1 z) + B_n^{III}(\mu)\sin(h_1 z)] & (L/2 < z \le L_0/2). \end{cases} \tag{4.33}$$

$$\vec{\mathcal{E}}_h(n,\Lambda_\mu^h) = \begin{cases} \frac{1}{-jk_0\epsilon_0}\nabla \times \mathcal{H}_h(n,\Lambda_\mu^h) & \text{(in regions I, III);} \\ \frac{1}{-jk_0\epsilon}\nabla \times \mathcal{H}_h(n,\Lambda_\mu^h) & \text{(in region II).} \end{cases} \tag{4.34}$$

In Eq.(4.33)

$$A_n^I(\mu) = 1, \tag{4.35}$$

$$B_n^I(\mu) = \frac{P_1}{e^{-jk_0 L_0 \sin\theta_0} - P_2}, \tag{4.36}$$

$$A_n^{II}(\mu) = P_3 + P_4 B_n^I(\mu), \tag{4.37}$$

$$B_n^{II}(\mu) = P_5 + P_6 B_n^I(\mu), \tag{4.38}$$

$$A_n^{III}(\mu) = [\cos(h_1 L_0) - \sin(h_1 L_0) B_n^I(\mu)] e^{jk_0 L_0 \sin\theta_0}, \tag{4.39}$$

$$B_n^{III}(\mu) = [\sin(h_1 L_0) + \cos(h_1 L_0) B_n^I(\mu)] e^{jk_0 L_0 \sin\theta_0}, \tag{4.40}$$

where

$$\begin{aligned} P_1 = {} & \cos(h_2 L)\sin(h_1 d) \\ & + \frac{h_{1\epsilon}}{h_2}\sin(h_2 L)\sin(h_1 L/2)\sin[h_1(L_0 - L/2)] \\ & + \frac{h_2}{h_{1\epsilon}}\sin(h_2 L)\cos(h_1 L/2)\cos[h_1(L_0 - L/2)], \end{aligned} \tag{4.41}$$

$$\begin{aligned} P_2 = {} & \cos(h_2 L)\cos(h_1 d) \\ & + \frac{h_{1\epsilon}}{h_2}\sin(h_2 L)\sin(h_1 L/2)\cos[h_1(L_0 - L/2)] \\ & - \frac{h_2}{h_{1\epsilon}}\sin(h_2 L)\cos(h_1 L/2)\sin[h_1(L_0 - L/2)], \end{aligned} \tag{4.42}$$

$$P_3 = \cos(h_1 L/2)\cos(h_2 L/2) + \frac{h_1\epsilon}{h_2}\sin(h_1 L/2)\sin(h_2 L/2), \tag{4.43}$$

$$P_4 = -\sin(h_1 L/2)\cos(h_2 L/2) + \frac{h_1\epsilon}{h_2}\cos(h_1 L/2)\sin(h_2 L/2), \tag{4.44}$$

$$P_5 = -\cos(h_1 L/2)\sin(h_2 L/2) + \frac{h_1\epsilon}{h_2}\sin(h_1 L/2)\cos(h_2 L/2), \tag{4.45}$$

$$P_6 = \sin(h_1 L/2)\sin(h_2 L/2) + \frac{h_1\epsilon}{h_2}\cos(h_1 L/2)\cos(h_2 L/2). \tag{4.46}$$

Applying the above procedure to the TE-mode case, we now expand the electric field in terms of $\vec{M}_n$:

$$\vec{E}_n^i = C_n^i \vec{M}_n^{(e)}(i) + D_n^i \vec{M}_n^{(o)}(i), \tag{4.47a}$$

and

$$\vec{H}_n^i = \frac{1}{jk_0}\nabla \times \vec{E}_n^i. \tag{4.47b}$$

By noticing the similarity of Eq.(4.47) to Eq.(4.22), we follow the same discussion for the TM mode and obtain an eigenvalue equation similar to Eq.(4.32), except $\tau = 1$. By solving this equation, the eigenvalues Λ_μ^e and the corresponding expansion coefficients, $C_n^i(\mu)$ and $D_n^i(\mu)$, are obtained. The explicit form of these two expansion coefficients are in exact accord with the expansion coefficients $A_n^i(\mu)$ and $B_n^i(\mu)$ for the TM-mode case, except the explicit apperance of ϵ is now replaced by 1. We denote the eigenfunctions for the TE mode by $\vec{\mathcal{E}}_e(n, \Lambda_\mu^e)$ and $\vec{\mathcal{H}}_e(n, \Lambda_\mu^e)$.

The actual field configuration excited by an incident wave in region $r \leq a$ can now be a linear combination of $\{\vec{\mathcal{E}}_h, \vec{\mathcal{H}}_h\}$ and $\{\vec{\mathcal{E}}_e, \vec{\mathcal{H}}_e\}$. Therefore, in general, in $r \leq a$

$$\vec{H}_c = \sum_n \sum_\mu \left[\alpha_\mu^n \vec{\mathcal{H}}_h(n, \Lambda_\mu^h) + \beta_\mu^n \vec{\mathcal{H}}_e(n, \Lambda_\mu^e)\right] \tag{4.48a}$$

$$\vec{E}_c = \sum_n \sum_\mu \left[\alpha_\mu^n \vec{\mathcal{E}}_h(n, \Lambda_\mu^h) + \beta_\mu^n \vec{\mathcal{E}}_e(n, \Lambda_\mu^e) \right] \tag{4.48b}$$

α_μ^n and β_μ^n are expansion coefficients to be determined by fitting the boundary conditions at $r = a$.

4.2.5. Rigorous Scattering Solution

The problem is now reduced to the determination of the expansion coefficients a_m^n, b_m^n, α_μ^n, and β_μ^n. The boundary conditions at interface $r = a$ are

$$E_{I\phi} + E_{s\phi} = E_{c\phi}, \tag{4.49a}$$

$$E_{Iz} + E_{sz} = E_{cz}, \tag{4.49b}$$

$$H_{I\phi} + H_{s\phi} = H_{c\phi}, \tag{4.49c}$$

$$H_{Iz} + H_{sz} = H_{cz}, \tag{4.49d}$$

Since all the functions of Eq(4.49) have the same phase factor of $e^{jn\phi}$, it is clear that each nth component of Eq(4.49) is decoupled from all other components and therefore can be solved independently. The nth-component equations of Eq.(4.49) can be solved by expanding all the z-dependent functions in terms of the periodic Fourier basis $e^{j2\pi kz/L_0}$. Multiplying both sides of these equations by $e^{-j2\pi mz/L_0}$ and integrating z over one period yields, after some algebra rearrangements,

$$a_m^n = \sum_\mu \Omega_{m\mu}^n \beta_\mu^n + (\tilde{H}_z)_m^n, \tag{4.50a}$$

$$b_m^n = \sum_\mu \Psi_{m\mu}^n \alpha_\mu^n + (\tilde{E}_z)_m^n, \tag{4.50b}$$

$$a_m^n + \Gamma_{mm}^n b_m^n = \sum_\mu (\Pi_{m\mu}^n \alpha_\mu^n + \Delta_{m\mu}^n \beta_\mu^n) + (\tilde{E}_\phi)_m^n, \tag{4.50c}$$

$$\Gamma_{mm}^n a_m^n + b_m^n = \sum_\mu (\Theta_{m\mu}^n \alpha_\mu^n + \Xi_{m\mu}^n \beta_\mu^n) + (\tilde{H}_\phi)_m^n, \tag{4.50d}$$

In Eq.(4.50), a tilde above the E and H denotes symbolically the resulting terms associated with incident waves after the integration over z and the algebric rearrangement. The explicit forms of all the matrix elements $\Omega^n_{m\mu}$, $\Psi^n_{m\mu}$, $\Gamma^n_{m\mu}$, $\Pi^n_{m\mu}$, $\Delta^n_{m\mu}$, $\Theta^n_{m\mu}$, $\Xi^n_{m\mu}$, $\tilde{E}^n_{zm}$, $\tilde{E}^n_{\phi m}$, $\tilde{H}^n_{zm}$, and $\tilde{H}^n_{\phi m}$ are given in Appendix A. In terms of matrix notation, solution of Eq.(4.50) is

$$\alpha = \left[(\Psi - \Theta) - (\Xi - \Gamma\Omega)(\Delta - \Omega)^{-1}(\Gamma\Psi - \Pi)\right]^{-1} \times (\tilde{H}_\phi - \tilde{E}_z - \Gamma\tilde{H}_z - (\Xi - \Gamma\Omega)(\Delta - \Omega)^{-1}[\tilde{E}_\phi - \tilde{H}_z - \Gamma\tilde{E}_z]), \quad (4.51a)$$

$$\beta = (\Delta - \Omega)^{-1}((\Gamma\Psi - \Pi)\alpha - \tilde{E}_\phi - \tilde{H}_z - \Gamma\tilde{E}_z), \quad (4.51b)$$

$$a = \Omega\beta + \tilde{H}_z, \quad (4.51c)$$

$$b = \Psi\alpha + \tilde{E}_z. \quad (4.51d)$$

Substitution of Eq.(4.51) into Eq.(4.16) and Eq.(4.48) gives the exact solution for the electromagnetic waves in the entire space.

Various electromagnetic properties of the particle chain may be obtained from the rigorous scattering solution presented above. For instance, the scattering efficiency[10] of the periodic chain is readily derived as

$$Q_{sca} \equiv \frac{1}{2aL_0I_i}\int_0^{L_0}\frac{1}{2}\mathrm{Re}(\vec{E}_s \times \vec{H}_s^*)\cdot \hat{e}_r a\, d\phi\, dz$$

$$= \frac{2}{k_0 a}\sum_n \sum_{|m|\le m_{max}} (|a_m^n|^2 + |b_m^n|^2)\frac{1-\tilde{\gamma}_m^2}{\cos^2\theta_0} \quad (4.52)$$

where I_i is the intensity of the incident wave, $\tilde{\gamma}_m^2 = (\sin\theta_0 + 2\pi m/k_0L_0)^2$, and m_{max} is the maximum integer that satisfies $\tilde{\gamma}_m^2 \le 1$ for the scattering waves. ($m > m_{max}$ gives exponentially decaying evanescent waves). In the derivation of Eq.(4.52) we have used the asymptotic forms of $\vec{E}_s$ and $\vec{H}_s$ at $r/a \gg 1$. The total extinction efficiency by definition is

$$Q_{ext} \equiv \frac{-1}{2aL_0 I_i} \int_0^{L_0} \frac{1}{2} \mathrm{Re}(\vec{E}_I \times \vec{H}_s^* + \vec{E}_s \times \vec{H}_I^*) \cdot \hat{e}_r a \, d\phi \, dz$$

$$= \frac{2}{k_0 a} \sum_n \mathrm{Re}(b_0^n) \tag{4.53}$$

for the TM-polarized incident wave and

$$Q_{ext} = -\frac{2}{k_0 a} \sum_n \mathrm{Im}(a_0^n) \tag{4.54}$$

for the TE-polarized incident wave. From the definition of Q_{ext} the absorption efficiency can be obtained from Eqs.(4.52), (4.53), and (4.54) as

$$Q_{abs} = Q_{ext} - Q_{sca} \tag{4.55}$$

One can also study the angle- or wave-vector-dependent scattering behaviors of the chain. In particular, the effect of high-multipole couplings on the depolarized scattering, defined as the component of the scattered waves with electric field perpendicular to that of the incident field vector, can be examined. In next section we numerically evaluate the characteristics of absorption and scattering from our model and compare them with experimental data.

The key step in our formulation is the construction of an eigenvalue problem for the field in $r \leq a$ to capture the electromagnetic coupling between the cylinders. The eigenvalues are given by the roots of Eq.(4.32) for both TM ($\tau = \epsilon$) and TE ($\tau = 1$) polarizations. We first illustrate the properties of the eigenvalues by plotting in Fig.4.2 the left-hand side of Eq.(4.32), denoted as F, as a function of Λ^2. Here the wavelength is taken to be 7200 Å, the separation distance between the adjacent cylinders is 150 Å, and the wave is assumed to be normally incident. We have omitted the small imaginary part in the dielectric constant for the purpose of illustration. The zero crossings of the curve represent the solutions of Eq.(4.32), i.e., eigenvalues. It is noted from the plot that there

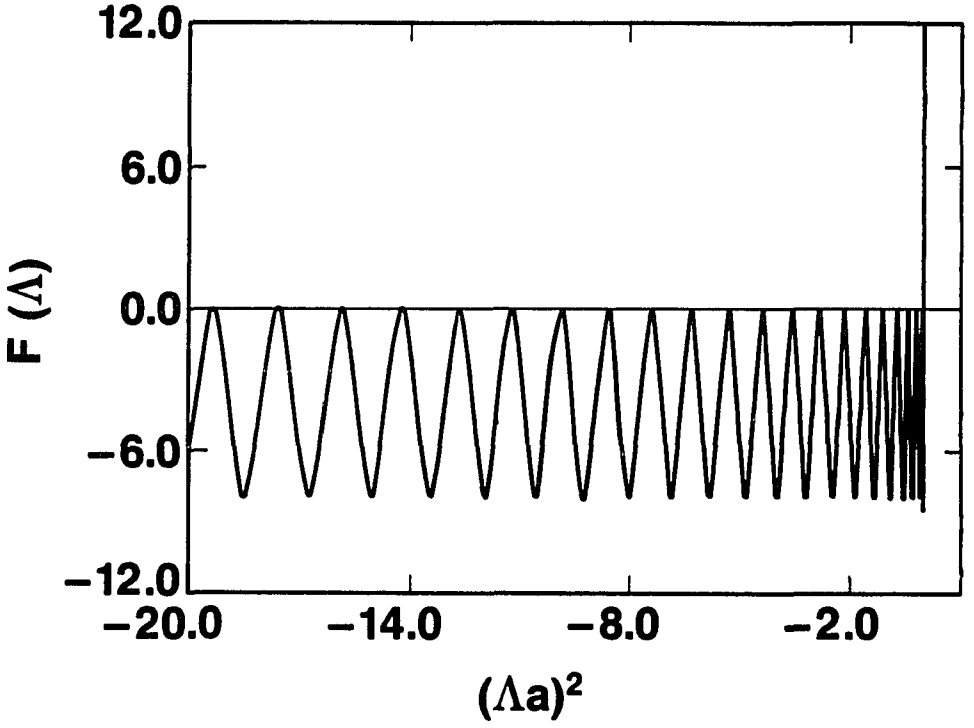

Figure 4.2a F[left-hand side of Eq.(4.32) with $\tau = \epsilon$] vs the dimensionless separation constant $(\Lambda a)^2$ for the TM mode. Here $\lambda_0 = 7200$ Å, $L = 150$ Å, and $d = 150$ Å. The zero crossings of F represent the eigenvalues. The maximum eigenvalue in this case is $(\Lambda a)^2 = (0.008944, 0.4227 \times 10^{-4})$, which corresponds to the lowest eigenmode.

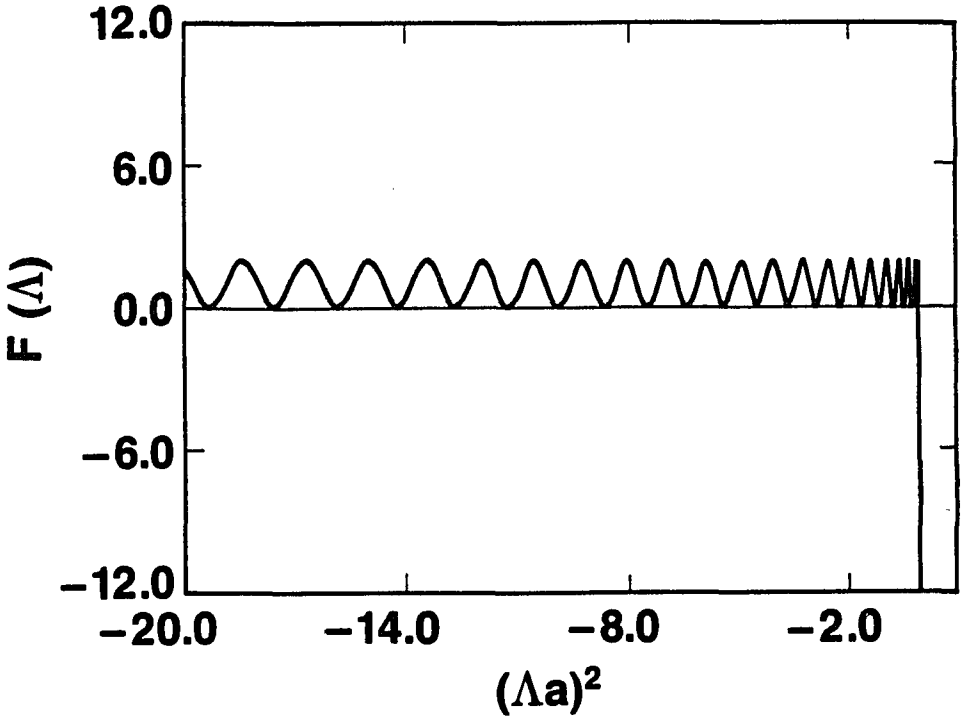

Figure 4.2b F[left-hand side of Eq.(4.32) with $\tau = 1$] vs the dimensionless separation constant $(\Lambda a)^2$ for the TE mode. The parameters are the same as those in the TM mode. The maximum eigenvalue in this case is $(\Lambda a)^2 = (-0.03538, 0.00246)$.

is always a maximum value for the real part of the eigenvalue. This enables us to order the eigenvalues according to the size of their real parts in the numerical calculation. The actual solutions of Eq.(4.32) in our calculation are obtained by a non-linear-equation solver routine with accurate trial solutions provided by the method discussed in Appendix B. Linear combinations of the eigenfields give the field configurations excited in the region $r \leq a$. We plot in Fig.4.3 for the same parameters the function $Z_i(z)$ of Eq.(4.25) to illustrate the z dependence of the eigenfunctions for the ground and excited states in both polarizations.

With the knowledge of the eigenvalues, the main task of the calculation is in calculating the matrix elements and obtaining the solution of Eq.(4.51). Since one cannot compute with infinite-order matrices, a resonable cutoff value for the matrix order indices m and μ is needed. In our case, a cutoff number for the order of the matrix is obtained when the expansion coefficients show indiscernable change by further increasing m and μ in the calculation. We found that $m \approx 15$ and $n = 6$ are sufficient for an accurate result. It is helpful to note for this part of the calculation that when the argument of Bessel and Henkel functions is large, it may pose problems for the accuracy for the matrix inversion. In this case, a redefinition (or scaling) of a_m^n, b_m^n, α_μ^n, and β_μ^n in Eq.(4.50) can make the problem well-posed again.

4.3 ABSORPTION CHARACTERISTICS

From experiments we set the parameters of our model as $L = 150$ $\mathring{A}$ and $a = 75$ $\mathring{A}$ corresponding to small spheres of diameter 150 $\mathring{A}$ in the aggregates[2,3]. The dielectric constant of the cylinder is obtained from the bulk dielectric constant of gold with the Drude collision time corrected due to the small particle size[12]. The matrix is water with an optical index of refraction of 1.33. In our numerical

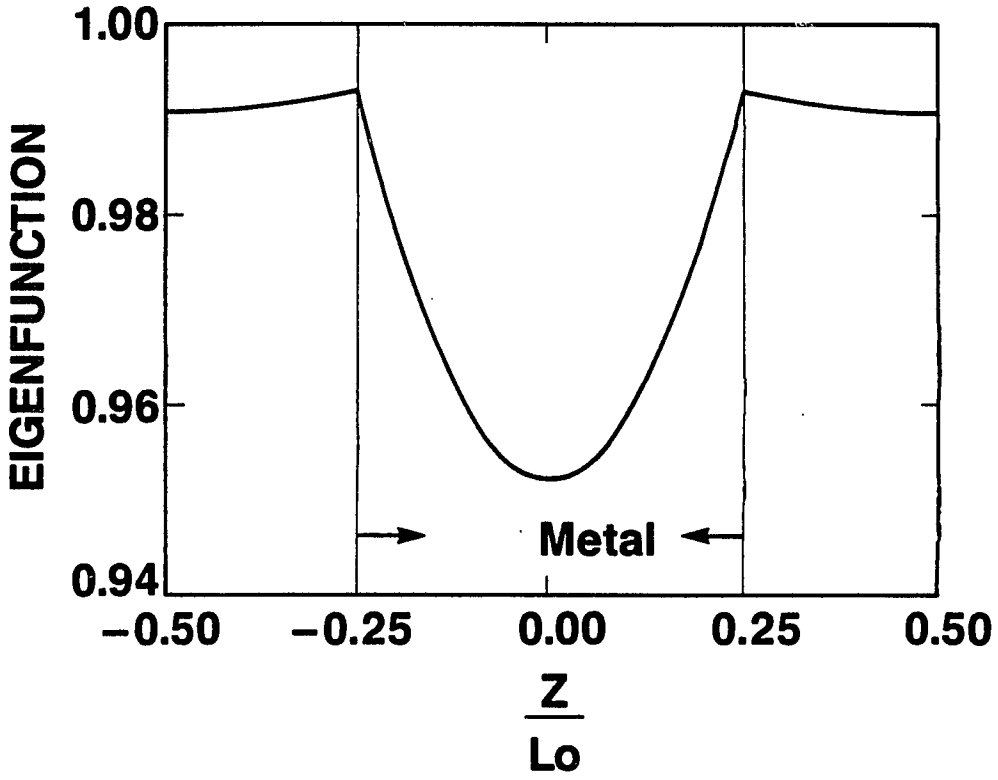

Figure 4.3a Plot of the ground-state eigenfunction $Z(z)$ in the TM mode.

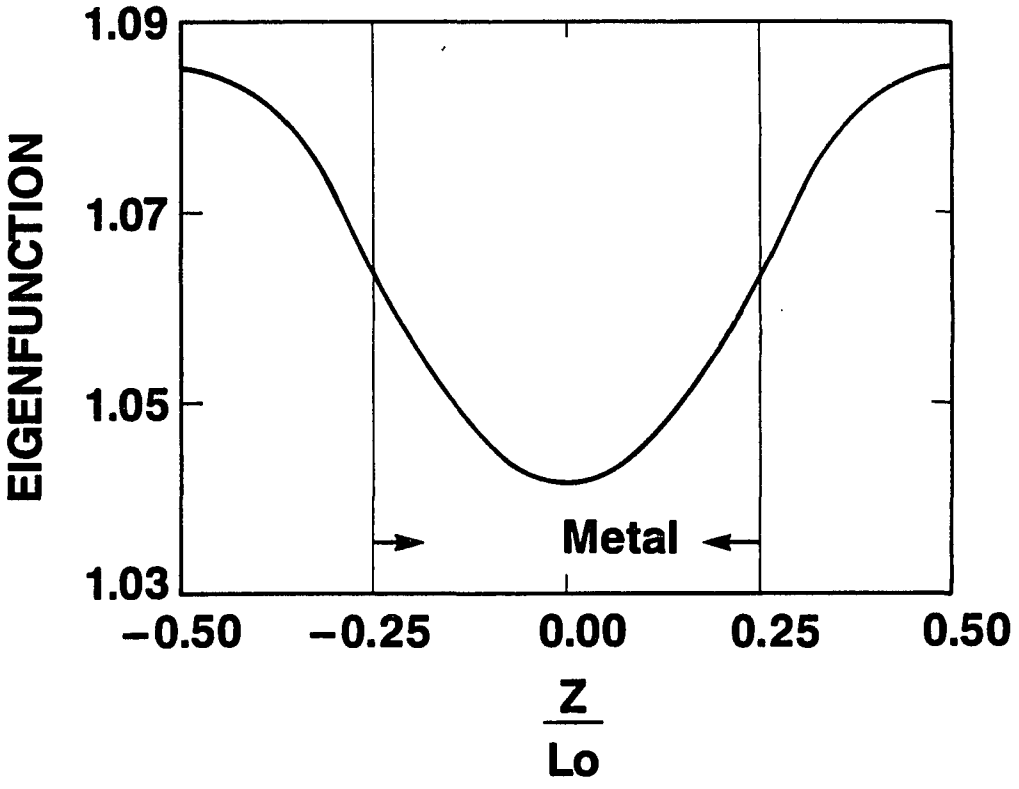

Figure 4.3b Plot of the ground-state eigenfunction $Z(z)$ in the TE mode.

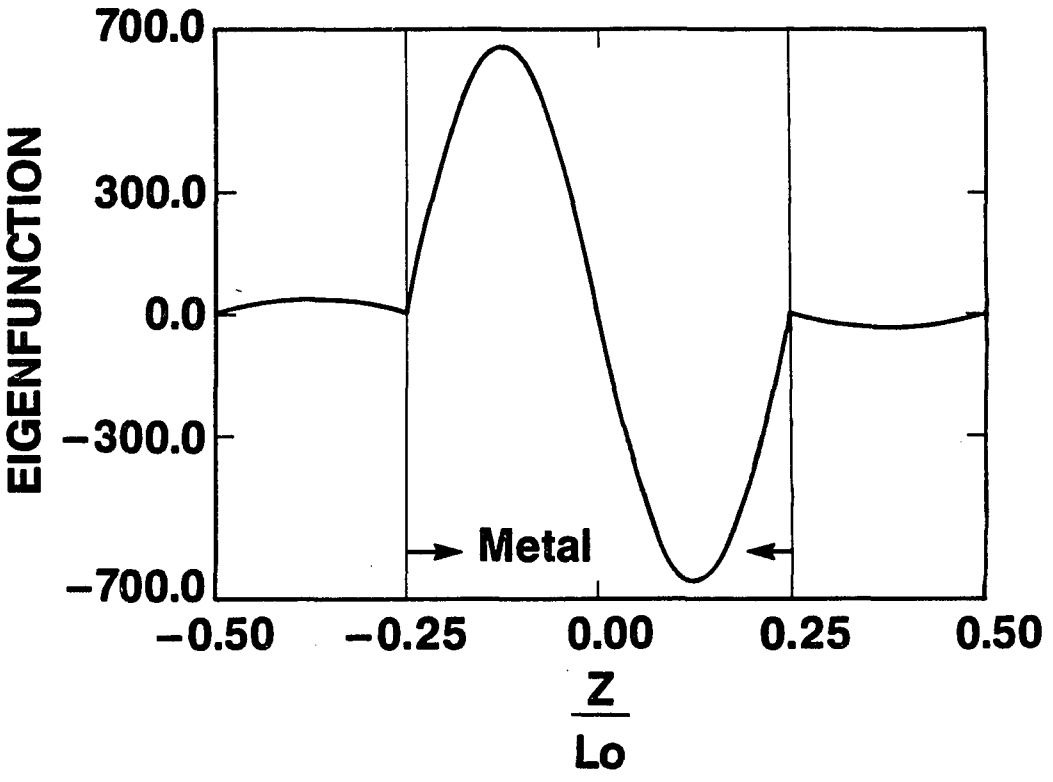

Figure 4.3c Plot of the excited eigenfunction $Z(z)$ in the TM mode.

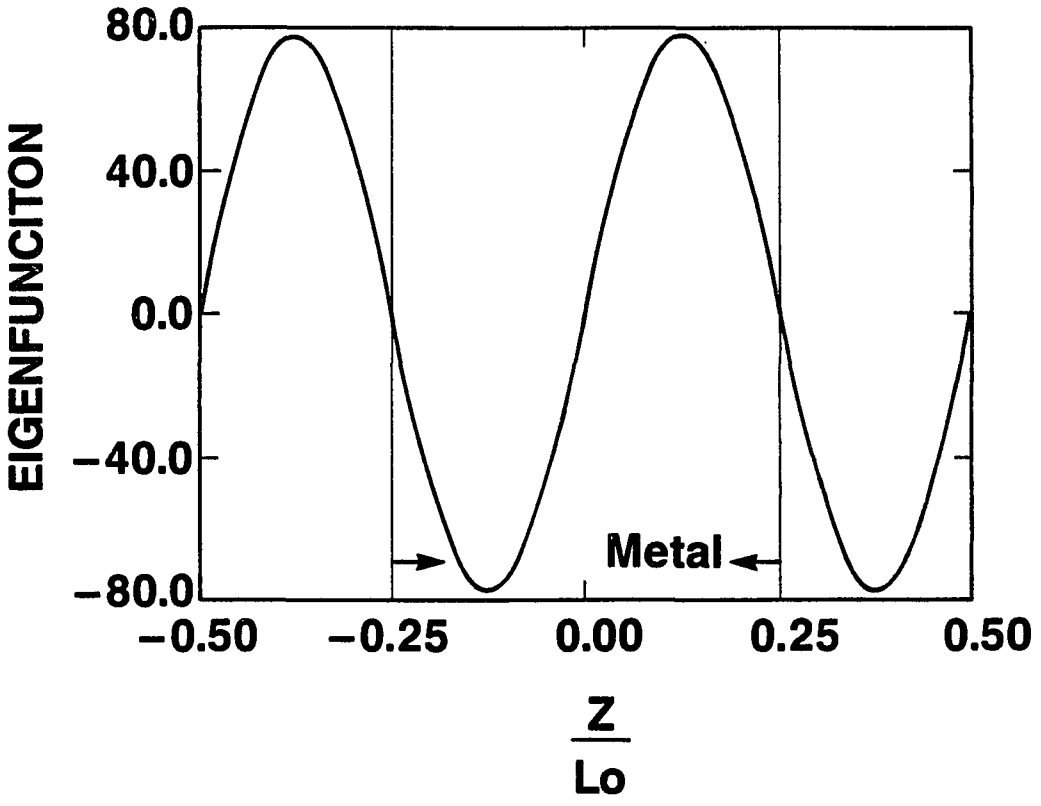

Figure 4.3d Plot of the excited eigenfunction $Z(z)$ in the TE mode.

calculations, we will concentrate on the properties in the optical frequencies.

Plotted in Fig.4.4 is the spectrum of absorption efficiency for different separation distances d when a normally incident wave is polarized perpendicular to the chain axis (TE mode). In this case one expects the electromagnetic excitations in adjacent cylinders to be weakly coupled. Indeed, the absorption is peaked within a very narrow frequency band around $\lambda = 5300$ $\mathring{A}$ which coincides with the Mie resonance for a single gold sphere*. This indicates that in the TE mode each particle absorbes independently. However, when the incident wave has an electric field component along the chain axis as in the TM mode, the single-particle character may be changed by the strong coupling of the electromagnetic fields between the adjacent cylinders. This is evident in the results shown Fig.4.5. For normal incidence the component of the oscillating incident electric field along the chain axis induces a collective excitation at longer wavelength with a magnitude much larger than the single-particle peaks shown in Fig.4.4. In fact, since Q_{abs} can be interpreted as the ratio of the absorption cross section to the geometric cross section, it is seen that the induced collective excitation absorbs nearly a factor of 5-10 times the intensity incident on the geometric cross section. The collective excitation peak positions are noted to be strongly dependent on the separation distance between the adjacent cylinders. In Fig.4.6 the peak frequency, normalized by the single-particle Mie-resonance frequency, is shown as a function of d/L. It is clear that when the cylinders are far apart, the collective excitation peak is positioned near the Mie-resonance peak, and as d decreases it shifts to lower and lower frequencies and eventually disappears into $\omega = 0$, recovering the solution for a homogeneous infinite cylinder[10]. Since the incident wavelength in

* For particle diameter between 50 and 200 Å, the Mie-resonance position is relatively independent of the particle size and is determined by the Frölich condition of $\epsilon + 2\epsilon_0 = 0$.

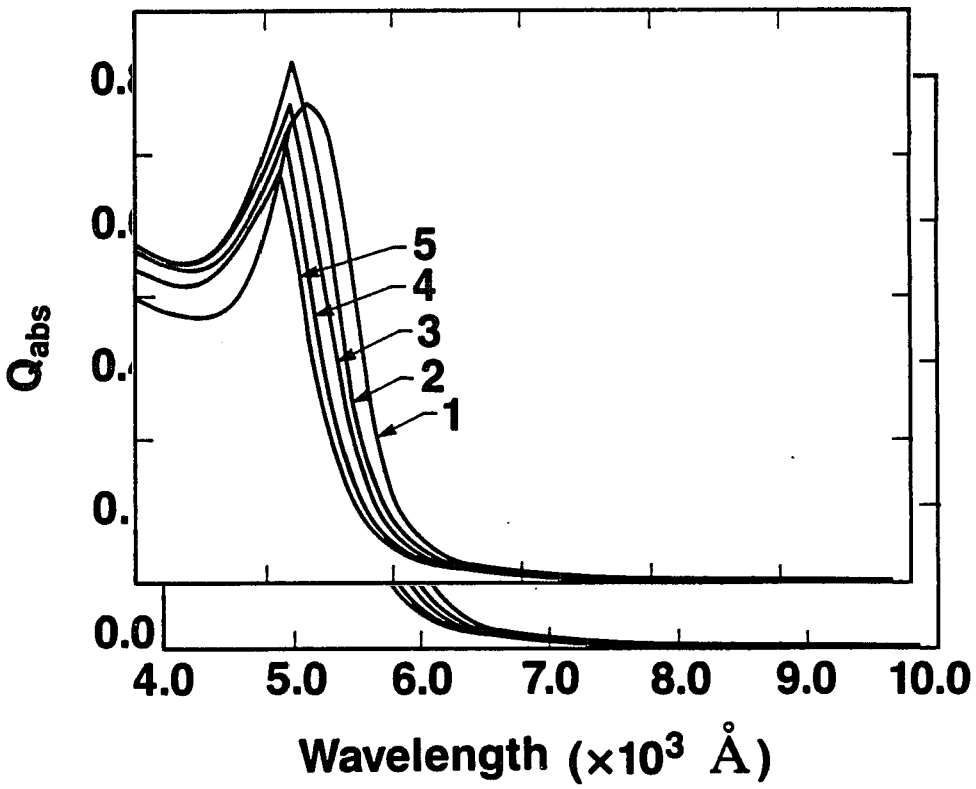

Figure 4.4 Spectra of absorption efficiency for a normally incident wave with electric field polarized perpendicular to the chain axis. The absorption characteristics with different separation distances are similar, with a peak around $\lambda = 5300$ Å. The number for each curve corresponding to the separation distances as follows: curve 1, $d = 150$ Å; curve 2, $d = 60$ Å; curve 3, $d = 40$ Å; curve 4, $d = 20$ Å; curve 5, $d = 10$ Å.

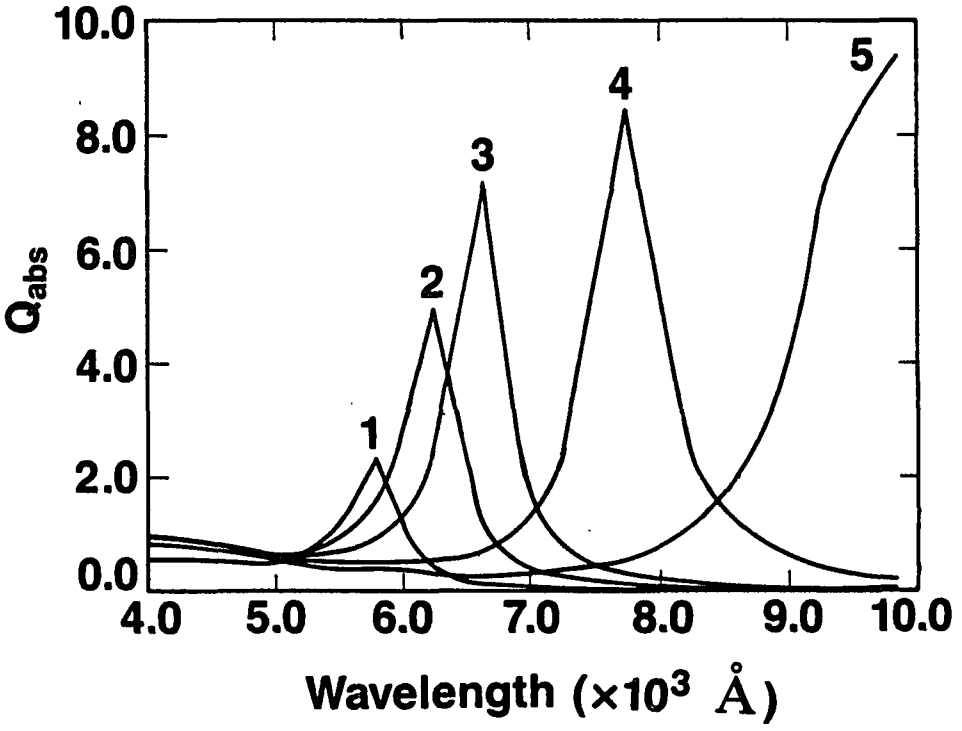

Figure 4.5 Spectra of absorption efficiency for a normally incident wave with electric field polarized along the chain axis. The position of the low-frequency absorption peak is noted to be strongly dependent on the separation distance d between adjacent cylinders. The value of d associated with each curve is the same as those indicated in Fig.4.4.

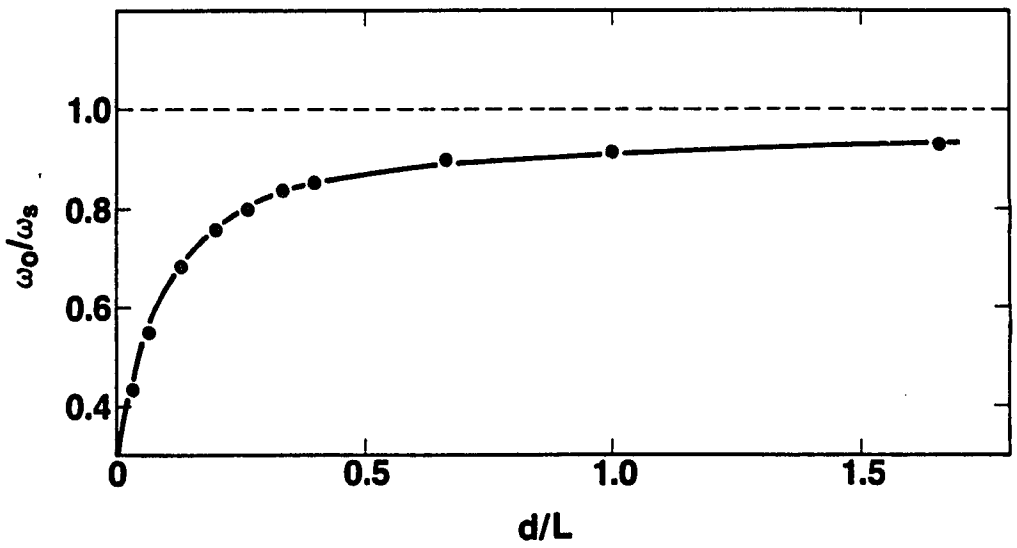

Figure 4.6 The red-shifted absorption peak position ω_0 normalized by the single-particle Mie-resonance frequency ω_s, plotted against d/L for a normally incident TM wave.

our problem is much larger than the particle sizes, the $m = 0$ mode is dominant in the calculated absorption characteristics. We note, however, that while the red shift is predominantly a dipolar effect, yet the magnitude of the shift does depend on the sum of all higher-order multipole interactions. Traditionally, the effect of these higher-order multipole interaction has been equated to the appearance of multiple peaks in the absorption spectrum. Since this phenomenon is not apparent in our present calculation, we have performed separate calculations on tin particles where the multiple peaks have been obtained by Fuchs *et al*[4]. Our results, presented in Appendix C, show that multiple peaks indeed appear in that case. We therefore conclude that the appearance or nonappearance of multiple peaks is also dependent on the dielectric constant and is not necessarily an indication of the presence or absence of multipole interactions. Another point we wish to note here is that the simplicity of our calculational method remains as one goes beyond the long-wavelength limit.

In Fig.4.7(a). we show the absorption spectra for a TM wave incident at two different angles away from normal. The separation distance d is set at 30 Å. It is clear that in both cases there are two peaks appearing simultaneously. By coupling this fact with the absorption characteristics of TE wave incident at these angles as shown in Fig.4.7(b), we conclude that when an aggregate cluster with locally chain-like structures is illuminated by an arbitrary incident wave, the absorption spectrum should display a double-peak character as seen experimentally[2]. Plotted in Fig.4.8 are the calculated solid-angle-averaged absorption efficiency, $< Q_{abs} >= \int Q_{abs}(\theta_0, \phi_0) d\Omega_0 / \int d\Omega_0$ (dashed line) and the experimental results (solid line). The value of d is set at 24 Å, which is calculated by equating the capacitance $C = \epsilon_0 \pi a^2 / 4\pi d$ for a capacitor of area πa^2 and separation d with that of two touching spheres of radius a, given by $2a \ln 2$. The agreement with

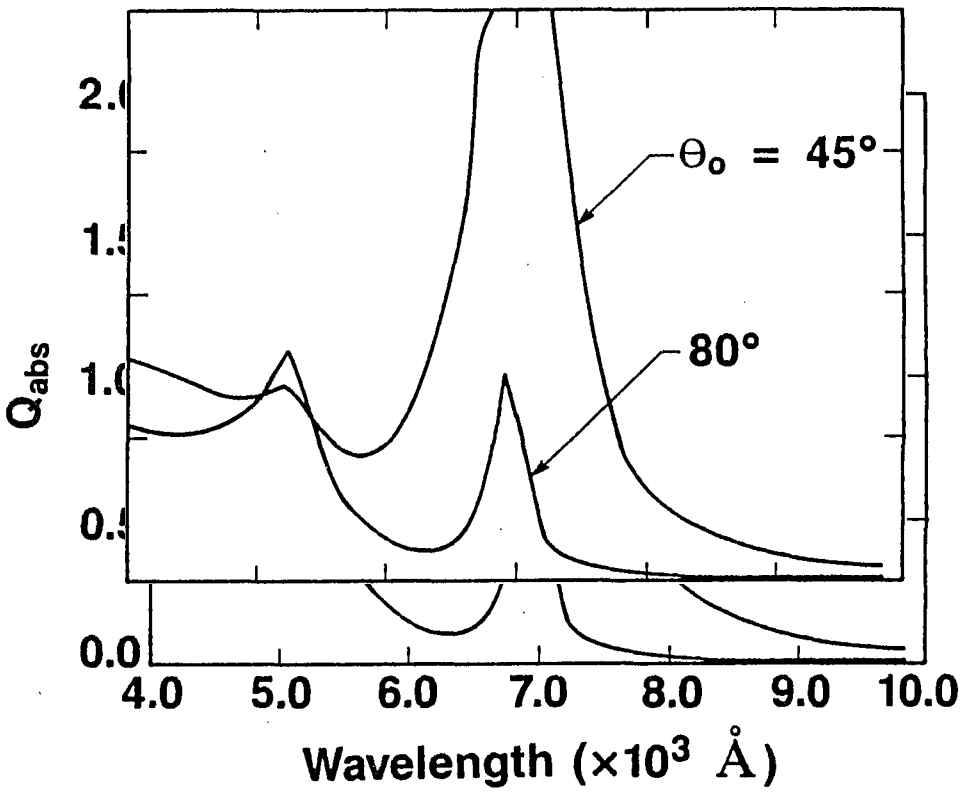

Figure 4.7a Spectra of absorption efficiency for a TM wave at two different incident angles. Two absorption peaks appear simultaneously in the spectra. When the incident angle is further away from the normal, the single-particle Mie-resonance peak becomes larger relative to the low-frequency excitation peak.

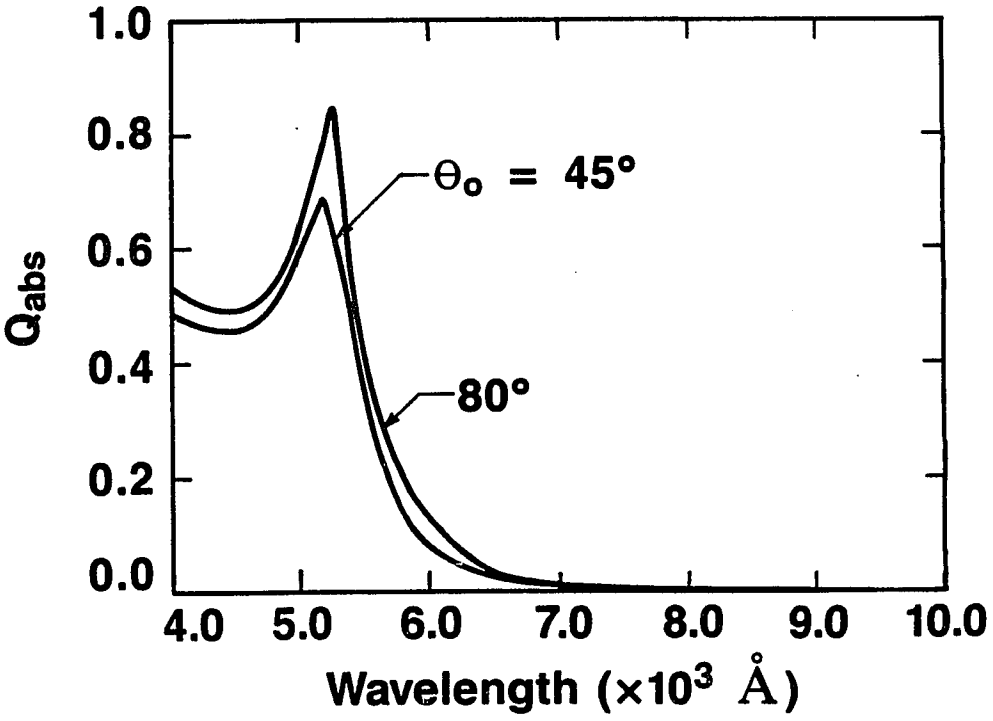

Figure 4.7b Spectra of absorption efficiency for a TE wave at two different incident angles. In contrast to the TM wave as shown in (a), only one absorption peak appears at the single-particle Mie-resonance frequency.

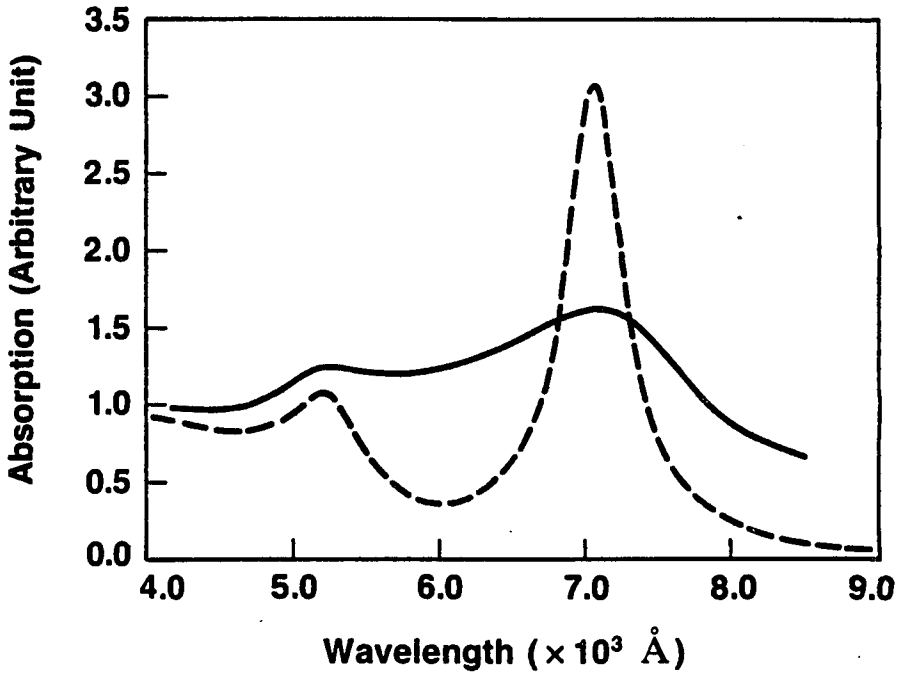

Figure 4.8 Comparison of the calculated solid-angle-averaged absorption coefficient (dashed line) with the experimental result of the fractal gold aggregates (solid line). The calculated result has been normalized to the experimental result at $\lambda = 4000\ \mathring{A}$

the experimentally observed low-frequency peak position is seen to be excellent. The overall agreement is very good in view of the simplicity of our model. The difference in width and strength of the low-frequency peak is probably due to the finite chain length and its broad size distribution. Nevertheless, the appearance of the low-frequency absorption peak is a clear indication that the anisotropic multipole interaction plays an important role in the optical-absorption characteristics of aggregate clusters.

4.4 SCATTERING NEAR COLLECTIVE EXCITATION

Now let us examine the scattering characteristics of the model. Figure 4.9 shows a typical spectrum of scattering efficiency. The incident wave is polarized along the chain axis with an incident angle $\theta_0 = 60^0$ and the separation distance $d = 30$ Å. Scattering is greatly enhanced at the low-frequency collective excitation frequency, in agreement with the experiment. However, the calculated results predicts a narrower width and sronger intensity than experimental result, as expected. (The effects of the collective excitation on the q-dependence of the polarized scattering has been discussed in Chapter 3). Since the optical extinction is the sum of the absorption and scattering, the above results imply that the optical extinction is greatly enhanced at this frequency due to the electromagnetic coupling between the cylinders.

A direct observable manifestation of the collective excitation is the magnitude of the depolarized scattering, which can be characterized by means of a ratio of the depolarized scattering, $R = I_{VH}/I_{VV}$, where $I_{VH}(I_{VV})$ is the depolarized (polarized) scattering intensity. In Fig.4.10 we compare the calculated R (after solid-angle averaging) with the experiment. The magnitude of the calculated polarized scattering has been normalized to the value measured at 4880 Å. Here

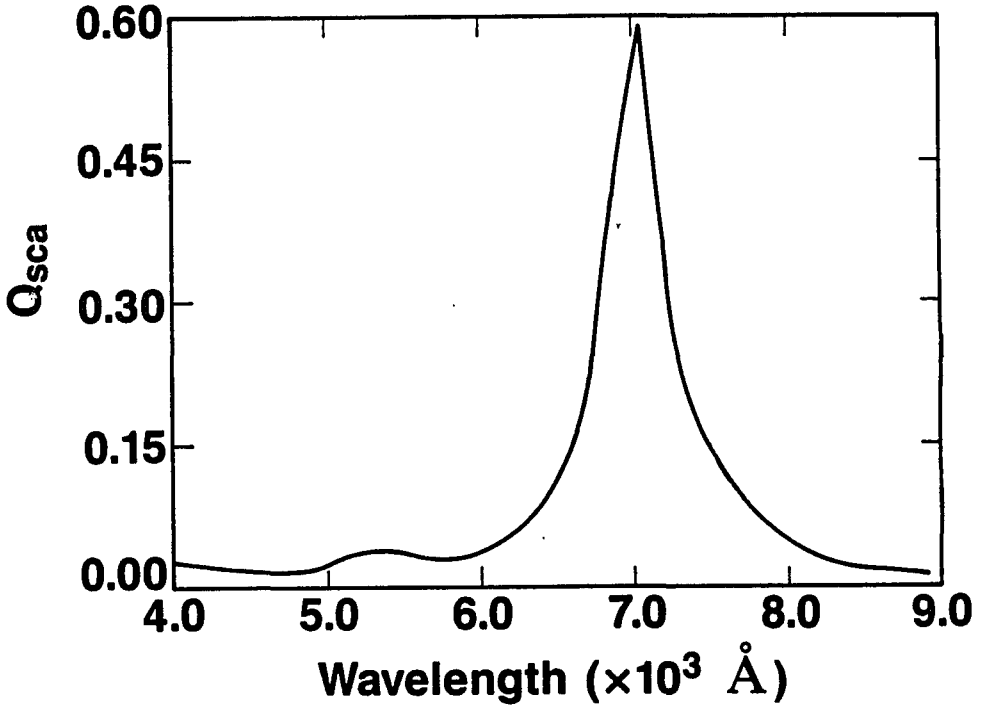

Figure 4.9 Scattering efficiency plotted as a function of λ. The incident wave is polarized in the incident plane with the incident angle at 60^0. The value of d is set at 30 $\mathring{A}$. The scattering is seen to be enhanced near the peak of the low-frequency excitation.

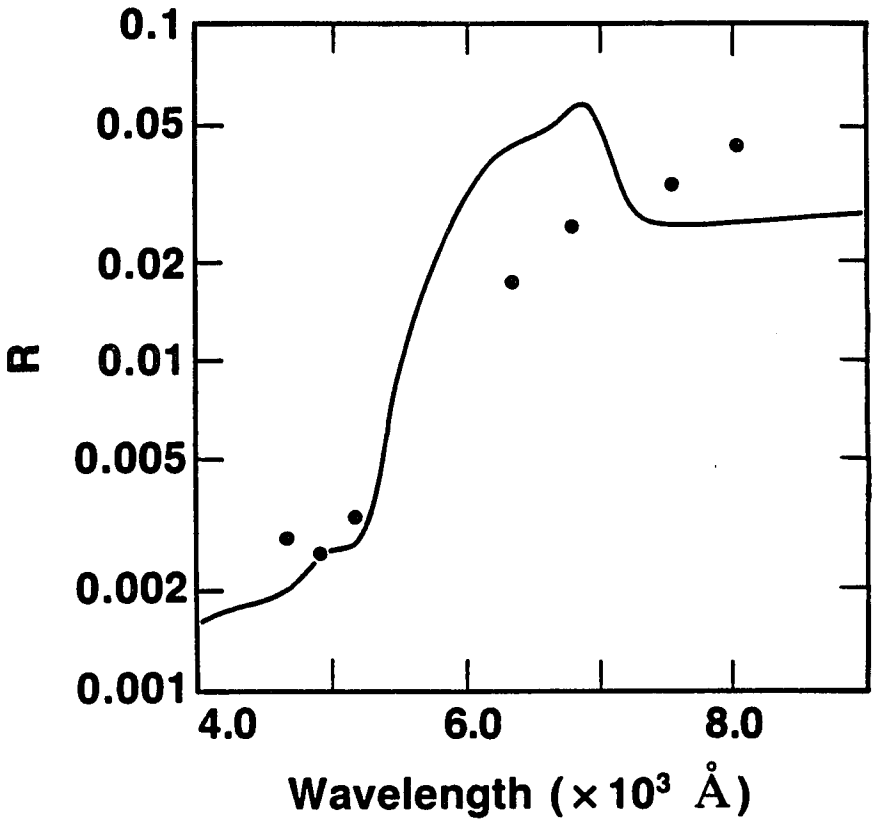

Figure 4.10 Comparison of the depolarized ratio between the calculated (solid-angle-averaged) result and the experiment. The calculated and measured polarized scatterings are normalized at $\lambda = 4880$ Å.

the d is set again at 24 Å. Since the polarized scattering is highly wave-vector dependent, the experimental data are all measured at the same $q = 0.01$ nm^{-1}. The agreement with our theoretical calculation is very good, correctly accounting for the rise in R as I_{VV} increases due to the collective excitation.

4.5 SUMMARY

We have formulated a simple method for the rigorous solution of the electromagnetic scattering properties of a periodic chain of cylinders. The model allows a detailed study of the electromagnetic coupling between cylinders and its relationship to the geometric sizes and material compositions of the chain. Application of the model to the elucidation of optical characteristics of small gold-particle aggregates indicates that the second absorption peak as well as the enhanced depolarized scattering arise from high-multipole interaction between neighboring particles, with the position of peak controlled by the strength of capacitive coupling. However, we note that the structure of real aggregates is much more complicated than the simple periodic chain and accurate modeling of its optical behavior would require much more effort. Yet the rigorous solution of our simple model indicates what may result if one has the ability to control the precise microstructure and actually produce cylindrically segmented particles. One application would be the control over position of the absorption peak which would be useful in infrared detection. In fact, further study in this direction has already revealed rich infrared and far-infrared absorption characteristics[13] associated with the variation in the geometric parameters.

Appendix A

The matrix elements of Eq.(4.50) are as follows:

$$\Omega^n_{m\mu} = \left(\frac{\Lambda^e_\mu}{\tilde{u}_m\eta}\right)^2 \frac{J_n(\Lambda^e_\mu)}{H^{(1)}_n(\tilde{u}_m\eta)} I^{(a)}_{m\mu}(\Lambda^e_\mu), \tag{A.1}$$

$$\Psi^n_{m\mu} = j\left(\frac{\Lambda^h_\mu}{\tilde{u}_m\eta}\right)^2 \frac{J_n(\Lambda^h_\mu)}{H^{(1)}_n(\tilde{u}_m\eta)} I^{(b)}_{m\mu}(\Lambda^h_\mu), \tag{A.2}$$

$$\Pi^n_{m\mu} = \frac{nJ_n(\Lambda^h_\mu)}{\tilde{u}_m\eta H^{(1)}_n{}'(\tilde{u}_m\eta)} J^{(b)}_{m\mu}(\Lambda^h_\mu), \tag{A.3}$$

$$\Delta^n_{m\mu} = \frac{\Lambda^e_\mu J_n{}'(\Lambda^e_\mu)}{\tilde{u}_m\eta H^{(1)}_n{}'(\tilde{u}_m\eta)} I^{(a)}_{m\mu}(\Lambda^e_\mu), \tag{A.4}$$

$$\Theta^n_{m\mu} = j\frac{\Lambda^h_\mu J_n{}'(\Lambda^h_\mu)}{\tilde{u}_m\eta H^{(1)}_n{}'(\tilde{u}_m\eta)} I^{(a)}_{m\mu}(\Lambda^h_\mu), \tag{A.5}$$

$$\Xi^n_{m\mu} = \frac{nJ_n(\Lambda^e_\mu)}{j\tilde{u}_m\eta H^{(1)}_n{}'(\tilde{u}_m\eta)} J^{(a)}_{m\mu}(\Lambda^e_\mu), \tag{A.6}$$

$$\Gamma^n_{mm} = \frac{nH_n(\tilde{u}_m\eta)}{j\tilde{u}_m\eta H^{(1)}_n{}'(\tilde{u}_m\eta)} J^{(a)}_{m\mu}(\Lambda^e_\mu), \tag{A.7}$$

and the corresponding components of incident waves for case (1), the TM mode, are

$$(\tilde{E}^{(1)}_Z)_m = -E_n \frac{J_n(\eta\cos\theta_0)}{H^{(1)}_n(\eta\cos\theta_0)}\delta_{m0}, \tag{A.8}$$

$$(\tilde{E}_{\phi}^{(1)})_m = -E_n \frac{n \sin\theta_0 J_n(\eta \cos\theta_0)}{\eta \cos\theta_0 H_n^{(1)\prime}(\eta \cos\theta_0)} \delta_{m0}, \tag{A.9}$$

$$(\tilde{H}_{Z}^{(1)})_m = 0, \tag{A.10}$$

$$(\tilde{H}_{\phi}^{(1)})_m = -E_n \frac{J_n'(\eta \cos\theta_0)}{H_n^{(1)\prime}(\eta \cos\theta_0)} \delta_{m0}. \tag{A.11}$$

For case (2), the TE mode, we have

$$(\tilde{E}_{Z}^{(2)})_m = 0, \tag{A.12}$$

$$(\tilde{E}_{\phi}^{(2)})_m = jE_n \frac{J_n'(\eta \cos\theta_0)}{H_n^{(1)\prime}(\eta \cos\theta_0)} \delta_{m0}, \tag{A.13}$$

$$(\tilde{H}_{Z}^{(2)})_m = jE_n \frac{J_n(\eta \cos\theta_0)}{H_n^{(1)}(\eta \cos\theta_0)} \delta_{m0}, \tag{A.14}$$

$$(\tilde{H}_{\phi}^{(2)})_m = jE_n \frac{n \sin\theta_0 J_n(\eta \cos\theta_0)}{\eta \cos\theta_0 H_n^{(1)\prime}(\eta \cos\theta_0)} \delta_{m0}. \tag{A.15}$$

Here $\eta = k_0 a$, $\tilde{\gamma}_m = \sin\theta_0 + 2\pi m/k_0 L_0$, and $\tilde{u}_m = (1-\tilde{\gamma}_m^2)^{1/2}$, δ is the Kronecker delta function, E_n is given by Eq.(), the prime denotes the derivative with respect to the entire argument, and

$$I_{m\mu}^{(a,b)}(\Lambda_\mu) = \frac{1}{L_0} \int_0^{L_0} \mathcal{F}^{(a,b)}(\Lambda_\mu) e^{-jk_0 \tilde{u}_m z} dz, \tag{A.16}$$

$$J_{m\mu}^{(a,b)}(\Lambda_\mu) = \frac{1}{L_0} \int_0^{L_0} \frac{\partial \mathcal{F}^{(a,b)}(\Lambda_\mu)}{\partial z} e^{-jk_0 \tilde{u}_m z} dz, \tag{A.17}$$

where $\mathcal{F}^{(a)}(\Lambda_\mu)$ corresponds to the function Z_i of Eq.(4.25) for each homogeneous region along the z direction and $\mathcal{F}^{(b)}(\Lambda_\mu)$ corresponds to Z_i/ϵ_i in the corresponding homogeneous region.

Appendix B

Maxwell's equation for the TM mode give two coupled equations relating H_ϕ and E_r:

$$\frac{\partial H_\phi}{\partial z} = jk_0\epsilon(z)E_r, \tag{B.1a}$$

$$\frac{\partial E_r}{\partial z} = jk_0\left(1 - \frac{\Lambda^2}{\epsilon(z)k_0^2}\right)H_\phi \tag{B.1b}$$

Similar equations hold between H_z and E_ϕ. The Fourier transform of the above equations yields

$$\gamma_m \mathcal{H}_m = k_0 \sum_p \epsilon_{m-p}\mathcal{E}_p, \tag{B.2a}$$

$$\gamma_p \mathcal{E}_p = \sum_m \left(k_0\delta_{pm}\mathcal{H}_m - \frac{\Lambda^2}{k_0}\sigma_{p-m}\mathcal{H}_m\right) \tag{B.2b}$$

In Eq.(B.2) $\mathcal{H}$ and $\mathcal{E}$ represent the Fourier components of the fields. Substituting Eq.(B.2b) into Eq.(B.2a), we have

$$AX = \Lambda^2 BX, \tag{B.3}$$

where X denotes the field components, Λ^2 is the separation constant, and the matrix elements of A nad B are

$$A_{ij} = k_0^2\frac{\epsilon_{i-j}}{\gamma_j} - \gamma_j\delta_{ij}, \tag{B.4}$$

$$B_{ij} = \sum_{k=-\infty}^{\infty} \epsilon_{i-k}\frac{1}{\gamma_k}\sigma_{k-j}, \tag{B.5}$$

in which δ is the Kronecker delta function,

$$\epsilon_k = \frac{1}{L_0}\int_0^{L_0} \epsilon(z)e^{j(2\pi k/L_0)z}dz, \tag{B.6}$$

$$\sigma_k = \frac{1}{L_0}\int_0^{L_0} \frac{1}{\epsilon(z)}e^{j(2\pi k/L_0)z}dz, \tag{B.7}$$

and

$$\gamma_j = k_0 \sin\theta_0 + \frac{2\pi j}{L_0}. \tag{B.8}$$

The solution of the eigenvalue equation (B.3) would thus provide fairly accurate trial solution to Eq.(4.32) in the text.

For the TE mode, we also have two coupled equations

$$\frac{\partial E_r}{\partial z} = jk_0\epsilon(z)H_\phi, \tag{B.9a}$$

$$\frac{\partial H_\phi}{\partial z} = jk_0\left(\epsilon(z) - \frac{\Lambda^2}{k_0^2}\right)E_r, \tag{B.9b}$$

and the equation between E_ϕ and H_r are similar to Eq.(B.9). The Fourier components of the field satisfy an equation similar to Eq.(B.3) with

$$A_{ij} = k_0\epsilon_{i-j} - \gamma_j^2\delta_{ij}, \tag{B.10}$$

$$B_{ij} = \delta_{ij}. \tag{B.11}$$

Appendix C

In this Appendix, we present a comparison of our calculation on a chain of tin particles with that of Fuchs *et al.*[4] on two tin spheres in order to illustrate the effect of higher-order multipole interactions.

The parameters used in Ref. 12a are as follows: the radius of a sphere $a = 30$ Å, the separation between two centers of the spheres $D = 61$ Å, and the dielectric constant is given by Drude model with a plasmon frequency $\omega_p = 1.17 \times 10^6$ sec^{-1}, Fermi velocity $v_F = 1.24 \times 10^8$ cm/sec, and electron mean free path $\ell \sim a$. The main feature in the spectrum that is attributed to multipole interaction is the presence of multiple peaks.

In our calculation, we use the same dielectric constant and set the radius of the cylinder at 30 $\mathring{A}$ and the length of the cylinder at 60 Å. Since our model consists of a chain of particles, instead of two spheres, there can not be an exact comparison. However, in Fig. 11 we show that if the particle separation is set at 30 Å, there is a very close qualitative correspondence with the calculated spectrum of Fuchs *et al.*[4] In particular, the multiple peaks that have been attributed to multipole interaction have all been reproduced.

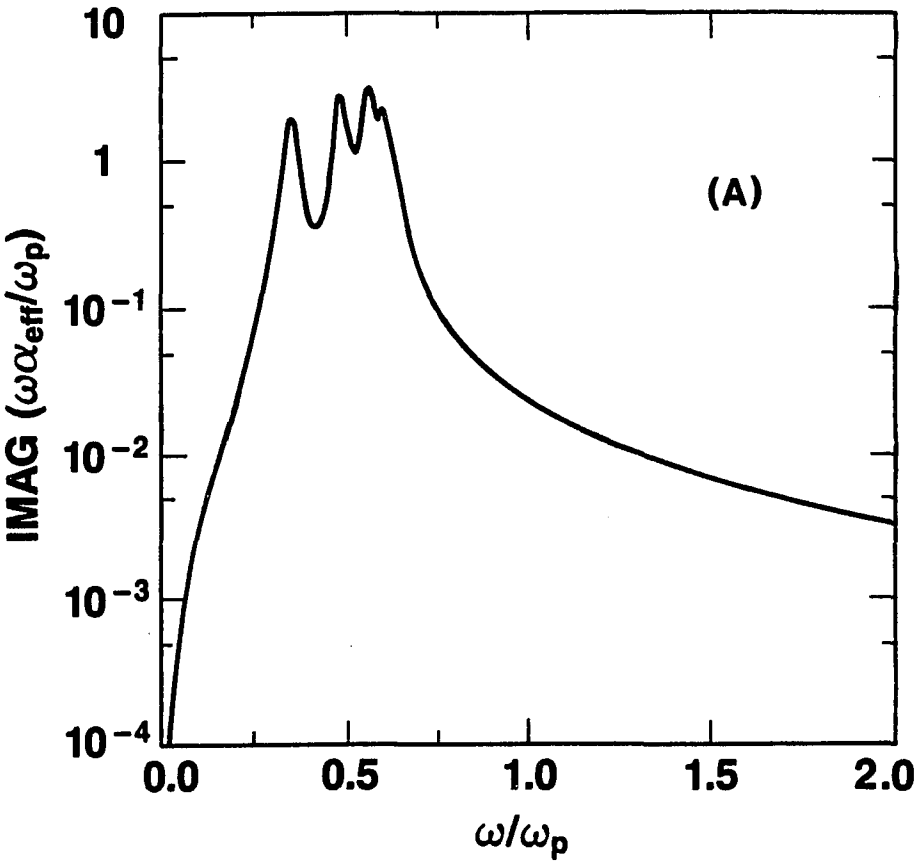

Figure 4.11a Illustration of the effect of high-order multipole interaction for tin particles. Plotted here is the result of Fuchs *etal* for two tin spheres. Parameters used are discussed in Appendix C.

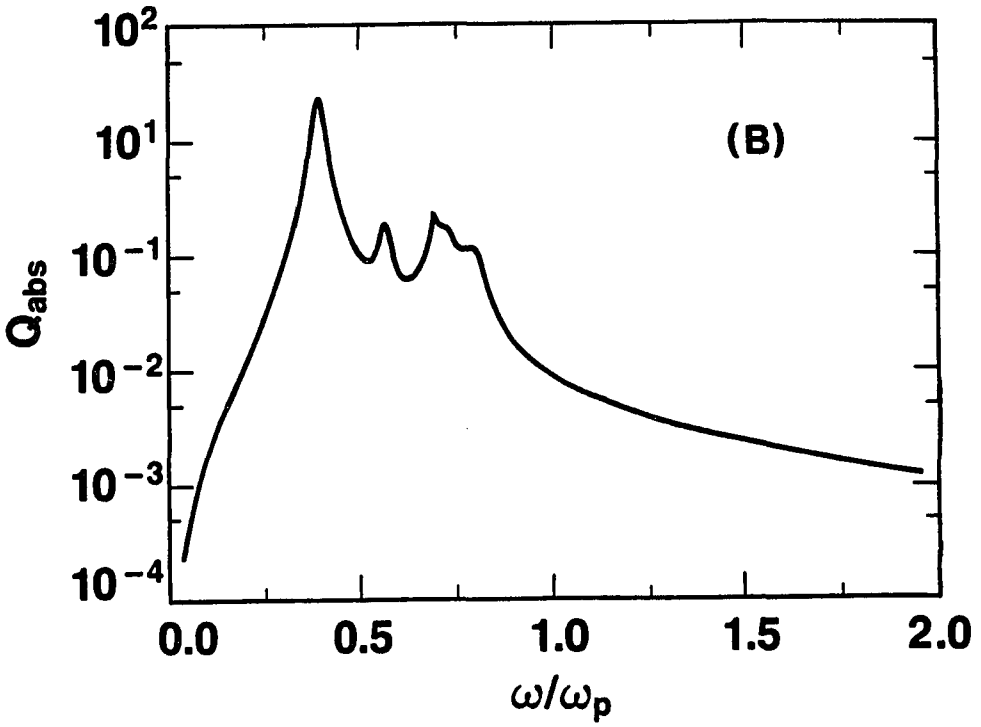

Figure 4.11b Absorption spectrum of a chain of tin particles. Parameters used are discussed in Appendix C. The magnitude of absorption plotted here and in the figure 4.11a differs by a calibration factor. It is appearant from this plot that all the multiple peaks traditionally attributed to the high-order multipole interaction are reproduced in our calculation.

REFERENCES

1. R. Landauer, in *Electrical Transport and Optical Properties of Inhomogeneous Media* (American Institute of Physics, New York, 1978), p.2; D. Stroud and F. P. Pan, *Phys. Rev. B* **17**, 1602 (1978).

2. M. H. Lindsay, M. Y. Lin, D. A. Weitz, P. Sheng, Z. Chen, R. Klein, and P. Meakin, Faraday Discuss. Chem. Soc. **83**, 153, (1987).

3. D. A. Weitz, M. Y. Lin, J. S. Huang, T. A. Witten, S. K. Sinha, J. S. Geljner, and R. C. Ball, in *Scaling Phenomena in Disordered Systems*, Vol. 133 of *NATO Advanced Study Institute Conference, Series B*, edited by R. Pynn and A. Skjeltorp (Plenum, New York, 1985).

4. R. Fuchs and F. Claro, *Phys. Rev. B* **35**, 3722 (1987); F. Claro, *ibid*, 30, 4989, 1984; and references therein.

5. J. M. Gerardy and Ausloos, *Phys. Rev. B* **22**, 4950 (1980), and references therein.

6. P. Clippe, E. Evrard, and A. A. Lucas, *Phys. Rev. B* **14**, 1715 (1976).

7. U. Kreibig, A Althoff, and M. Pressmann, *Surf. Sci.* **106**, 308 (1981); M. Quinten and U. Kreibig, *ibid*, 172, 557, 1986.

8. K. Ohtaka and Inoue, *Phys. Rev. B* **19**, 5057 (1979); **25**, 689 (1982); **26**, 3487 (1982); *J. Phys. Jpn.* **52**, 1457 (1982).

9. Z. Chen and P. Sheng, *Phys. Rev. B* , 39, 9816 (1989).

10. see, for example, C. F. Bohren and D. R. Huffman, *Absorption and Scattering of Light by Small Particles* (wiley, New York, 1983).

11. P. Sheng, R. S. Stepleman, and P. N. Sanda, *Phys. Rev. B* , 26, 2907 (1973).

12. R. W. Cohen, G. D. Cody, M. D. Coutts, and B. Abeles, *Phys. Rev. B* **8**, 3689 (1973).

13. M. Y. Zhou, P. Sheng, Z. Chen, and S. T. Chui, (unpublished).

BIBLIOGRAPHY

Alder, B. L., J. -J. Weis and H. L. Strauss, *Phys. Rev.* **A7**, 281 (1973).

Berry, M. V. and I. C. Percival, *Opt. Acta.* **33**, 577 (1986).

Billmeyer, S. W. and M. Saltzman, *Principles of Color Technology* (Wiley, New York, 1967).

Bohren, C. F. and D. R. Huffman, *Absorption and Scattering of Light by Small Particles* (wiley, New York, 1983).

Born, M. and E. Wolf, *Principles of Optics* (Pergamon Press, Oxford, 1975), 5th edition, P. 100.

Bragg, W. L. and A. B. Pippard, *Acta. Cryst.* **6**, 865 (1953).

Brown, W. F. Jr., *J. Chem. Phys.* **23**, 154 (1955).

Bruggeman, D. A. G., *Ann. Physik (Leipz.)* **24**, 636 (1935).

Bruggeman, D. A. G., *Ann. Physik (Leipz.)* **24**, 665 (1935).

Bruggeman, D. A. G., *Ann. Physik (Leipz.)* **25**, 645 (1936).

Chen, Z. and P. Sheng, *Phys. Rev. B* , 39, 9816 (1989).

Chen, Z., P. Sheng, D. A. Weitz, M. H. Lindsay, M. Lin, and P. Meakin, *Phys. Rev. B* **37**, 5232 (1988).

Claro, F., *Phys. Rev. B* **30**, 4989 (1984).

Clausius, R., *Die Mechanische Behandlung der Electricität*, (Vieweg-Verlag, Brunswick, 1879), Vol. II.

Clippe, P., E. Evrard, and A. A. Lucas, *Phys. Rev. B* **14**, 1715 (1976).

Cohen, R. W., G. D. Cody, M. D. Coutts, and B. Abeles, *Phys. Rev. B* **8**, 3689 (1973).

de Boer, J., F. ran der Maesen, and C. A. tan Seldam, *Physica* **19**, 265 (1955).

Debye, P., *Polar Molecules* (The Chemical Catalog Company, Inc., New York, 1929), P.27.

DeRis, J., *Seventeenth Symposium (International) on Combustion* (Combustion Institute, Pittsburg, PA, 1978), P.1103.

Family, F. and D. P. Landau, editors, *Kinetics of Aggregation and Gelation* (Elsevier, Amsterdam, 1984).

Felderhof, B. U., *J. Phys.* **C15**, 3943 (1982).

Felderhof, B. U., *J. Phys.* **C15**, 3953 (1982).

Felderhof, B. U., G. W. Ford, and E. G. D. Cohen, *J. Stat. Phys.* **28**, 649 (1982).

Felderhof, B. U., G. W. Ford, and E. G. D. Cohen, *J. Stat. Phys.* **33**, 241 (1983).

Foldy, L. L., *Phys. Rev.* **67**, 107 (1945).

Frölich, H. *Theory of Dielectrics* (Oxford University Press, 1958), 2nd edition.

Fuchs, R. and F. Claro, *Phys. Rev. B* **35**, 3722 (1987).

Garnett, J. C. M., *Philos. Trans. R. Soc. Lond.* **203**, 385 (1904).

Gebelein, C. G., editor *Polymer Materials and Artificial Organs* (American Chemical Society, Washington, D. C., 1984).

Gebelein, C. G., P. J. Williams, and R. D. Deanin, editors, *Polymer in Solar Energy Utilization* (American Chemical Society, Washington, D. C., 1983).

Geigenmüuer, U. and P. Mazar, *Physica* **136A**, 316 (1986).

Gerardy, J. M. and Ausloos, *Phys. Rev. B* **22**, 4950 (1980).

Gittleman, J. I. and B. Abeles, *Phys. Rev. B* , 15, 3273 (1977).

Hashin, Z. and S. Strikman, *J. Appl. Phys.* **33**, 3125 (1962).

Hellwarth, R. W., *Phys. Rev.* **152**, 152 (1966).

Jackson, J. D., *Classical Electrodynamics* (Wiley & Sons, New York, 1975), 2nd edition.

Johnson, D. L. and P. N. Sen, editors, *Physics and Chemistry of Porous Media* (American Institute of Physics, New York, 1984).

Kirkwood, J. G., *J. Chem. Phys.* **4**, 592 (1936).

Kirkwood, J. G. and E. M. Boggs, *J. Chem. Phys.* **10**, 392 (1942).

Kittel, C., *Introduction for Solid State Physics* (Wiley & Sons, New York, 1976), 5th edition.

Kreibig, U., A. Althoff, and M. Pressmann, *Surf. Sci.* **106**, 308 (1981).

Landauer, R., in *Electrical Transport and Optical Properties of Inhomogeneous Media*, 1977, edited by J. C. Garland and D. B. Tanner, AIP Conference Preceeding No. 40 (American Institute of Physics, New York, 1978), P.2.

Landauer, R. and J. W. F. Woo, *Phys. Rev. B* , 5 (1189), 1972.

Lax, M., *Rev. Mod. Phys.* **23**, 287 (1951).

Lindsay, M. H., M. Y. Lin, D. A. Weitz, P. Sheng, Z. Chen, R. Klein, and P. Meakin, *Faraday Discuss. Chem. Soc.* **83**, 153 (1987).

Lorentz, H. A., *The Theory of Electrons* (Reprint: Dover, New York, 1952).

Mandelbrot, B. B., *The Fractal Geometry of Nature* (Freeman, San Francisico, 1982).

Matsushita, M., K. Sumida, and Y. Sawada, *J. Phys. Soc. Jpn.* **54**, 2786 (1985).

Maxwell, J. C., *A Treatise on Electricity and Magnetism*, Vol. 1 (Dover, New York, 1954), P.440.

Meakin, P., *Phys. Lett.* **107A**, 269 (1985).

Mossotti, O., *Mem. math. fis. Modena*, **24**, II, 49 (1850).

Mott, N. F., *Metal-Insulator Transitions*, (Taylor and Francis, London, 1974).

Mott, N. F. and E. A. Davis, *Electronic Process in Non-Crystalline Materials* (Oxford University Press, London, 1979), 2nd edition.

Nagaoka, Y. and H. Fukuyama, editors, *Anderson Localization* (Springer Verlag, 1982).

Ohtaka, K. and Inoue, *Phys. Rev. B* **19**, 5057 (1979).

Ohtaka, K. and Inoue, *Phys. Rev. B* **25**, 689 (1982).

Ohtaka, K. and Inoue, *Phys. Rev. B* **26**, 3487 (1982).

Ohtaka, K. and Inoue, *J. Phys. Jpn.* **52**, 1457 (1982).

Onsager, L., *J. Am. Chem. Soc.* **58**, 1486 (1936).

Patton, T. C., *Paint Flow and Pigment Dispersion* (Wiley-Interscience, New York, 1979).

Percus, J. K. and G. L. Yevick, *Phys. Rev.* **110**, 1 (1958).

Pohl, H. A. and M. Pollak, *J. Chem. Phys.* , 66, 4031 (1977).

Pollak, M. and M. Knotek, *J. Non-Cryst. Solids* **4**, 459 (1970).

Pollak, M., *Proc. R. Soc. Lond.* **A325**, 383 (1971).

Purcell, E. M., C. K. Pennypackw, *The Astrophysical Journal* **186**, 705 (1973).

Quinten, M. and U. Kreibig, *Surf. Sci.* **172**, 557 (1986).

Schaefer, D. W., J. E. Martin, P. Wiltzius, and D. S. Cannell, *Phys. Rev. Lett.* **52**, 2371 (1984).

Sheng, P., in *Homogenization and Effective Moduli of Materials and Media*, edited by J. L. Ericksen, The IMA volumes in mathematics and its applications, vol. 1 (Springer-Verlag, New York, 1986).

Sheng, P., editor, *Scattering and Localization of Classical Wave in Random Media* (World Scientific, Singapore, 1989).

Sheng, P. and Z. Chen, *Phys. Rev. Lett.* **60**, 227 (1988).

Sheng, P., R. S. Stepleman, and P. N. Sanda, *Phys. Rev. B* , 26, 2907 (1973).

Stell, G. and G. S. Rushbrooke, *Chem. Phys. Lett.* **24**, 531 (1974).

Stauffer, D., *Introduction to Percolation Theory* (Taylor and Francis, London, 1985).

Vleck, Van, *J. Chem. Phys.* **5**, 320 (1937); **5**, 556 (1937).

Weitz, D. A. and M. Oliveria, *Phys. Rev. Lett.* **52**, 1433 (1984).

Weitz, D. A., M. Y. Lin, J. S. Huang, T. A. Witten, S. K. Sinha, J. S. Geljner, and R. C. Ball, in *Scaling Phenomena in Disordered Systems*, Vol. 133 of *NATO Advanced Study Institute Conference, Series B*, edited by R. Pynn and A. Skjeltorp (Plenum, New York, 1985).

Weitz, D. A., J. S. Huang, M. Y. Lin, and J. Sung, *Phys. Rev. Lett.* **54**, 1416 (1985).

Wiener, O., *Abhandlungen der Mathematish-Physischen Klasse der Koenigl. Saechsischen Gesellschaft der Wissenschaften* **32**, 509 (1912).

Yvon, J., *Recherches sur la théorie cinétique des liquides II* (Hermann, Paris, 1937).

Zallen, R., *The Physics of Amorphous Solids* (Wiley, New York 1983).

Zhou, M. Y., P. Sheng, Z. Chen, and S. T. Chui, Preprint.